Imperial College London
Department of Electrical and Electronic Engineering

Performance Analysis of Large Wireless Networks: A Stochastic Geometry Approach

Mudasar Bacha

2018

Supervised by Dr. Bruno Clerckx

Submitted in part fulfilment of the requirements for the degree of
Doctor of Philosophy in Electrical and Electronic Engineering of Imperial College London
and the Diploma of Imperial College London

Statement of Originality

I declare that this thesis is the result of my own work. The information and ideas derived from the work of others have been acknowledged in the text and a list of references is given in the bibliography. The material of this thesis has not been and will not be submitted for another degree at any other university or institution.

Copyright Declaration

To my parents for their love and support

Abstract

In recent years, stochastic geometry has emerged as a powerful tool for the modeling, analysis, and design of wireless networks with random topologies. Stochastic geometry has been demonstrated to provide a tractable yet an accurate approach for the performance analysis of wireless networks, when the network nodes are modeled as a Poisson point process. This thesis develops analytical frameworks to study the performance of various large-scale wireless networks with random topologies. Firstly, it develops a mathematical model for the uplink analysis of heterogeneous cellular networks when the base stations have multiple antennas. Further, it studies how the gains of downlink and uplink decoupling can be optimized in such a network. Secondly, this thesis also models, analyzes, and designs an ad-hoc network architecture that utilizes both the wireless power transfer and backscatter communications. The performance of such a network is further compared with a regular powered network. Finally, this thesis for the first time develops a scheduling algorithm for cellular networks that has an information theoretic justification. Then using tools from stochastic geometry, this thesis quantifies the gains of such scheduling algorithm over the traditional scheduling algorithm for the downlink transmission. Furthermore, to find the optimal system parameters that provide the maximum gains, this thesis performs asymptotic analysis and provides a simple optimization algorithm. The accuracy of all the mathematical models have been verified with extensive Monte Carlo simulations.

Acknowledgements

I would like to express my sincere gratitude to my supervisor Dr. Bruno Clerckx for his guidance and support throughout my PhD. Working with Bruno was a rewarding experience - both professionally and personally. The flexibility and freedom Bruno provided in formulating my research problem, helped me to grow as a researcher. I am grateful for his insightful suggestions and feedback on my research papers.

I am thankful to Dr. Marco Di Renzo for hosting me at CetraleSupelec. The discussion with Marco was always intellectually stimulating and rewarding. I also acknowledge his excellent feedback on Chapter 4 of this thesis.

I am also thankful to Dr. Justin P. Coon and Prof. Danilo Mandic for their helpful comments on this thesis.

I was fortunate to make some excellent friends at Imperial College and I would miss the time spent with them. Especially, I want to thank Shanxiang, Enrico, Tricia, Hamdi, Firdus, and Fawwaz.

Last, but by no mean the least, my heartfelt thanks to my Mother and Father, for their support and encouragement throughout my life. I am also thankful to my siblings for their support and love.

Mudasar Bacha, London, May 2018.

Contents

List of Tables

List of Figures

List of Abbreviations

5G	Fifth generation mobile networks
AWGN	Additive white Gaussian noise
BNs	Backscatter nodes
BPP	Binomial point process
BS	Base station
CCDF	Complementary cumulative distribution function
CDF	Cumulative distribution function
CoMP	Coordinated multipoint
CSI	Channel state information
CW	Continuous wave
D2D	Device-to-device
DL	Downlink
DUDe	Downlink and uplink decoupling
FBS	Femto base station
FPC	Fractional power control
HCPP	Matérn hard core point process
HetNets	Heterogeneous networks
i.i.d	Independent and identically distributed
IAFPC	Interference aware fractional power control
IC	Integrated circuit
ICIC	Intercell interference coordination
INR	Interference-to-noise ratio

IoT	Internet of Things
LTE-A	Long term evolution-advanced
MAC	Medium access control
MBS	Macro base station
MIMO	Multiple input multiple output
MRC	Maximal ratio combining
PBs	Power beacons
PCP	Poisson cluster point process
PDF	Probability density function
PGFL	Probability generating functional
PPP	Poisson point process
RFID	Radio Frequency IDentification
RPN	Regularly powered network
SIMO	Single input multiple output
SINR	Signal-to-interference-and-noise ratio
SIR	Signal-to-interference ratio
SISO	Single input single output
SNR	Signal-to-noise ratio
TDMA	Time-Division Multiple Access
TIN	Treating interference as noise
UE	User equipment
UL	Uplink
WPBN	Wireless powered backscatter communications network
WPT	Wireless power transfer

1. Introduction

A fundamental property of electromagnetic signals is that they are attenuated when passing through a wireless medium. This distance-dependent attenuation of electromagnetic signals is called *path loss*. For the correct data recovery of the attenuated signal, the strength of the received signal must be greater than the power of the thermal noise, such that, the signal-to-noise power ratio (SNR) is greater than a certain threshold, defined for correct data recovery. As a result, when the distance between the transmitter and receiver is greater than beyond a certain distance, it is not possible for the receiver to distinguish the signal from the thermal noise. Therefore, for correct data recovery, the transmitter is required to transmit with enough power to compensate for the path loss and to achieve the required SNR. Hence, the transmit power is one of the important design parameters in wireless communications. Another important design parameter in wireless communications is the available spectrum, which is usually divided into multiple frequency channels. Independent communication links can be established over non-overlapping frequency channels. The relation between the SNR, the bandwidth, and the maximum data rate supported by each channel is given by Shannon's formula as follows:

$$\mathcal{C} = W \log_2 (1 + \mathrm{SNR}), \tag{1.1}$$

where W represents the bandwidth and $\mathcal{C}$ is in bits per seconds. In single link wireless networks, the desired SNR level can be maintained by properly adjusting the transmission power.

In order to accommodate a large number of devices, the same frequency channel is shared and reused by multiple devices. In this multiple access channel, for correct data recovery at the receiver, the signal-to-interference-and-noise ratio (SINR) should be greater than a specific threshold. Shannon's formula for the multiple access channel is given by

$$\mathcal{C} = W \log_2 (1 + \mathrm{SINR}), \tag{1.2}$$

where the interference from other users is treated as noise. Unlike single link wireless networks, in the multiple-access networks, the required SINR level cannot be just maintained by increasing the transmit power of all the transmitters, as this will increase both the signal power as well as the interference power, and might degrade the SINR and hence the data rate. Therefore, maintaining the required SINR level is a design problem and depends on different network parameters. Two fundamental network parameters that highly affect the

SINR are network geometry and the medium access control.

The relative position of network nodes in the spatial domain makes the network geometry or network topology. The network geometry depends on the type of network and application. For instance, cellular networks are carefully planned to provide coverage to a certain geographical area and often have a regular network topology, while sensor networks usually have random topology. To mediate access to the shared wireless medium a medium access control (MAC) protocol is utilized. The purpose of a MAC is to select multiple users that can simultaneously share the same spectrum while maintaining a sufficient SINR at each link, and to ensure some kind of fair access to the shared spectrum among the users.

In multiple access networks, SINR is one of the main performance metrics and its value depends on the location of transmitters (network topology) and the transmit power of the transmitters. Some of the important performance metrics that depend on the SINR are the following.

- **Coverage Probability**: Let Θ be the SINR decoding threshold. The coverage probability is the probability that the SINR at the receiver is greater than Θ. Mathematically, it can be defined as $\mathcal{C} = \mathbb{P}\left[\text{SINR} \geq \Theta\right]$.
- **Rate Coverage Probability**: Let W be the frequency resources, Ω be the load on a base station (BS)[1], and ρ be the rate threshold, then the rate coverage probability can be defined as $\mathcal{R} = \mathbb{P}\left[\frac{W}{\Omega}\log_2\left(1+\text{SINR}\right) > \rho\right]$.
- **Average Rate or Spectral Efficiency**: Average data rate or spectral efficiency is the average rate supported per channel per hertz and can be defined as $\mathcal{R}_{\mathcal{SE}} = \log_2\left[1+\text{SINR}\right]$.

Other SINR-based performance metrics are spatial frequency reuse, delay and energy efficiency. After looking at the importance of SINR in wireless networks, next we discuss different approaches used in the literature for the mathematical modeling of SINR-based performance in large-scale wireless networks.

1.1. Background and Motivation

The mathematical modeling of wireless networks has always been a non-trivial task. The well-known Wyner model completely ignores the network geometry and only incorporates the distance dependent path-loss into the channel fading [1]. These simplistic assumptions make the Wyner model tractable, but the accuracy is compromised, which leads to disputable insights [2]. Another over-simplified approach is a two-cell model in which interference is assumed from a single cell only [3]. This model neglects most sources of interference in the network and fails to capture the effect of network topology. A widely

[1] In cellular networks, it is the number users in the coverage region of the BS.

accepted and used model in the industry for large-scale infrastructure-based wireless networks is the grid-based model [4]. In the grid-based model, a 2-D network of base stations (BSs) is modeled on a hexagonal lattice or a square lattice. However, the real network deployment is far from the hexagonal-grid, and the grid-based model represents a very idealistic deployment of the cellular networks. In particular, the heterogeneous deployment of BSs will further increase randomness in the network topological structure. Moreover, the grid-based model makes the analysis of the network very complicated and often requires time-consuming Monte-Carlo simulations for the numerical evaluation of the complicated expressions [2]. All these approaches either ignore the effect of network topology or assume simple and deterministic network topology. The only mathematical tool that can capture the effect of the random topology of a network and provide tractable yet accurate expressions is stochastic geometry [5–9].

1.1.1. Stochastic Geometry: A Powerful Mathematical Tool for the Analysis of Random Wireless Networks

Stochastic geometry is the branch of applied probability which permits the study of the average performance, over many spatial realizations, of a network whose nodes are distributed according to some probability distribution [10]. In other words, stochastic geometry allows spatial averaging of all possible network realizations weighted by their probability of occurrence [11]. Stochastic geometry uses point processes to model the spatial distribution of the network elements such as BSs and user equipments (UEs). The commonly used point processes are the Poisson point process (PPP), Binomial point process (BPP), Poisson cluster point process (PCP) and the Matérn hard core point process (HCPP). The selection of a particular point process is dependent on the deployment scenario. In the given point process, PPP is the simplest and most widely used. In this thesis, PPP will be adopted for the spatial modeling of the network elements.

PPP has two important properties; firstly, the number of points in a bounded area follows the Poisson distribution. Secondly, the numbers of points in disjoint areas are independent. The independent property of the points makes the PPP simple and the resulting analysis tractable. A spatial point process $\Phi = \{x_i; i \in \mathbb{N}\}$ is a random, finite or countably-infinite collection of points in the $d-$dimensional Euclidean space $\mathbb{R}^d$, where $x_i \in \mathbb{R}^d$ represents the coordinates of the ith point. For a PPP, let $\mathbf{A} \subset \mathbb{R}^2$, the number of points $\Phi(\mathbf{A}) = |\Phi \cap \mathbf{A}| \sim Poisson(\lambda)$ with the following probability mass function

$$\mathbb{P}[\Phi(\mathbf{A}) = n] = \mathrm{e}^{-\lambda L(\mathbf{A})} \frac{(\lambda L(\mathbf{A}))^n}{n!}, \tag{1.3}$$

where λ is the intensity of the point process and $L(.)$ represents the Lebesgue measure [12]. The PPP results in pure random deployment of network elements and makes the mathematical analysis tractable; however, due to this random deployment some of the network nodes can become arbitrary close to each other. PPP is not suitable for a network

with repulsion between nodes, where the locations of the nodes are correlated. To model the repulsion among the nodes, the PCP and HCPP can be used. Nevertheless, the non-PPP based abstraction models are generally not mathematically as tractable as the PPP based abstraction models.

In the following, some of the important properties and statistical measures of the homogenous PPP are discussed that will be utilized throughout the main technical chapters. More details about the point process can be found in the notable references [5, 7–9, 13].

1. **Campbell's theorem:** Let Φ be a PPP of density λ and $f : \mathbb{R}^d \to \mathbb{R}$ be measurable function, then Campbell's theorem states that

$$\mathbb{E}\left[\sum_{x_i \in \Phi} f(x_i)\right] = \int_{\mathbb{R}^d} \lambda f(x)\, \mathrm{d}x. \tag{1.4}$$

   Note that the Campbell's theorem converts an expectation of a random sum over a PPP to an integral and can be used to compute the mean interference in a cellular network.

2. **Probability generating functional (PGFL):** Let Φ be a PPP of density λ and $f : \mathbb{R}^d \to [0, 1]$ be a real value function, then the PGFL states that

$$\mathbb{E}\left[\prod_{x_i \in \Phi} f(x_i)\right] = \exp\left(-\lambda \int_{\mathbb{R}^d} (1 - f(x))\, \mathrm{d}x\right). \tag{1.5}$$

   The PGFL converts the expectation of a random product over a PPP to an integral. As discussed later, the PGFL is very useful in the determination of the Laplace transform of interference.

3. **Slivnyak's theorem:** Slivnyak's theorem for a PPP states that conditioning on a point at a certain location, x_i, does not change the statistical properties of the PPP[2]. In other words, the PPP observed from any arbitrary location remains the same irrespective of having a point on that location. Mathematically, it can be written as

$$\mathbb{E}\left[\sum_{x_i \in \Phi} f(x_i, \Phi \backslash (x_i))\right] = \int_{\mathbb{R}^d} \mathbb{E}\left[f(x, \Phi)\right] \lambda \mathrm{d}x. \tag{1.6}$$

   This suggests that adding or removing a point does not change the distribution of other points of the process. Slivnyak's theorem is important in the analysis of cellular networks because it allows the modeling of the interfering points as a PPP, while removing a point (for example, a serving BS in the downlink analysis of a cellular network) from the PPP.

[2]The reduced Palm distribution of a PPP is equal to the distribution of the PPP itself [7–9].

4. **Independent thinning:** The independent selection of points of a PPP with probability p and discarding those with probability $(1-p)$ results in two independent PPPs of densities $p\lambda$ and $(1-p)\,\lambda$, respectively. The medium access control (MAC) protocol such as Time-Division Multiple Access (TDMA) in cellular networks usually leads to a thinning of the UEs. If the underlying UEs are modeled as a PPP, the resulting thinned UEs also form a PPP.

5. **Superposition:** Let $\Phi_1, \cdots, \Phi_n$ be the n independent homogeneous PPPs with densities $\lambda_1, \cdots, \lambda_n$, respectively, the superposition of these point processes results in a PPP $\Phi = \bigcup_i^n \Phi_n$ with density $\lambda = \sum_i^n \lambda_i$. The superposition property of the PPP is generally exploited in the modeling of multi-tier cellular networks.

6. **Displacement:** When the points of a PPP are displaced by a random translation vector $\mathbf{V}_{x_i}$, the resulting point process is again a PPP. Mathematically, we write as

$$\Phi' = \{x_i \in \Phi : x_i + \mathbf{V}_{x_i}\}, \tag{1.7}$$

where $\mathbf{V}_{x_i}$ are independent random variables, but their distribution may depend on x_i. This shows that the independent displacements preserves the Poisson nature of a PPP. The displacement property of the PPP is usually exploited in modeling mobility of nodes in a network.

In wireless networks, interference is one of the main network parameters. Stochastic geometry provides a systematic way to characterize interference. The interference[3] can be considered as a function of the point process. The interference depends on the time variant locations of the interfering network elements, modeled by the point process and the instantaneous channel gains. Interference can be completely characterized by its probability density function (PDF)[4]; however, generally there is no known PDF of the interference in large-scale wireless networks. Therefore, the interference is usually characterized by the Laplace transform (or characteristic function or moment generating function) of the PDF [5]. The Laplace transform of the interference I can be written as

$$\mathcal{L}_I(s) = \mathbb{E}\left[\mathrm{e}^{(-sI)}\right], \tag{1.8}$$

and the Laplace transform always exists because the interference is strictly a positive random variable. By considering interference as a function of the point process, i.e. $I = \sum_{x_i \in \Phi} f(x_i)$, the Laplace transform can be written as

$$\mathcal{L}_I(s) = \mathbb{E}\left[\exp\left(-s\sum_{x_i\in\Phi} f(x_i)\right)\right] = \mathbb{E}\prod_{x_i\in\Phi}\left[\exp\left(-sf(x_i)\right)\right]. \tag{1.9}$$

[3] from now onwards, interference is defined as aggregate interference.
[4] or equivalently its cumulative distribution function (CDF)

Now, we apply the PGFL of a PPP and as a result write the above equation as

$$\mathcal{L}_I(s) = \exp\left(-\lambda \int_{\mathbb{R}^d} \left(1 - \mathrm{e}^{-sf(x)}\right) \mathrm{d}x\right). \tag{1.10}$$

Note that the integration boundary represents the interference boundary (the region where the PPP exists). The detailed discussion about how to find the Laplace transform of the interference will be provided in the main technical chapters.

In literature, different techniques have been used to utilize the Laplace transform, the characteristic function, or the moment generating function to study network performance, such as coverage probability, average rate, and error probability. To the best of author knowledge, these are nine techniques which can be briefly summarized as follows:

- The first technique assumes that the desired link undergoes Rayleigh fading. With the Rayleigh fading assumption, the exact distribution of the signal-to-interference-and-noise ratio (SINR) can be obtained [5].
- The second technique only considers the most dominant interferer or the nearest n interferer to find a bound on the performance of the network [5].
- In the third approach, the PDF of the interference is approximated by some known distribution, such as Gaussian or shifted log-normal through empirical fitting [5].
- The fourth technique uses the Plancherel-Parseval theorem to avoid inverting the Laplace transform. This technique extends the stochastic geometry analysis to a general fading environment; however, the resulting expressions involve complicated integrals [5].
- In the fifth approach, the Laplace transform, the characteristic function, or the moment generating function is numerically inverted [5].
- A direct method for the computation of coverage probability without finding the Laplace transform has been proposed in [14].
- Equivalent-in-distribution representation of the other cell interference has been outlined in [15].
- A moment generating function representation of other cell interference has been used in [16] to find the average rate of the network. In order to find the average rate of the network, this technique does not require the computation of coverage probability.
- A mathematical framework for the computation of coverage probability and average rate based on Gil-Pelaez inversion theorem has been introduced in [17].

The detailed discussion of the related work has been postponed to the technical chapters, for the sake of an organized presentation. That is, in each technical chapter, a unique network is studied and its related literature and novelty are discussed there.

1.2. Outline and Contributions

This thesis utilizes stochastic geometry tools for the modeling, analysis, and design of different network topologies that have not been studied before. The central goal of the thesis is to develop generic frameworks for the design and analysis of large-scale wireless networks that take into account the network topology. This thesis extends stochastic geometry applications to new scenarios of large-scale wireless networks. The chapter-wise details are as follows:

- **Chapter 2: Downlink and Uplink Decoupling in Two-Tier Heterogeneous Networks with Multi-Antenna Base Stations**

  This chapter studies the gain provided by the downlink and uplink decoupling in two-tier heterogeneous networks where BSs have multiple antennas and UEs have single antennas. It considers Maximal ratio combining as a linear receiver at the BSs and derives the signal-to-interference ratio (SIR) coverage probability and the rate coverage probability in the form of mathematically tractable expressions. It then investigates how the beamforming gains of both tiers affects the gains of downlink and uplink decoupling. Furthermore, it studies how the optimal performance can be achieved by offloading UEs to the small BSs in case of high asymmetry in the beamforming gains of both tiers.

- **Chapter 3: Backscatter Communications for the Internet of Things**

  This chapter studies a unique ad-hoc network architecture that utilizes a combination of wireless power transfer and backscatter communications. The network consists of power beacons and passive backscatter nodes. The power beacons transmit a sinusoidal continuous wave in an isotropic direction and the backscatter nodes reflect back a portion of this signal through backscatter modulation, while harvesting the remaining energy. This chapter derives the coverage probability and capacity of such a network with the help of stochastic geometry. This chapter further compares the performance of such a network with the regular powered network in which the backscatter nodes have a reliable power source.

- **Chapter 4: Treating Interference as Noise in Cellular Networks**

  This chapter develops a scheduling algorithm for the cellular networks that is based on the optimality condition of treating interference as noise, a famous interference management technique in the information theory. The signal-to-interference-and-noise ratio (SINR) coverage probability and the spectral efficiency of the network, utilizing this scheduling algorithm, have been derived in tractable and easily computable expressions. This chapter then performs asymptotic analysis and provides a simple optimization algorithm that gives the optimal system parameters for the SINR coverage probability. These optimal system parameters provide the maximum

gains over the classical scheduling algorithm in terms of the SINR coverage probability. Moreover, the performance of this scheduling algorithm is compared with the classical scheduling algorithm, and the gains in terms of both the SINR coverage probability and the spectral efficiency are quantified.

- **Chapter 5: Conclusion**

  This chapter concludes the thesis and provides some further research directions.

1.3. Publications

This thesis has resulted in the following journal papers:

Submitted (under-review)

- **M. Bacha**, M. Di Renzo, and B. Clerckx, "Treating Interference as Noise in Cellular Networks: A Stochastic Geometry Approach," submitted to *IEEE Transactions on Wireless Communications*.

- **M. Bacha** and B. Clerckx, "Backscatter Communications for the Internet of Things: A Stochastic Geometry Approach," submitted to *IEEE Transactions on Communications*.

Published

- **M. Bacha**, Y. Wu, and B. Clerckx, "Downlink and Uplink Decoupling in Two-Tier Heterogeneous Networks with Multi-Antenna Base Stations," *IEEE Transactions on Wireless Communications,* vol. 16 , no. 5, pp. 2760-2775, May 2017.

2. Downlink and Uplink Decoupling in Two-Tier Heterogeneous Networks with Multi-Antenna Base Stations

In order to improve the uplink performance of future cellular networks, the idea to decouple the downlink (DL) and uplink (UL) association has recently been shown to provide significant gains in terms of both coverage and rate performance. However, all the work is limited to single input single output (SISO) network. Therefore, to study the gain provided by the DL and UL decoupling in multi-antenna BSs setup, this chapter studies a two tier heterogeneous network consisting of multi-antenna BSs, and single antenna UEs. It uses maximal ratio combining (MRC) as a linear receiver at the BSs and using tools from stochastic geometry, it derives tractable expressions for both SIR coverage probability and rate coverage probability. It is observed that as the disparity in the beamforming gain of both tiers increases, the gain in terms of SIR coverage probability provided by the decoupled association over non-decoupled association decreases. Furthermore, it is observed that when there is asymmetry in the number of antennas of both tiers, then further biasing towards the femto-tier is required on the top of decoupled association to balance the load and to get the optimal rate coverage probability.

2.1. Introduction

The demand for high data rates is ever-growing and it is projected that over the next decade a factor of a thousand times increase in wireless network capacity will be required [18]. In order to meet this challenge, a massive densification of the current wireless networks characterized by the dense deployment of low power and low cost small cells is required, which will convert the existing single-tier homogeneous networks into multi-tier heterogeneous networks (HetNets) [19]. HetNets that consist of different types of base stations (Macro, Micro, Pico and Femto) cannot be operated in the same way as a single-tier homogeneous network (consisting of macro base stations only) and need some fundamental changes in their design and deployment to meet the high data rate demand.

Cellular networks have been designed mainly for downlink (DL) because initially the traffic was asymmetric (mostly in the downlink direction). However, with the increase in real-time applications, online social-networking, and video-calling, the traffic in UL has greatly increased, which necessitates the need for the uplink (UL) optimization. In current

cellular networks, cell association is based on downlink average received power, which is viable for homogeneous networks where the transmit power of all the base stations (BSs) is the same. However, in heterogeneous networks there is a big disparity in the transmit power of different BSs, and the association scheme based on downlink received power is highly inefficient, therefore, the idea of downlink and uplink decoupling (DUDe) has been proposed for fifth generation mobile networks (5G) in [20–22].

2.1.1. Related Work

A simulation study has been performed on a two-tier live network where the UL association is based on minimum path-loss while the DL association is based on DL received power [23]. This kind of association divides the users into three groups: users attached to a macro base station (MBS) both in the DL and UL, users attached to a femto base station (FBS) both in the DL and UL, and users attached to an MBS in the DL and an FBS in the UL. The authors in [23] showed that the gain in UL throughput is quite high when the UL association is based on minimum path-loss. The gain comes from those UEs which are connected to an MBS in the DL and an FBS in the UL because they have a better channel to the femto-cell and they create less interference to the macro-cell. A network consisting of macro-tier and femto-tier is studied using tools from stochastic geometry in [24], where the throughput gain due to decoupling has been shown. In [25], the analytical results obtained from a stochastic geometry-based model have been compared with the results obtained from the simulation in [23], and they found that both of them match each other. They also found that the association probability mainly depends on the density of the deployment and not on the process used to generate the deployment geometry. It has been shown in [26] that DUDe provides gain in term of system rate, spectrum efficiency, and energy efficiency. A joint study of DL and UL for k tier SISO network has been performed in [27], while considering a weighted path-loss association and UL power control.

Stochastic geometry has emerged as a powerful tool for the analysis of cellular networks after the seminal work of [28]. It has been shown that stochastic geometry-based models are equally accurate as grid based models. In addition, they provide more tractability and their accuracy becomes better as the heterogeneity of the network increases. Most of the work that considered stochastic geometry-based models, mainly studied the DL performance of the HetNets. For instance, SISO HetNets have been studied in [11,16,29–46], multiple input multiple output (MIMO) HetNets in [47–55]. A complete survey can be found in [5,6] and the references therein. However, only limited work has been carried out in UL because it is more involved due to UL power control and correlation among interferers. The UL power control is required because an interfering user may be closer to the BS than the scheduled user, which creates an additional source of randomness in the UL modeling. The correlation among interfering users comes due to the orthogonal channels assignment within a cell, which prohibits the use of the same channel in a cell. In other words, there is only one UE randomly located within the coverage region of the BS, which transmits in a given resource

block. Therefore, the interference does not originate from the PPP distributed UEs but instead from Voronoi perturbed lattice process [27]. The exact interference characterization is not available [27], and thus makes the UL analysis even more involved.

An uplink model for the single tier network has been derived in [56], which uses fractional power control (FPC) in the UL. A multi-tier UL performance has been studied in [27, 57], where each tier differs only in terms of density, cut-off threshold, and transmit power. In [57], a truncated channel power inversion is used due to which mobile users suffer from truncation outage in addition to SINR outage. The performance gain of DUDe is only studied for a SISO network and there is no work which studies the decoupled association in the MIMO network[1]. Therefore, this chapter considers multi-antenna BSs and also considers UL biasing with the DUDe.

2.1.2. Contributions and Outcomes

The main challenge in modeling the UL multi-antennas HetNets, in addition to the generic challenges discussed above, is to select an analytically tractable technique from the number of possible multi-antenna techniques. The present chapter considers maximal ratio combining (MRC) at the BSs and assumes that the channel is perfectly known at the receiver. A receiver has knowledge about the channel between the transmitter and itself, but it does not have any knowledge about the interfering channel. Furthermore, it considers power control in the UL, which partially compensates for the path-loss [27, 56]. This chapter assumes Rayleigh fading in addition to path-loss[2].

We use a cell association technique with biasing[3], which can be used in any MIMO HetNets. This association completely decouples the DL and UL association, and is generic and simple. Cell biasing in the UL can be used to balance the load across the tiers. This association scheme is motivated by the technique used in [24] for SISO HetNets. Due to the DUDe, users are divided into three disjoint groups as shown in Fig. 2.1; (I) users attached to the MBS both in the DL and UL, (II) users attached to the FBS both in the DL and UL, and (III) users attached to the MBS in the DL and FBS in the UL. The gain in the UL performance comes from the last kind of UE because they have a strong connection to the FBS (low path-loss) and they create less interference to the MBS (due to a larger distance).

This chapter studies both the SIR and rate coverage probability of a two tier network where the association is based on DL and UL decoupling. The novel and insightful findings of this chapter are as follows:

[1] [58] studies the UL performance in multi antennas BSs network. However, our analysis approach is significantly different than [58]. We explicitly take into account the beamforming gain in the cell association and uses the Faà di Bruno's formula [59] to find the high order derivative of the Laplace transform of the interference, whereas [58] does not consider beamforming gain in the cell association and uses the Gil-Pelaez inversion theorem to avoid finding the higher order derivative.

[2] For the sake of simplicity, shadowing in not considered in this work. Shadowing in a similar setup can be found in [27, 58].

[3] The biasing can be considered as the artificial increase in the transmit power of a given network tier.

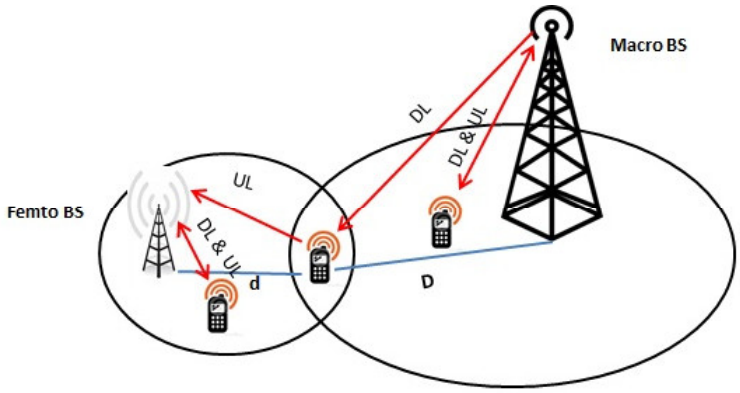

Figure 2.1.: System Model.

- The gain in terms of the SIR coverage probability provided by the DUDe association over a no-DUDe association (association based on DL maximum received power averaged over fading) decreases as the difference in the number BS's antennas in the femto and macro-tier increases. When the number of MBS antennas is larger than that of FBS, the association region of an MBS is enlarged due to the larger beamforming gain provided by the MBS. As a result of which UEs closer to the FBSs become associated with MBSs. These boundary UEs, which are connected to the macro-tier, create strong interference at nearby FBSs when they transmit to their serving MBSs. On the other hand, when both tiers have the same beamforming gain, the coverage region of both tiers are the same and the interference created by the boundary UEs is not that strong. Thus, the DUDe gain over No-DUDe is high when both tiers have the same beamforming gain.

- It has been shown in [23, 24, 26, 27] that the DUDe association improves the load balance and provides fairness in the UL performance of different UEs. In [27] it is shown that in the UL the optimal rate coverage is provided by the minimum path-loss association. However, we observe that in the single input multiple output (SIMO) network, DUDe association does not completely solve the load imbalance problem and the optimal rate coverage is not provided by the minimum path-loss association. In the SIMO network, this load imbalance problem comes from the different beamforming gain of the femto and macro-tier, therefore, we still need biasing towards the femto-tier to balance the load. We show that when the beamforming gain of the macro-tier is high as compared to the femto-tier then biasing towards the femto-tier improves the rate coverage probability.

The rest of the chapter is organized as follows. In Section 2.2, we present our system model and assumptions. In Section 2.3, we derive some enabling results, in particular, the association probabilities and the distance distribution of a user to its serving BS. Section 2.4 is the main technical section, we develop the mathematical framework for the SIR

Table 2.1.: List of Notations for Chapter 2.

Notation	Description
Φ_K, Φ_U	PPP of tier K BSs, PPP of UEs
λ_K, λ_U	density of tier K BSs, density of UEs
P_K, P_U	transmit power of each BS of the Kth tier , transmit power of a UE
X_K, α_K	distance between the *typical* UE and the *tagged* BS, path-loss exponent of Kth tier
X_{K_i}, X_{J_q}	distance between an interfering UE of Kth and Jth tier, and their serving BSs respectively
D_{K_i}, D_{J_q}	distance between an interfering UE of Kth and Jth tier, and the tagged BS respectively
$\mathcal{A}_K$, N_K	association probability of a *typical* UE to Kth tier, number of antennas at a Kth tier BS
B	bias factor, $B = \frac{B_F}{B_M}$, where B_F and B_M is biasing towards femto-tier and macro-tier respectively
τ_K, ρ_K, η	SIR threshold and rate threshold of Kth tier, UL power control fraction
$\mathcal{C}$, $\mathcal{C}_K$	SIR coverage probability of the network, SIR coverage probability of the Kth tier
$\mathcal{R}$, $\mathcal{R}_K$	rate coverage probability of the network, rate coverage probability of the Kth tier
$\Omega_K, \bar{\Omega}_K$, W	load on a Kth tier BS, average load on Kth tier BS, bandwidth in Hz
$\mathbf{h}_{K_0}, \mathbf{h}_{K_i}, \mathbf{h}_{J_q}$	complex channel gain between the tagged BS and typical UE, an interfering UE of Kth and Jth tier respectively

coverage probability and the rate coverage probability of the network. Section 2.5 presents simulations and numerical results, while Section 2.6 provides a summary of this chapter.

The key notations used in this chapter are given in Table 2.1.

2.2. System Model

2.2.1. Network Model

We consider a heterogeneous network that consists of macro base stations (MBSs), femto base stations (FBSs) and user equipments (UEs). The location of MBSs, FBSs and UEs are modeled as 2-D independent homogeneous Poisson Point Processes (PPPs). Let Φ_M, Φ_F, and Φ_U represent the PPPs for MBSs, FBSs and UEs respectively. Furthermore, let λ_M, λ_F, and λ_U be the density of Φ_M, Φ_F, and Φ_U respectively. The transmit power of a MBS and FBS are represented by P_M and P_F respectively, where $P_M > P_F$. We consider that MBSs have N_M and FBSs have N_F antennas and $N_M \geq N_F$, while UEs have single antenna. Throughout the system model, only inter-cell interference is considered i.e., a BS schedules a single UE in a given resource block. The analysis is performed for a *typical* UE located

at the origin and the BS serving this typical UE is referred to as the *tagged* BS, thanks to Slivnyak's theorem [7].

2.2.2. Uplink Power Control

We consider a fractional power control in the uplink that partially compensates for path-loss [60]. Let X_K be the distance between a UE and its serving Kth-tier BS. The UE transmits with $P_U = P_0 X_K^{\eta\alpha_K}$, where α_K is the path-loss exponent of the Kth-tier, P_0 is the transmit power of the UE before applying the UL power control, and $0 \leq \eta \leq 1$ is the power control fraction. If $\eta = 1$, the path-loss is completely inverted by the power control, and if $\eta = 0$, no channel inversion is applied and all UEs transmit with the same power. We do not consider the maximum transmit power constraint for the tractability of the analysis. However, the analysis can be extended to include the maximum power constraint similar to [57, 58].

2.2.3. Signal Model

The received signal vector $\mathbf{Y}_{K_0}$ at a tagged BS when a typical UE u_0 is served by a Kth tier BS having N_K antennas is given by

$$\mathbf{Y}_{K_0} = \sqrt{P_0 X_K^{\alpha_K(\eta-1)}}\mathbf{h}_{K_0} s_{K_0} + \underbrace{\sum_{i\in\Phi'_K\setminus u_0} \sqrt{P_0 X_{K_i}^{\alpha_K\eta} D_{K_i}^{-\alpha_K}}\mathbf{h}_{K_i} s_{K_i}}_{\text{interference from } K\text{th tier scheduled UEs}} + \underbrace{\sum_{q\in\Phi'_J} \sqrt{P_0 X_{J_q}^{\alpha_J\eta} D_{J_q}^{-\alpha_K}}\mathbf{h}_{J_q} s_{J_q}}_{\text{interference from } J\text{th tier scheduled UEs}} + \mathbf{n}, \quad (2.1)$$

where α_K is the path-loss exponent of Kth tier ($\alpha_K > 2$); $\mathbf{h}_{K_i} = \left[h_{K_1}, h_{K_2}, \ldots h_{K_{N_K}}\right]^T$ is the complex channel gain and the magnitude of each h_i follows Rayleigh distribution (we assume Rayleigh fading channel); X_{J_q} represents the Euclidean distance between the qth UE of the Jth tier and its serving BS; D_{J_q} is the Euclidean distance between the qth interfering UE of the Jth tier to the tagged BS; s_{J_q} is the signal transmitted by the qth UE of the Jth tier having unit power; $\mathbf{n} = [n_1, n_2, \cdots, n_{N_K}]^T$ is the vector of complex additive white Gaussian noise at the tagged BS; Φ'_K and Φ'_J represent the point processes formed by the thinned PPP of the scheduled UEs of the Kth and Jth tier respectively. Since, we assume multiple antennas' BS, we apply a receiver combiner $\mathbf{g_0}$ to s_{K_0} of a typical UE. By

using maximal ratio combining (MRC), $\mathbf{g}_0 = \mathbf{h}_{M_0}^H$, (2.1) can be written as

$$Z_{K_0} = \mathbf{h}_{K_0}^H \mathbf{Y}_{K_0} = \sqrt{P_0 X_K^{\alpha_K(\eta-1)}} \left\|\mathbf{h}_{K_0}\right\|^2 s_{K_0} + \sum_{i \in \Phi_K' \setminus u_0} \sqrt{P_0 X_{K_i}^{\alpha_K \eta} D_{K_i}^{-\alpha_K}} \mathbf{h}_{K_0}^H \mathbf{h}_{K_i} s_{K_i} + \sum_{q \in \Phi_J'} \sqrt{P_0 X_{J_q}^{\alpha_J \eta} D_{J_q}^{-\alpha_K}} \mathbf{h}_{K_0}^H \mathbf{h}_{J_q} s_{J_q} + \mathbf{h}_{K_0}^H \mathbf{n}. \quad (2.2)$$

Similarly, the SINR γ_{K_0} at the tagged BS K_0 can be written as

$$\gamma_{K_0} = \frac{P_0 \left\|\mathbf{h}_{K_0}\right\|^2 X_K^{\alpha_K(\eta-1)}}{\sum\limits_{i \in \Phi_K' \setminus u_0} P_0 \left|\frac{\mathbf{h}_{K_0}^H \mathbf{h}_{K_i}}{\left\|\mathbf{h}_{K_0}\right\|}\right|^2 X_{K_i}^{\alpha_K \eta} D_{K_i}^{-\alpha_K} + \sum\limits_{q \in \Phi_J'} P_0 \left|\frac{\mathbf{h}_{K_0}^H \mathbf{h}_{J_q}}{\left\|\mathbf{h}_{K_0}\right\|}\right|^2 X_{J_q}^{\alpha_J \eta} D_{J_q}^{-\alpha_K} + \sigma_n^2}, \quad (2.3)$$

where $\left\|\mathbf{h}_{K_0}\right\|^2 \sim \text{Gamma}\left(N_K, 1\right)$, whereas $\left|\frac{\mathbf{h}_{K_0}^H \mathbf{h}_{K_i}}{\left\|\mathbf{h}_{K_0}\right\|}\right|^2$ and $\left|\frac{\mathbf{h}_{K_0}^H \mathbf{h}_{J_q}}{\left\|\mathbf{h}_{K_0}\right\|}\right|^2$ both follow independent exponential distribution [61].

We assume high density for the UEs such that each BS has at least one UE in its association region and UEs always have data to transmit in the UL (saturated queues). Throughout the chapter the Kth tier will always be the serving tier of the typical UE while Jth tier will be the interfering tier. We will use the terms UE and user, and typical user and random user interchangeably.

2.2.4. Cell Association

The long term average received power (accounting for beamforming gain) at a typical UE when a Kth tier BS transmits is $P_K N_K X_K^{-\alpha_K}$. Similarly, in the UL, the long term average received power at a typical Kth tier BS is $P_0 N_K X_K^{-\alpha_K}$ (before employing UL power control). In the DL, a UE is associated to a BS from which it receives the maximum average power, while in the uplink it is associated to a BS that receives the maximum average power. In the UL, each UE has the same transmit power, so the association is actually related to the number of antennas and the path-loss. Due to the cell association criterion, there are three sets of UEs: 1) UEs connected to the MBSs both in the DL and the UL, 2) UEs associated to the MBSs in the DL and FBSs in the UL, and 3) UEs connected to the FBSs both in the DL and the UL as shown in Fig. 2.1. In the DL, the load imbalance problem arises due to the high transmit power and beamforming gain of the MBS as compared to the FBS, whereas in the UL it is only due to the larger number of antennas at the MBS. In order to balance the load among the macro-tier and femto-tier in the UL, we use bias factor $B = \frac{B_F}{B_M}$, where B_F and B_M are the biases towards femto- and macro-tier respectively. A biasing $B > 1$ offloads UEs from the macro-tier to the femto-tier, $B < 1$ offloads UEs from the femto-tier to the macro-tier, and $B = 1$ means no biasing. The association criterion is based on long-term average biased-received power and the UEs in different regions can be written as:

- Case1- UEs connected to MBS both in the UL and DL:

$$\left\{\underbrace{\left(P_M N_M X_M^{-\alpha_M} > P_F N_F X_F^{-\alpha_F}\right)}_{\text{DL association rule}} \bigcap \underbrace{\left(N_M B_M X_M^{-\alpha_M} > N_F B_F X_F^{-\alpha_F}\right)}_{\text{UL association rule}}\right\},$$

- Case2- UEs connected to MBS in the DL and FBS in the UL:

$$\left\{\left(P_M N_M X_M^{-\alpha_M} > P_F N_F X_F^{-\alpha_F}\right) \bigcap \left(N_M B_M X_M^{-\alpha_M} \leq N_F B_F X_F^{-\alpha_F}\right)\right\},$$

- Case3- UEs connected to FBS both in the UL and DL:

$$\left\{\left(P_M N_M X_M^{-\alpha_M} \leq P_F N_F X_F^{-\alpha_F}\right) \bigcap \left(N_M B_M X_M^{-\alpha_M} \leq N_F B_F X_F^{-\alpha_F}\right)\right\}.$$

2.3. Preliminaries

In this section, we find the association probabilities of UEs and the distance distribution of a UE to its serving BS. These will be required in the next section to find the SIR coverage probability and rate coverage probability of the network.

2.3.1. Association Probability

In this subsection, we find the association probabilities of the UEs.

Lemma 2.1. *The probability that a typical UE is associated with the MBS both in the UL and the DL is given by*

$$\mathbb{P}\left(case1\right) = 2\pi\lambda_M \int_0^\infty X_M e^{-\pi\left[\lambda_F \Upsilon_1^{2/\alpha_F}\left(X_M^{\alpha_M/\alpha_F}\right)^2 + \lambda_M X_M^2\right]} \mathrm{d}_{\mathrm{X_M}}, \tag{2.4}$$

where for $\frac{B_F}{B_M} \geq \frac{P_F}{P_M}$, $\Upsilon_1 = \frac{B_F N_F}{B_M N_M}$ *and for* $\frac{B_F}{B_M} < \frac{P_F}{P_M}$, $\Upsilon_1 = \frac{P_F N_F}{P_M N_M}$. *The association probability is independent of the density of the UEs.*

Proof. See Appendix A.1. □

Lemma 2.2. *The probability that a typical UE is associated with a MBS in the DL and a FBS in the UL is*

$$\mathbb{P}\left(case2\right) = 2\pi\lambda_F \left[\int_0^\infty X_F e^{-\pi\left[\lambda_M \Upsilon_1'^{2/\alpha_M}\left(X_F^{\alpha_F/\alpha_M}\right)^2 + \lambda_F X_F^2\right]} \mathrm{d}_{\mathrm{X_F}} - \int_0^\infty X_F e^{-\pi\left[\lambda_M \Upsilon_2'^{2/\alpha_M}\left(X_F^{\alpha_F/\alpha_M}\right)^2 + \lambda_F X_F^2\right]} \mathrm{d}_{\mathrm{X_F}}\right], \tag{2.5}$$

where when $\frac{B_F}{B_M} \geq \frac{P_F}{P_M}$, *then* $\Upsilon'_1 = \frac{B_M N_M}{B_F N_F}$ *and* $\Upsilon'_2 = \frac{P_M N_M}{P_F N_F}$ *and when* $\frac{B_F}{B_M} < \frac{P_F}{P_M}$ *then* $\Upsilon'_1 = \frac{P_M N_M}{P_F N_F}$ *and* $\Upsilon'_2 = \frac{B_M N_M}{B_F N_F}$.

Proof. The proof follows similar steps as Lemma 2.1. □

Lemma 2.3. *The probability that a typical UE associates with the FBS both in the DL and the UL can be written as*

$$\mathbb{P}\left(case3\right) = 2\pi\lambda_F \int_0^\infty X_F e^{-\pi\left[\lambda_M \Upsilon_2'^{2/\alpha_M}\left(X_F^{\alpha_F/\alpha_M}\right)^2 + \lambda_F X_F^2\right]} \mathrm{d}_{\mathrm{X_F}}, \tag{2.6}$$

where when $\frac{B_F}{B_M} \geq \frac{P_F}{P_M}$, *then* $\Upsilon'_2 = \frac{P_M N_M}{P_F N_F}$ *and when* $\frac{B_F}{B_M} < \frac{P_F}{P_M}$ *then* $\Upsilon'_2 = \frac{B_M N_M}{B_F N_F}$.

Proof. It can be easily proved by following the same steps as in Lemma 2.1. □

From Lemma 2.1, 2.2 and 2.3, the tier-association probabilities in the UL can be easily obtained. Thus the probability that a typical UE is associated with Kth-tier BS is given by

$$\mathcal{A}_K = 2\pi\lambda_K \int_0^\infty X_K e^{-\pi\left[\lambda_J \Upsilon^{2/\alpha_J}\left(X_K^{\alpha_K/\alpha_J}\right)^2 + \lambda_K X_K^2\right]} \mathrm{d}_{\mathrm{X_K}} \tag{2.7}$$

where $K, J \in \{M, F\}$ and $K \neq J$ and for $\frac{B_F}{B_M} \geq \frac{P_F}{P_M}$, $\Upsilon = \frac{B_J N_J}{B_K N_K}$ and for $\frac{B_F}{B_M} < \frac{P_F}{P_M}$, $\Upsilon = \frac{P_J N_J}{P_K N_K}$. It is important to mention that the condition $\frac{B_F}{B_M} < \frac{P_F}{P_M}$ in Lemma 2.1, 2.2, 2.3 and (2.7) is very unlikely to be true because usually we need to offload the UEs towards the femto-tier instead of the macro-tier. However, we specifically mentioned it so that the expression in Lemma 2.1, 2.2, 2.3 and (2.7) holds for the entire range of the bias B.

For $\alpha_K = \alpha_J = \alpha$, (2.7) simplifies to

$$\mathcal{A}_K = \frac{\lambda_K}{\lambda_K + \Upsilon^{2/\alpha}\lambda_J}. \tag{2.8}$$

The probability that a typical UE associates to the Kth tier increases with increasing the density of Kth tier BS, or biasing towards Kth tier or placing more antennas at Kth tier BSs. However, the increase due to biasing and the beamforming gain is not the dominant factor due to the presence of the exponent $2/\alpha$ where $\alpha > 2$.

2.3.2. Distance Distribution to the Serving BS

In this subsection, we find the distance distribution of the scheduled user to the serving BS.

Lemma 2.4. *The distribution of the distance* X_K *between the typical UE and the tagged BS is*

$$f_{X_K}\left(X_K\right) = \frac{2\pi\lambda_K}{\mathcal{A}_K} X_K \exp\left\{-\pi\left(\lambda_K X_K^2 + \lambda_J\left(\frac{B_J N_J}{B_K N_K}\right)^{2/\alpha_J} X_K^{2(\alpha_K/\alpha_J)}\right)\right\}, \tag{2.9}$$

where $K, J \in \{M, F\}$ *,* $K \neq J$*, and* $\mathcal{A}_K$ *is the tier association probability.*

Proof. We provide the proof in Appendix A.2. □

Remark 2.1. *It is important to mention that the distance distribution of an interfering UE to its serving BS is different from the distribution of the typical UE and the tagged BS because the distance between an interfering UE and its serving BS is upper bounded by a function of the distance between an interfering UE and the tagged BS. Specifically, let both the typical UE* u_0 *and an interfering UE* u_i *belong to the* K*th tier and let the distance between* u_i *and its serving BS be* X_{K_i}*, and* D_{K_i} *be the distance between* u_i *and the tagged BS, then* $0 \leq X_{K_i} \leq D_{K_i}$*. Similarly, if* u_i *belongs to the* J*th tier (interfering tier) and the distance between* u_i *and its serving BS is* X_{J_i} *and the distance between* u_i *and the tagged BS is* D_{J_i}*, then* $0 \leq X_{J_i} \leq \left(\frac{N_J B_J D_{J_i}^{\alpha_K}}{N_K B_K}\right)^{1/\alpha_J}$.

Remark 2.2. *Based on the association rule in the previous section, we define the interference boundary here. For a UE who is associated to* K*th tier and the association distance is* X_K*, the interference boundary* I_{X_J} *for the* J*th tier is given by* $I_{X_J} = D_J > \left(\frac{N_J B_J}{N_K B_K}\right)^{1/\alpha_J} X_K^{\alpha_K/\alpha_J}$.

Thus, both Remark 2.1 and Remark 2.2 define the regions where the interfering UEs can be located and these regions come due to the association rule defined in the previous section.

2.4. SIR and Rate Coverage Probability

2.4.1. SIR Coverage Probability

The UL SIR coverage probability[4] can be defined as the probability that the instantaneous UL SIR at a randomly chosen BS is greater than some predefined threshold. The UL SIR coverage probability $\mathcal{C}$ of our system model can be written as

$$\mathcal{C} = \mathcal{C}_F \mathcal{A}_F + \mathcal{C}_M \mathcal{A}_M, \tag{2.10}$$

where $\mathcal{C}_F$, $\mathcal{C}_M$, $\mathcal{A}_F$, and $\mathcal{A}_M$ are the coverage and association probability of the femto- and macro-tier respectively. The Kth-tier coverage probability $\mathcal{C}_K$ for a target SIR τ_K can be defined as

$$\mathcal{C}_K \triangleq \mathbb{E}_{X_K}\left[\mathbb{P}\left[\mathrm{SIR}_{X_K} > \tau_K\right]\right]. \tag{2.11}$$

In the UL, the interfering UEs do not constitute a homogeneous PPP due to the correlation among the interfering UEs. This correlation is due to the orthogonal channel assignment within a cell and can be better modeled by a soft-core process [62]. However,

[4]We consider an interference-limited network similar to [34] and therefore study the SIR coverage probability instead of the SINR coverage probability.

soft core processes are generally analytically not tractable [5]. Therefore, in most of the UL analysis, the interfering UEs are approximated as a single homogeneous PPP (because in the UL the transmit power of the UEs are the same and the association regions of BSs form a Voronoi tessellation) [24–26, 57]. However, in this system model, it can not be approximated as a single homogeneous PPP due to biasing and different beamforming gain for the femto and macro-tier (the association regions of BSs form a weighted Voronoi tessellation). Therefore, we approximate it as two independent PPPs, i.e., the femto-tier interfering UEs constitute one homogeneous PPP while the macro-tier interfering UEs constitute another homogeneous PPP. However, we do not approximate the interfering UEs as PPPs in the entire 2-D plane but only in the regions defined in Remark 2.1 and 2.2. The constraints of Remark 2.1 and 2.2 are taken into consideration in the rest of the analysis.

The channel $\mathbf{h}_{K_0}$ follows Gamma $(N_K, 1)$, therefore, we need to find the higher order derivative of the Laplace transform of the interference, which is a common problem in MIMO transmission in the PPP network. In the literature, different techniques have been used to simplify the nth derivative of the Laplace transform. A Taylor expansion-based approximation is used in [63] while [64] uses special functions to approximate the nth derivative of the Laplace transform. However, both of these techniques are applicable to ad-hoc networks only. For a cellular network, a recursive-technique is used in [65], but their final expression is still complicated. Hence, we utilize Faà di Bruno's formula [59] to find the nth derivative of the Laplace transform of the interference.

We state the coverage probability of a random user associated to a Kth tier BS in the following theorem.

Theorem 2.1. *The UL coverage probability $\mathcal{C}_K$ of the typical UE when the serving BS is a Kth tier BS and the SIR threshold is τ_K for the system model in Section 2.2 is given by*

$$\mathcal{C}_K(\tau_K) = \frac{2\pi\lambda_K}{\mathcal{A}_K}\int_0^\infty X_K \exp\left\{-\pi\left(\lambda_K X_K^2 + \lambda_J(\zeta)^{2/\alpha_J} X_K^{2(\alpha_K/\alpha_J)}\right)\right\} \sum_{n=0}^{N_K-1}\frac{s^n(-1)^n}{n!}\mathcal{L}_I^n(s)\,\mathrm{d}_{\mathrm{X_K}}, \quad (2.12)$$

where $s = \tau_K X_K^{\alpha_K(1-\eta)}$, $\zeta = \frac{N_J B_J}{N_K B_K}$, $\mathcal{L}_I(s)$ is the Laplace transform of the interference given

$$\mathcal{L}_I(s) = \exp\left(\frac{-2\pi s}{\alpha_K - 2}\left[\lambda_K\int_0^\infty X_{K_i}^{2-\alpha_K(1-\eta)}\,{}_2\mathrm{F}_1\left[1, 1-\frac{2}{\alpha_K}, 2-\frac{2}{\alpha_K}; -sX_{K_i}^{-\alpha_K(1-\eta)}\right]\times f_{X_{K_i}}(X_{K_i})\,\mathrm{d}_{\mathrm{X_{K_i}}} + \lambda_J\zeta^{1-2/\alpha_K}\int_0^\infty X_{J_q}^{2\alpha_J/\alpha_K-\alpha_J(1-\eta)}\times {}_2\mathrm{F}_1\left[1, 1-\frac{2}{\alpha_K}, 2-\frac{2}{\alpha_K}; -s\zeta X_{J_i}^{-\alpha_J(1-\eta)}\right] f_{X_{J_q}}(X_{J_q})\,\mathrm{d}_{\mathrm{X_{J_q}}}\right]\right). \quad (2.13)$$

Both the $f_{X_{K_i}}(X_{K_i})$ and $f_{X_{J_q}}(X_{J_q})$ can be obtained from Lemma 2.4, and the $\mathcal{L}_I^n(s)$

represents the nth derivative of the $\mathcal{L}_I(s)$*. In order to find* $\mathcal{L}_I^n(s)$*, the Faà di Bruno's formula [59] is utilized which can be written as*

$$\mathcal{L}_I^n(s) = \sum \frac{n!}{b_1! b_2! \cdots b_n!} \mathcal{L}_I^k(s) \left(\frac{f'(s)}{1!}\right)^{b_1} \left(\frac{f''(s)}{2!}\right)^{b_2} \cdots \left(\frac{f^n(s)}{n!}\right)^{b_n},$$

where $f(s)$ *is the term inside the exponential of* (2.13) *and the summation is to be performed over all different solutions in non-negative integers* $b_1, \cdots, b_n$ *of* $b_1 + 2b_2 + \cdots + nb_n = n$ *and* $k = b_1 + \cdots + b_n$*.*

Proof. See Appendix A.3. □

It can be noticed that as the number of antennas N_K increases, the summation term becomes larger, and after taking the nth derivative, the expression becomes very lengthy. Hence, numerically computing the coverage probability is computationally very expensive.

2.4.2. Special Cases

The SIR coverage in Theorem 2.1 can be simplified for the following plausible special cases.

Corollary 2.1. *The* K*th tier SIR coverage probability without the UL power control* $(\eta = 0)$ *is given by* (2.12)*, while* $\mathcal{L}_I(s)$ *simplifies to*

$$\mathcal{L}_I(s) = \exp\left(\frac{-2\pi\tau_K}{\alpha_K - 2}\left[\lambda_K s^{2/\alpha_K} {}_2\mathrm{F}_1\left[1, 1 - \frac{2}{\alpha_K}, 2 - \frac{2}{\alpha_K}; -\tau_K\right] + \lambda_J \zeta^{\frac{2-\alpha_K}{\alpha_J}} s^{\frac{2+\alpha_J-\alpha_K}{\alpha_J}} {}_2\mathrm{F}_1\left[1, 1 - \frac{2}{\alpha_K}, 2 - \frac{2}{\alpha_K}; \frac{-\tau_K s^{1-\alpha_K/\alpha_J}}{\zeta^{\alpha_K/\alpha_J}}\right]\right]\right), \quad (2.14)$$

where $s = X_K^{\alpha_K}$ *and the rest of the variables have the predefined meaning.*

The coverage probability can be found by evaluating just a single integral.

Corollary 2.2. *The* $\mathcal{C}_K$ *with full channel inversion* $(\eta = 1)$ *is given by* (2.12)*, while* $\mathcal{L}_I(s)$ *simplifies to*

$$\mathcal{L}_I(s) = \exp\left(\frac{-2\pi s}{\alpha_K - 2}\left[\lambda_K {}_2\mathrm{F}_1\left[1, 1 - \frac{2}{\alpha_K}, 2 - \frac{2}{\alpha_K}; -s\right]\int_0^\infty X_{K_i}^2 f_{X_{K_i}}(X_{K_i})\,\mathrm{d}_{\mathrm{X_{K_i}}} + \lambda_J \zeta^{1-2/\alpha_K} {}_2\mathrm{F}_1\left[1, 1 - \frac{2}{\alpha_K}, 2 - \frac{2}{\alpha_K}; -s\zeta\right]\int_0^\infty X_{J_q}^{2\alpha_J/\alpha_K} f_{X_{J_q}}(X_{J_q})\,\mathrm{d}_{\mathrm{X_{J_q}}}\right]\right), \quad (2.15)$$

where $s = \tau_K$ *while the rest of the parameters remain the same.*

Corollary 2.3. *For* $B_K N_K = B_J N_J$ *and* $\alpha_K = \alpha_J = \alpha$ *the* $\mathcal{C}_K$ *is given by*

$$\mathcal{C}_K(\tau_K) = \frac{2\pi\lambda_K}{\mathcal{A}_K}\int_0^\infty X_K \exp\left\{-\pi\lambda X_K^2\right\} \sum_{n=0}^{N_K-1} \frac{s^n(-1)^n}{n!} \mathcal{L}_I^n(s)\,\mathrm{d}_{\mathrm{X_K}}, \quad (2.16)$$

where $\lambda = \lambda_K + \lambda_J$ *and* $\mathcal{L}_I(s)$ *is given by*

$$\mathcal{L}_I(s) = \exp\left(\frac{-2\pi s\lambda}{\alpha - 2}\int_0^\infty X_i^{2-\alpha(1-\eta)}{}_2\mathrm{F}_1\left[1, 1-\frac{2}{\alpha}, 2-\frac{2}{\alpha}; -sX_i^{-\alpha(1-\eta)}\right] f_{X_i}(X_i)\,\mathrm{d}_{\mathrm{X_i}}\right). \tag{2.17}$$

The coverage probability behaves as if the interference is from a single tier network with density $\lambda = \lambda_K + \lambda_J$.

Corollary 2.4. *For* $N_K = N_J$, $B_K = B_J$, $\alpha_K = \alpha_J = \alpha$, $\tau_K = \tau_J = \tau$ *and* $\lambda_K = \lambda_J = \lambda$ *then the coverage probability is given by*

$$\mathcal{C} = \mathcal{C}_K = \mathcal{C}_J = \frac{2\pi\lambda}{\mathcal{A}}\int_0^\infty X_K \exp\left\{-2\pi\lambda X_K^2\right\}\sum_{n=0}^{N_K-1}\frac{s^n(-1)^n}{n!}\mathcal{L}_I^n(s)\,\mathrm{d}_{\mathrm{X_K}}, \tag{2.18}$$

where $\mathcal{A} = \mathcal{A}_K = \mathcal{A}_J$ *and* $\mathcal{L}_I(s)$ *is*

$$\mathcal{L}_I(s) = \exp\left(\frac{-4\pi s\lambda}{\alpha - 2}\int_0^\infty X_i^{2-\alpha(1-\eta)}{}_2\mathrm{F}_1\left[1, 1-\frac{2}{\alpha}, 2-\frac{2}{\alpha}; -sX_i^{-\alpha(1-\eta)}\right] f_{X_i}(X_i)\,\mathrm{d}_{\mathrm{X_i}}\right). \tag{2.19}$$

The network coverage probability $\mathcal{C}$ becomes equal to the tier coverage probability $\mathcal{C}_K$, $\mathcal{C}_J$.

Corollary 2.5. *For* $\eta = 0$, $B_K N_K = B_J N_J$, $\alpha_K = \alpha_J = \alpha$ *the* $\mathcal{C}_K$ *is given by* (2.16), *while* $\mathcal{L}_I(s)$ *simplifies to*

$$\mathcal{L}_I(s) = \exp\left(\frac{-2\pi\tau_K s^{2/\alpha}\lambda}{\alpha - 2}{}_2\mathrm{F}_1\left[1, 1-\frac{2}{\alpha}, 2-\frac{2}{\alpha}; -\tau_K\right]\right), \tag{2.20}$$

where $s = X_K^\alpha$ *and* $\lambda = \lambda_K + \lambda_J$.

The coverage probability is in the form of single integral and the interference behaves as if it originates from a single tier network.

Corollary 2.6. *For* $\eta = 0$, $N_K = 1$, $\alpha_K = \alpha_J = \alpha$ *the* $\mathcal{C}_K$ *is*

$$\mathcal{C}_K(\tau_K) = \frac{\lambda_k}{\mathcal{A}_K\left[\lambda_K + \lambda_J\zeta^{-2/\alpha} + \frac{2\tau_K}{\alpha-2}\mathrm{G}(\alpha, \tau_K, \zeta, \lambda_K, \lambda_J)\right]}, \tag{2.21}$$

where $\mathrm{G}(\alpha, \tau_K, \zeta, \lambda_K, \lambda_J) = \lambda_K{}_2\mathrm{F}_1\left[1, 1-\frac{2}{\alpha}, 2-\frac{2}{\alpha}; -\tau_K\right] + \lambda_J\zeta^{2/\alpha-1}$ ${}_2\mathrm{F}_1\left[1, 1-\frac{2}{\alpha}, 2-\frac{2}{\alpha}; -\frac{\tau_K}{\zeta}\right]$, *and* $\zeta = \frac{B_K}{N_J B_J}$.

The coverage probability reduces to a closed form.

Corollary 2.7. *For* $\eta = 0$, $N_K = N_J = 1$ $B_K = B_J = 1$, $\alpha_K = \alpha_J = \alpha$ *the the* $\mathcal{C}_K$ *can*

further be simplified to

$$\mathcal{C}_K(\tau_K) = \frac{1}{1 + \frac{2\tau_K}{\alpha-2}{}_2\mathrm{F}_1\left[1, 1-\frac{2}{\alpha}, 2-\frac{2}{\alpha}; -\tau_K\right]}. \tag{2.22}$$

The coverage probability becomes density invariant. Similar observation has been made in [37, 57].

2.4.3. Rate Coverage Probability

In this subsection, we find the rate coverage probability of the network, which is the probability that a randomly chosen user can achieve a target rate, or the average fraction of users that achieve the target rate. The rate coverage probability of the network can be written as

$$\mathcal{R} = \mathcal{A}_F\mathcal{R}_F + \mathcal{A}_M\mathcal{R}_M, \tag{2.23}$$

where $\mathcal{R}_F$ and $\mathcal{R}_M$ are the rate coverage probabilities, and $\mathcal{A}_F$ and $\mathcal{A}_M$ are the association probabilities of the femto- and macro-tier respectively. The rate coverage $\mathcal{R}_K$ of the Kth tier when the rate threshold is ρ_K can be written as

$$\mathcal{R}_K \triangleq \mathbb{P}\left[\frac{W}{\Omega_K}\log_2\left(1+\mathrm{SIR}_K\right) > \rho_K\right], \tag{2.24}$$

where W is the frequency resources and Ω_K is the load on a Kth-tier BS. The rate distribution captures the effect of both SIR and load, which in turn depends on the corresponding association area. The distribution of the association area is complex and not known. However, by using the association area approximation in [66], the probability mass function of the load is given by

$$\mathbb{P}\left(\Omega_K = n\right) = \frac{3.5^{3.5}}{(n-1)!}\frac{\Gamma\left(n+3.5\right)}{\Gamma\left(3.5\right)}\left(\frac{\lambda_U\mathcal{A}_K}{\lambda_K}\right)^{n-1}\left(3.5+\frac{\lambda_U\mathcal{A}_K}{\lambda_K}\right)^{-(n+3.5)}, n \geq 1, \tag{2.25}$$

where $\Gamma(t) = \int_0^\infty x^{t-1}\exp(-x)\,\mathrm{dx}$ is a gamma function.

We state the rate coverage probability $\mathcal{R}_K$ in the following Theorem.

Theorem 2.2. *The $\mathcal{R}_K$ when the rate threshold is ρ_K for the system model under consideration is given by*

$$\mathcal{R}_K(\rho_K) = \sum_{n\geq 1}\frac{3.5^{3.5}}{(n-1)!}\frac{\Gamma\left(n+3.5\right)}{\Gamma\left(3.5\right)}\left(\frac{\lambda_U\mathcal{A}_K}{\lambda_K}\right)^{n-1} \times \left(3.5+\frac{\lambda_U\mathcal{A}_K}{\lambda_K}\right)^{-(n+3.5)}\mathcal{C}_K\left(2^{\rho_K n/W}-1\right), \tag{2.26}$$

where $\mathcal{C}_K$ is given by (2.12).

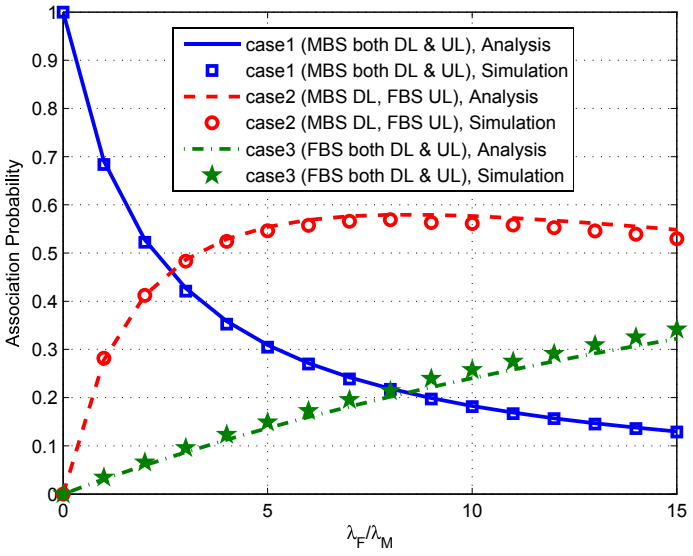

Figure 2.2.: UL Association probabilities vs. λ_F/λ_M, $(\alpha = 4, N_M = 5, N_F = 1, B = 1)$.

Proof. The rate coverage probability of the Kth tier for threshold ρ_K can be written as

$$\mathcal{R}_K(\rho_K) = \mathbb{P}\left[\frac{W}{\Omega_K}\log_2(1+\mathrm{SIR}_K) > \rho_K\right] \quad = \mathbb{P}\left[\mathrm{SIR}_K > 2^{\rho_K\Omega_K/W} - 1\right]. \tag{2.27}$$

By the definition of the SIR coverage probability, the above expression becomes

$$\mathcal{R}_K(\rho_K) = \mathbb{E}_{\Omega_K}\left[\mathcal{C}_K\left(2^{\rho_K\Omega_K/W} - 1\right)\right] \quad = \sum_{n\geq 1}\mathbb{P}(\Omega_K = n)\,\mathcal{C}_K\left(2^{\rho_K n/W} - 1\right). \tag{2.28}$$

By inserting (2.25) in the above expression, we obtain (2.26). □

The rate coverage probability expression in (2.26) can be further simplified by using the mean load approximation used in [66]. The mean load is given by

$$\bar{\Omega}_K = \mathbb{E}[\Omega_K] = 1 + \frac{1.28\lambda_U\mathcal{A}_K}{\lambda_K}, \tag{2.29}$$

where $K \in \{M, F\}$. By using the mean load $\bar{\Omega}_K$ the summation over n is removed from (2.26).

2.5. Results and Discussion

First, we discuss the accuracy of our analysis and system model. The MBSs, FBSs and UEs are deployed according to the system model. We fix the $P_M = 43$ dBm, $P_F = 20$ dBm, $P_0 = -100$ dBm/Hz, and $W = 10$ MHz. All the densities, $(\lambda_M, \lambda_F$ and $\lambda_U)$, are per square kilometers /Km^2. We consider the same SIR thresholds $(\tau = \tau_M = \tau_F)$, rate thresholds $(\rho = \rho_M = \rho_F)$ and path-loss exponents $(\alpha = \alpha_M = \alpha_F)$ for both tiers.

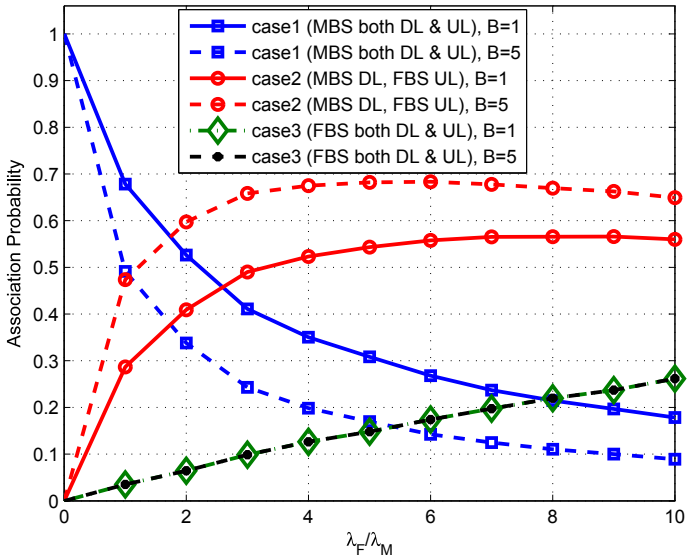

Figure 2.3.: Effect of biasing on the UL association probabilities, ($\alpha = 4, N_M = 5, N_F = 1, B = 5$).

Fig. 2.2 shows the association probabilities of UEs to different cases (mentioned in Section 2.2) versus ratio of λ_F and λ_M, (λ_F/λ_M), for the given parameters. The solid lines show analytical results, derived using (2.4), (2.5), and (2.6) while marked points are obtained using Monte Carlo simulations. It can be noticed that as the density of the FBS, λ_F, increases, the number of UEs in $case2$ and $case3$ also increases, whereas the number of UEs in $case1$ decreases. It can be further noticed that initially the association probability of $case2$ increases very rapidly and reaches a maximum value, $(\lambda_F/\lambda_M = 7)$, and then starts decreasing since a larger number of UEs become attached to FBSs both in the DL and UL. The figure provides an estimate of the load in different tiers for design engineers. We can observe that at $\lambda_F/\lambda_M = 5$, 30% of the UEs are attached to the macro-tier ($case1$) while 70% of UEs are attached to the femto-tier ($case2$+$case3$), but if we increase $N_M = 25$ and keep the rest of the parameters the same then 50% of the UEs will be attached to the macro-tier and 50% to the femto-tier (using (2.7)). This shows that even when using DUDe and a higher density for the femto-tier, we still need to balance the load between the tiers. Therefore, we use biasing to balance the load and Fig. 2.3 shows the effect of biasing on different UEs' type.

Fig. 2.3 depicts the effect of biasing on association probabilities. It can easily be noticed that by using $B = 5$ the association probability of $case2$ increases while the association probability of $case1$ decreases. When $B > 1$ it offloads the boundary UEs of the macro-tier and these UEs become attached to femto-tier. Similarly, when $B < 1$ the boundary UEs of the femto-tier are offloaded to the macro-tier, whereas $B = 1$ means no biasing. By changing B, we can balance the load among two tiers for optimal performance.

Fig. 2.4 compares the SIR coverage probability obtained through simulations and anal-

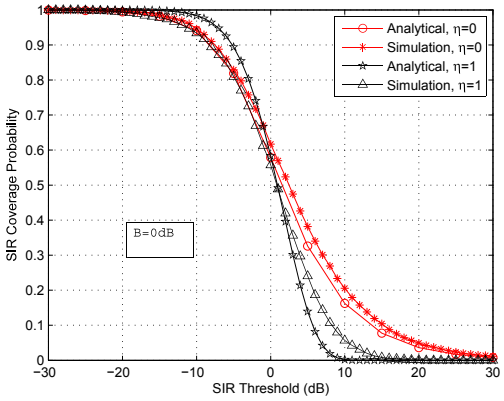

(a) $\lambda_M = 3, \lambda_F = 10, N_M = 4, N_F = 2, \alpha = 3$

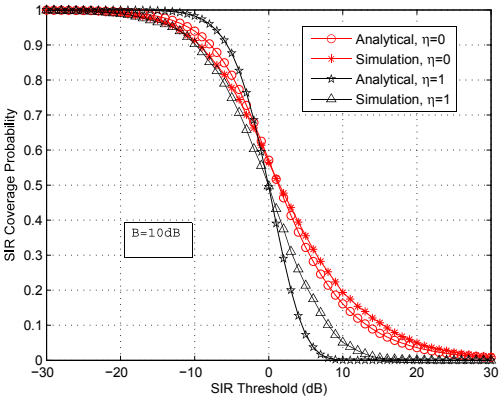

(b) $\lambda_M = 3, \lambda_F = 10, N_M = 4, N_F = 2, \alpha = 3$

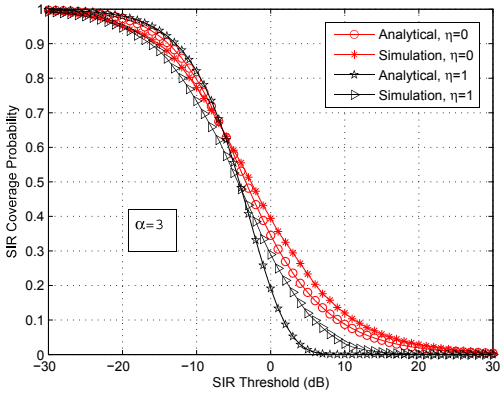

(c) $\lambda_M = 1, \lambda_F = 4, N_M = N_F = 1, B = 10\text{dB}$

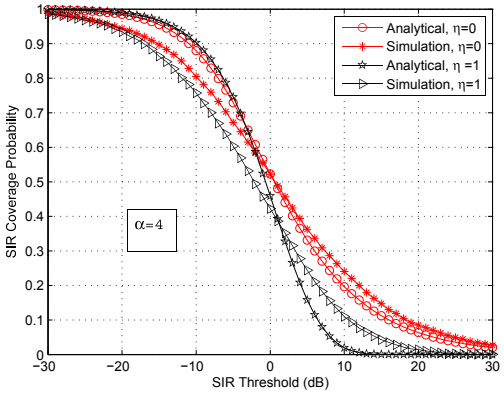

(d) $\lambda_M = 1, \lambda_F = 4, N_M = N_F = 1, B = 10\text{dB}$

Figure 2.4.: Comparison of the SIR coverage probability obtained through simulations and analysis.

ysis for various network parameters. It can be noticed that the analysis and simulations curves are close to each other, which shows that the independent homogeneous PPPs approximation of the interfering UEs is reasonably accurate. The gap between the simulation and the numerical curve is due to the homogeneous PPP approximation of the interfering UEs. There is some correlation among the interfering UEs as discussed in Section 2.4. However, it is quite challenging to model this correlation. Therefore, in most of the UL analysis this correlation is ignored [24,56–58]. The rest of the results in the current chapter are obtained through Monte Carlo simulations unless stated otherwise.

Fig. 2.5 shows the effect of η on the SIR coverage probability when the cell association is based on the maximum downlink received power and when it is based on DUDe. It can be observed that power control affects the cell-centered (corresponds to large SIR threshold) and cell-edged (corresponds to small SIR threshold) UEs differently, i.e., the centered UEs coverage decreases with power control, whereas the cell-edged UEs coverage increases with the middle value of $\eta = 0.5$ and with full channel inversion ($\eta = 1$) it decreases. With $\eta = 1$ the interference power becomes significant and hence decreases the overall coverage, therefore, η should be optimized accordingly. Furthermore, comparing Fig. 2.5a and Fig. 2.5b reveals that the effect of power control is more prominent when the association scheme is No-DUDe. This is due to the large cell size of the MBSs in the No-DUDe association as compared to the cell size of the MBSs in the DUDe association.

Fig. 2.6 shows how the gain provided by the DUDe association over No-DUDe association in term of SIR coverage probability changes with the beamforming gain of both tiers. It is important to mention that the UL coverage probability of the network when the association is based on maximum DL received power averaged over fading can be derived by similar tools and methods used in this chapter. It is clear from the figure that the gain of DUDe association over No-DUDe is maximum when both tiers have the same beamforming gain, and decreases otherwise. When N_M is large compared to N_F, the beamforming gain provided by a MBS increases, which enlarges the association region of a MBS. As a result of which UEs closer to the FBSs become associated with MBSs. These boundary UEs, which are connected to the macro-tier, create strong interference at nearby FBSs when they transmit to their serving MBSs. Whereas, when both tiers have the same beamforming gain, the coverage region of both tiers are the same and the interference created by the boundary UEs is not that strong. Thus, the DUDe gain over No-DUDe is high when both tiers have the same beamforming. In other words, we can say that as the difference in beamforming gain of both tiers increases, the gain provided by the DUDe over No-DUDe decreases. Fig. 2.7 shows the same effect when UL power control is not utilized.

Fig. 2.8 shows the effect of the number of MBS's antennas and biasing on rate coverage probability. For no biasing case $B = 1$, increasing N_M from 1 to 20 decreases the rate coverage. To explain this effect, we know that the rate coverage depends on the load on a BS (2.24). When N_M is high, the coverage region of the macro-tier increases and most of the UEs become attached to MBSs due to which, the macro-tier is overloaded. Thus

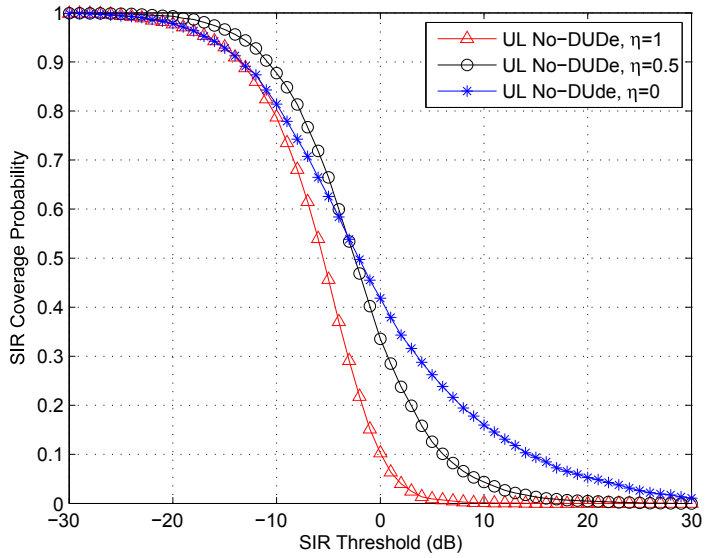

(a) No-DUDe

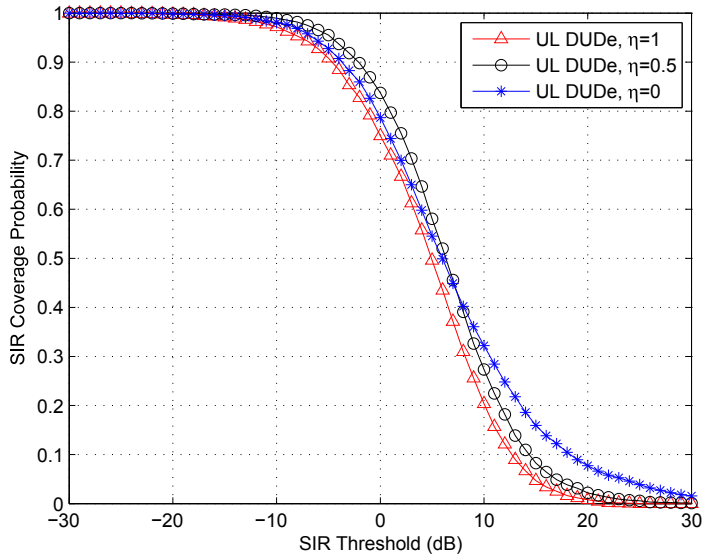

(b) DUDe

Figure 2.5.: Effect of Power Control fraction η on the SIR coverage Probability, ($\lambda_M = 2, \lambda_F = 12, \alpha = 3, N_M = 12, N_F = 4$, and $B = 1$).

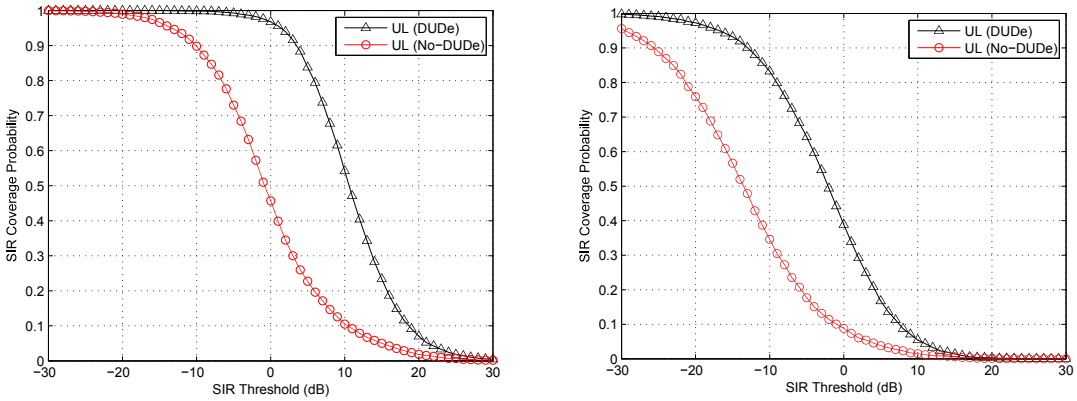

(a) $N_M = 12, N_F = 12$

(b) $N_M = 1, N_F = 1$

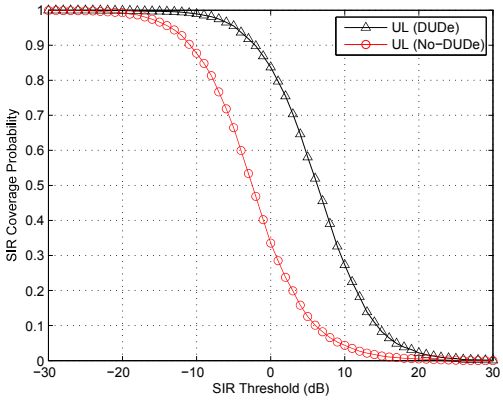

(c) $N_M = 12, N_F = 4$

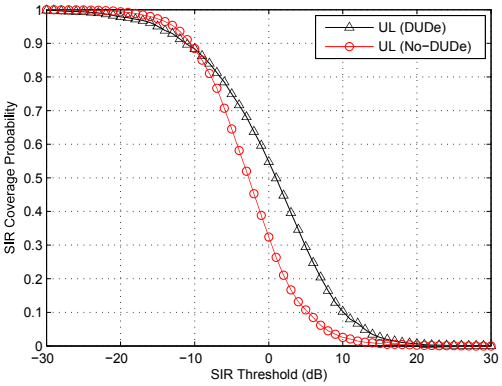

(d) $N_M = 12, N_F = 1$

Figure 2.6.: Beamforming gain effect on the DUDe gain in terms of the SIR coverage probability with power control, $(\eta = 0.5, \lambda_M = 2, \lambda_F = 12, \alpha = 3, B = 1)$.

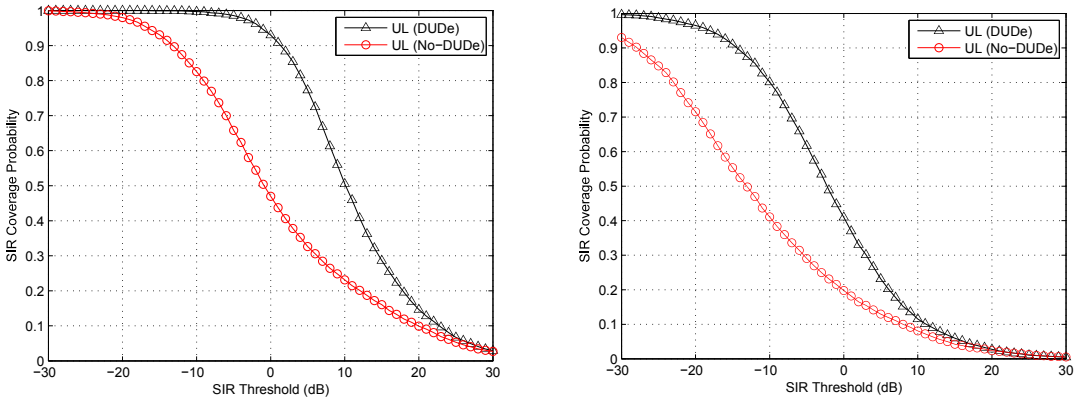

(a) $N_M = 12, N_F = 12$

(b) $N_M = 1, N_F = 1$

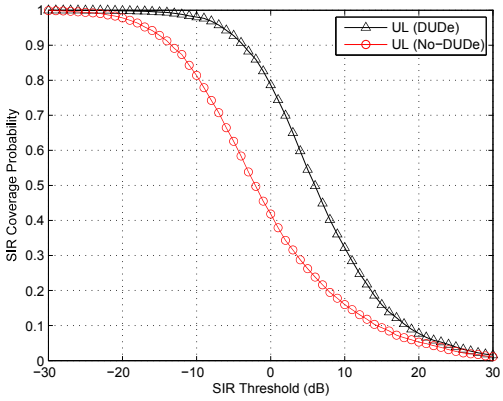

(c) $N_M = 12, N_F = 4$

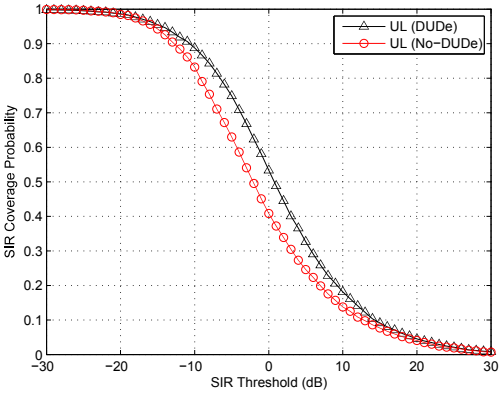

(d) $N_M = 12, N_F = 1$

Figure 2.7.: Beamforming gain effect on the DUDe gain in terms of the SIR coverage probability without power control, $(\eta = 0, \lambda_M = 2, \lambda_F = 12, \alpha = 3, B = 1)$.

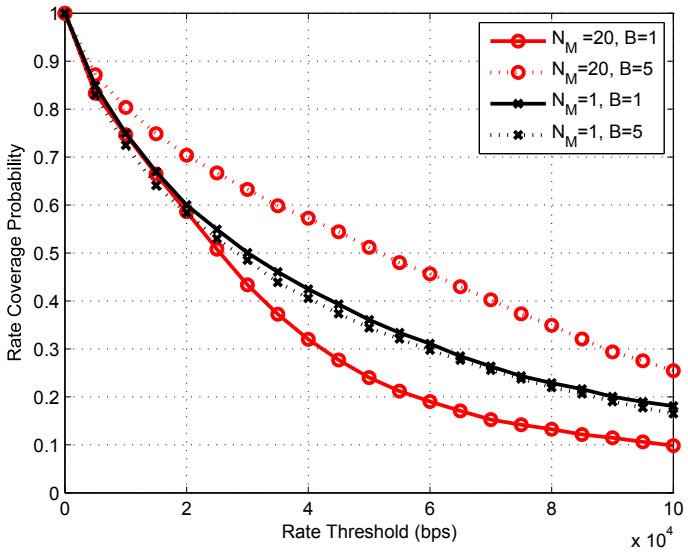

Figure 2.8.: Effect of number of MBS antennas and biasing on the rate coverage probability, $(\lambda_M = 3, \lambda_F = 18, \lambda_u = 3000, \alpha = 3, \eta = 1)$.

the overall rate coverage probability drops. Further, we can see from the figure that when $N_M = 1$, no-biasing gives us the maximum rate coverage, which is in accordance with the result of [27]. However, for higher N_M we see that biasing improves the rate coverage. From the network design perspective, we see that increasing N_M can degrade the rate coverage, therefore, to benefit from a large number of MBSs' antennas we need a suitable biasing towards the femto-tier.

Fig. 2.9 illustrates the effect of FBSs' density and path-loss exponent α on the rate coverage probability for the association scheme of DUDe and No-DUDe. It can be observed that changing α from 3 to 4 increases the rate coverage probability for both DUDe and No-DUDe, which comes from the decrease in the interference power. It can be further observed that an increase in λ_F increases the rate coverage for the DUDe case. This improvement in the rate coverage comes from the inherent property of the DUDe to better handle interference. On the other hand, for the No-DUDe association scheme, increasing λ_F slightly improves the rate coverage for centered UEs (large rate threshold) while decreases the rate coverage of cell-edged UEs (small rate threshold). When λ_F increases then the load on BS decreases due to which, the rate coverage improves for the cell-centered users. However, with the increase in λ_F, the cell size of a BS decreases and by using channel inversion the cell-edged UEs transmit power also reduces, thus the coverage of cell-edge UEs reduces.

2.5.1. Optimal bias and optimal power control fraction

Fig. 2.10 shows the effect of biasing on SIR coverage probability for $\eta = 0$ and $\eta = 1$. For $\eta = 0$ the optimal coverage probability is given by no biasing i.e., $B = \frac{B_F}{B_M} = 1$ or

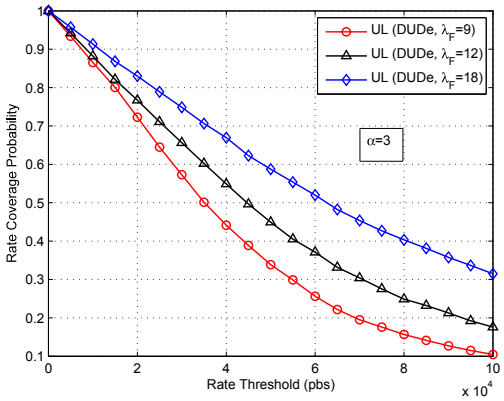

(a) $\alpha = 3$

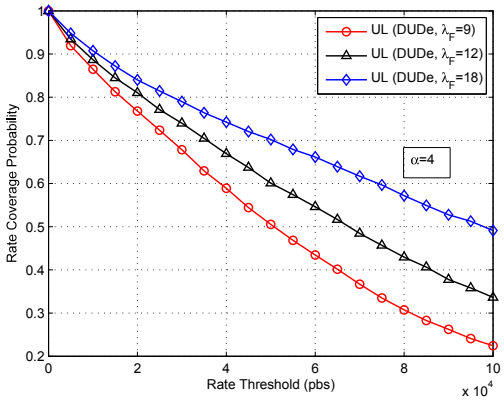

(b) $\alpha = 4$

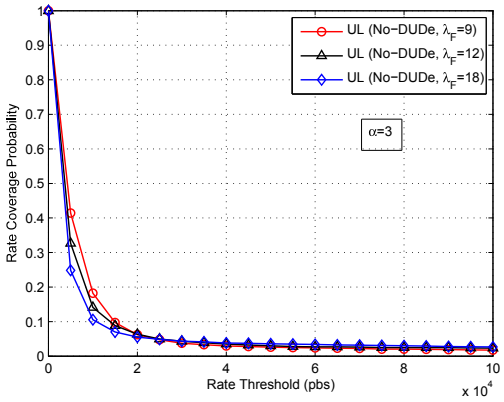

(c) $\alpha = 3$

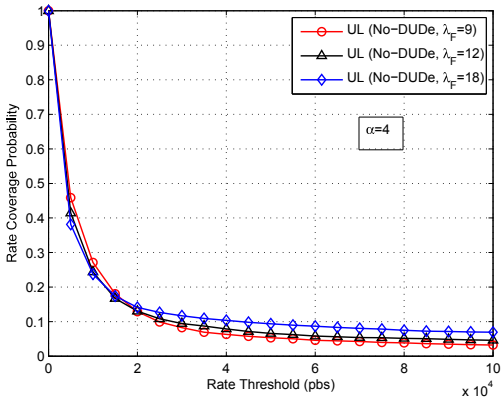

(d) $\alpha = 4$

Figure 2.9.: Effect of λ_F and α on the rate coverage probability for the DUDe and No-DUDe association ($\eta = 1, \lambda_M = 3, N_M = 6, N_F = 2, B = 5, \lambda_U = 3000$).

$B = 0$dB as shown by Fig. 2.10a. The SIR is independent of the load and depends on the density of BSs, path-loss, beamforming gain of the BSs, and the SIR threshold τ, and when $\eta = 0$ then all UEs transmit with the same power. By using biasing we force a UE to associate to a BS to which the UE connection is not strong, and thus the SIR coverage probability reduces. However, from Fig. 2.10b we see that when $\eta = 1$ the optimal SIR is given by $B = 5$dB. With power control, the transmit power of a UE is proportional to its distance from the BS and the transmit power of the cell-edged UEs is greater than the cell-centered UEs. Further, when the beamforming gain N_M of the macro-tier is greater than the femto-tier, cell-edged UEs of macro cells transmit with large power and generate high interference. Therefore, offloading these cell-edged UEs to the femto-tier improves the SIR coverage.

The rate depends on the load and using an appropriate value of biasing can maximize the rate coverage. To find a closed form expression for the optimal bias is beyond the scope of this work. However, the optimal value can be found by a linear search. Fig. 2.11 shows the rate coverage against biasing for different rate thresholds ρ. It is clear from the figure that the maximum rate coverage is given by offloading UEs towards the femto-tier. However, this optimal bias value changes with ρ. When ρ is small (corresponds to cell-edged UEs) we need a small value of B, whereas for large ρ (corresponds to cell-centered UEs) we need more aggressive biasing as shown in Fig. 2.11a and Fig. 2.11b, respectively. One can observe that for $B < 0$ dB the rate coverage is very low. When the beamforming gain of the macro-tier is high, the coverage region is also large as compared to femto-tier and biasing towards macro-tier further increases the coverage region of MBSs (see Fig. 2.3). Due to this enlargement of the coverage region, a large number of UEs becomes attached to the macro-tier and it becomes overloaded, which drops the rate coverage probability. In [27] it is shown that for a SISO network the UL rate coverage is maximized when the association is based on minimum path-loss. However, for MIMO setup this is not the case. Comparing the UL offloading with the DL, one can see that in the DL we need more aggressive offloading of UEs to the small cell, because there is a high disparity in both the transmit powers and beamforming gains of the macro and femto BSs. Whereas, in the uplink the load imbalance is only due to the difference in the beamforming gain of the macro and femto BSs.

Fig. 2.12 shows the rate coverage against η. The power control fraction η affects the cell-edged and cell-centered UEs differently. For the cell-edged UEs the optimal rate coverage is given by the median value of η, as shown in Fig. 2.12a. Whereas for cell-centered UEs the optimal rate coverage is given without uplink power control $\eta = 0$, as shown in Fig. 2.12b. Therefore, based on the target rate threshold, the appropriate value of η can be chosen to optimize the rate coverage.

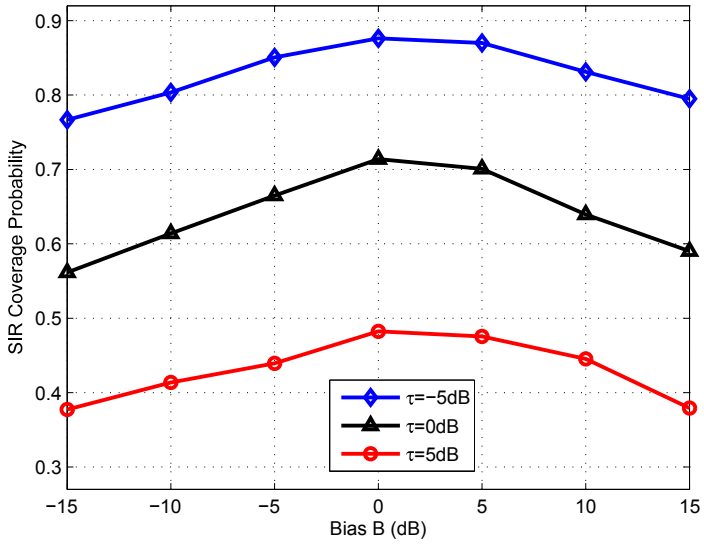

(a) $\eta = 0$

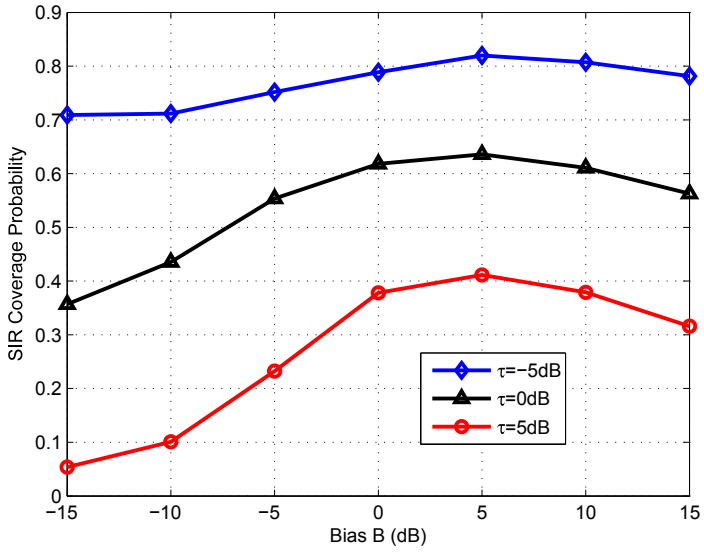

(b) $\eta = 1$

Figure 2.10.: Optimal bias for the SIR coverage probability ($N_M = 20, N_F = 2, \lambda_M = 2, \lambda_F = 10, \lambda_U = 3000, \alpha = 3$).

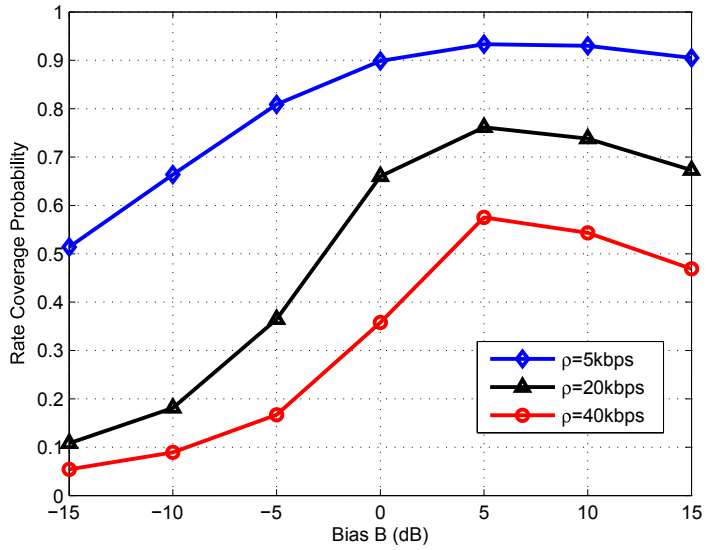

(a)

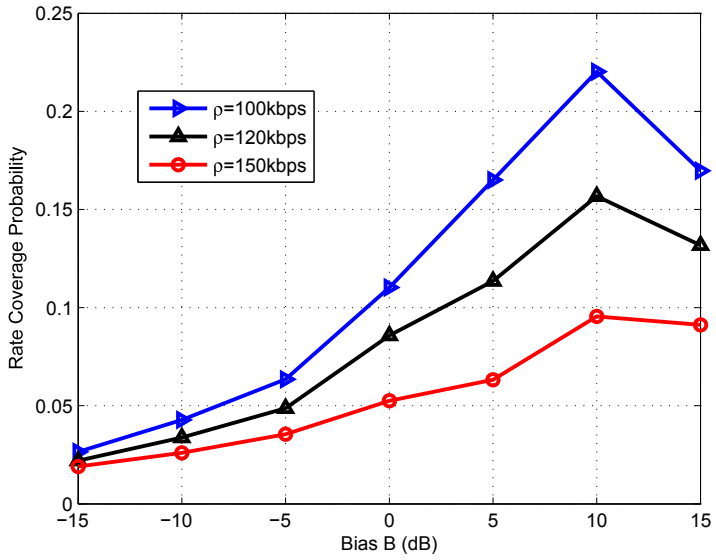

(b)

Figure 2.11.: Optimal bias for the rate coverage probability ($\eta = 1, N_M = 20, N_F = 2, \lambda_M = 2, \lambda_F = 10, \lambda_U = 3000, \alpha = 3$).

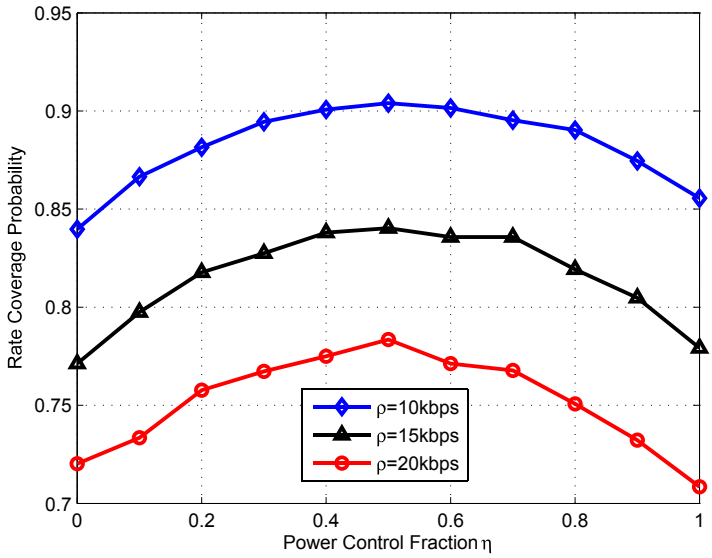

(a)

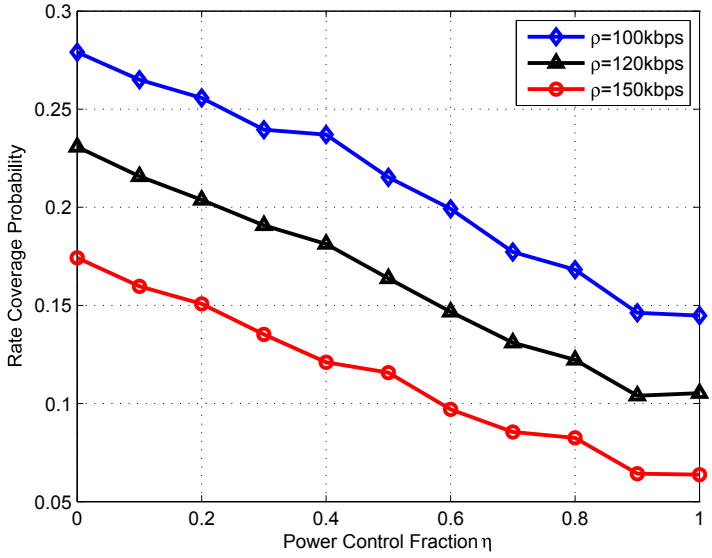

(b)

Figure 2.12.: Optimal η for the rate coverage probability ($N_M = 4, N_F = 2, \lambda_M = 2, \lambda_F = 10, \lambda_U = 3000, \alpha = 3$).

2.6. Chapter Summary

Using tools from stochastic geometry, the UL performance of a two-tier random network is studied, where the cell association is based on DL and UL decoupling. Multiple antennas are considered at BSs, and single antennas are considered at UEs. The position of the MBSs, FBSs, and UEs are modeled using a 2-D PPP. Maximal ratio combining has been used at the BS and tractable analytical expressions have been derived for the rate and SIR coverage probability. It has been shown that the gain (in term of SIR coverage probability) of the decoupled DL and UL association over the coupled DL and UL association is maximum when both tiers have the same number of antennas (same beamforming gain). It has also been observed that in order to leverage the benefits of multiple antennas in a DUDe network, offloading of UEs to the small cell is required.

In the next chapter, we study an ad-hoc network that utilizes a combination of wireless power transfers and backscatter communication. We develop an analytical framework for this ad-hoc network by exploiting the stochastic geometry tools.

3. Backscatter Communications for the Internet of Things

Motivated by the recent advances in the Internet of Things (IoT) and in Wireless Power Transfer (WPT), in this chapter, we study a network architecture that consists of power beacons (PBs) and passive backscatter nodes (BNs). The PBs transmit a sinusoidal continuous wave (CW) and the BNs reflect back a portion of this signal while harvesting the remaining part. A BN harvests energy from multiple nearby PBs and modulates its information bits on the composite CW through backscatter modulation. The analysis of this network architecture poses real challenges due to the double fading channel, and its dependence on the PPPs of both the BNs and PBs. However, with the help of stochastic geometry, we derive the coverage probability and the capacity of the network in tractable and easily computable expressions, which depend on different system parameters. We observe that the coverage probability decreases with an increase in the density of the BNs, while the capacity of the network improves. We further compare the performance of this network with a regular powered network in which the BNs have a reliable power source and show that for a very high density of the PBs, the coverage probability of the former network approaches that of the regular powered network.

3.1. Introduction

The emerging Internet of Things (IoT) is expected to connect billions of small computing devices to the Internet [67]. These tiny devices have processing, sensing and wireless communications capabilities. They are supposed to be deployed everywhere and can be accessed from anywhere at any time. However, powering these small devices is a major challenge (others are interoperability, management, security and privacy) [68,69]. It is very expensive and impractical to replace the batteries of such a massive number of devices or power them with wires. Therefore, harvesting energy from external sources for perpetual operation is a viable option [69]. The advancement in Wireless Power Transfer (WPT) has made it possible to power IoT devices [70].

In the current chapter, we study a random network consisting of passive backscatter nodes (BNs) and power beacons (PBs). The PBs are deployed for WPT and they transmit sinusoidal continuous waves (CW)[1]. The mobile nodes or backscatter nodes (BN), which

[1]Significant enhancements can nevertheless be obtained by proper multisine waveform designs [71, 72].

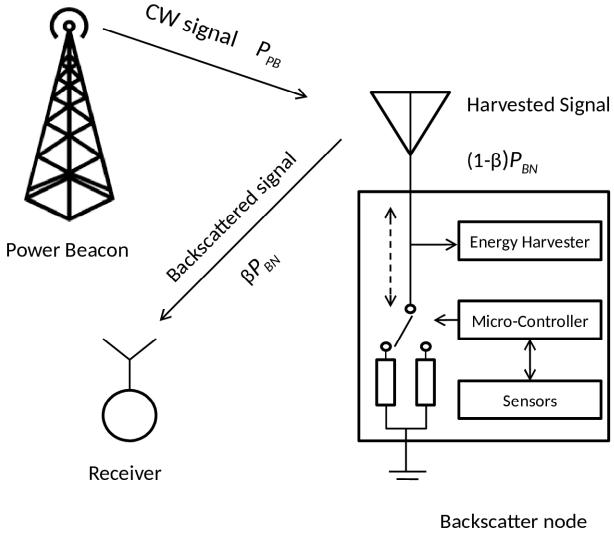

Figure 3.1.: Backscattering communication system.

are in the range of PBs will backscatter a portion of this CW to a nearby receiver by mismatching its antenna impedance, while harvesting the remaining power to operate its integrated circuit [73]. A BN modulates the data onto the backscattered signal by controlling its antenna impedance. A schematic diagram of a backscatter communication system is shown in Fig. 3.1. In contrast to conventional radio architecture relying on power hungry RF chains, the backscatter nodes do not have any active RF components. As a result, the BN has miniature hardware and very low power consumption. For more details on the backscatter operation, readers are referred to [73, 74], and the references therein. The aim of this work is to study the performance of this unique network, where the BNs are powered through wireless power transfer from the PBs. The analysis is performed using tools from the stochastic geometry.

3.1.1. Related Work

Backscatter communication is traditionally used in the Radio Frequency IDentification (RFID) systems, where an RFID-reader reads data from a nearby tag via backscatter modulation [73–75]. Recently, there have been some studies, which used backscatter communication by harvesting energy from ambient sources such as TV and Wi-Fi signals [76–78]. However, this ambient energy harvesting technique cannot be used in the large scale IoT due to a scalability issue [74, 79]. The authors in [80] consider a single cell network in which there is one reader in the center of the cell and the sensors nodes are distributed uniformly within this cell. They studied the decoding probability under different collisions

Table 3.1.: List of Notations for Chapter 3.

Notation	Description
Φ_{PB}, Φ_{BN}, λ_{PB}, λ_{BN}	PPP of the PBs, PPP of the BNs, density of the PBs, density of the BNs
P_{PB}, β, N_{PB}	transmit power of each PB, backscattering efficiency, average number of the PBs in the harvesting region
α^f, α^b	path loss exponent of the forward channel, path-loss exponent of the backward channel
P_{BN}, $\bar{P}_{BN}$	received power at BN, average received power at BN
$d_{i,j}$, $x_{j,k}$	distance between ith receiver and jth BN, distance between jth BN and kth PB
$\mathrm{Ei}(z)$	$\mathrm{Ei}(z)$ is the exponential integral function $\mathrm{Ei}(z) = \int_z^\infty \mathrm{e}^{-t}t^{-1}\mathrm{d}t$
$\mathcal{C}, \mathcal{T}, \mathbb{P}[.], \mathbb{E}_x$	coverage probability, transmission capacity, probability of an event, expectation with respect to x
$\Theta, N, \gamma'_{R_0}, \gamma_{R_0}$	SINR threshold, variance of the noise, SINR at typical receiver R_0, modified SINR at R_0
$h^f_{i,j}$	complex channel gain of the forward channel between the ith BN and jth PB while $\mathbf{h}^f_{i,j} = \left\lvert h^f_{i,j}\right\rvert^2$
$h^b_{j,k}$	complex channel gain of the backward channel between the jth receiver and kth BN while $\mathbf{h}^b_{j,k} = \left\lvert h^b_{j,k}\right\rvert^2$

resolution schemes such as using directional antennas, successive interference cancellation, and ultra-narrow band transmission. They observed that a combination of these techniques gives significant gains. A full-duplex backscatter communication setup is considered in [81] where a multiple access scheme based on a time-hopping spread-spectrum is proposed to reduce the interference. A comparison between multistatic and monostatic radio architecture has been done in [82], where it has been demonstrated that multistatic architecture outperforms the monostatic architecture in term of diversity order, bit error rate, energy outage and coverage.

Most of the above works considered a single-reader single-tag or single-reader multiple-tags, except [79], which considers a wireless powered backscatter communication network in which dense PBs are deployed to wirelessly power BNs. They model the network as a Poisson cluster point process (PCP), where PBs constitute the parent point process and the BNs form daughter point processes. Using tools from stochastic geometry they studied the coverage and network capacity of the network. However, they considered that a BN only harvests energy from a single PB and they also did not consider fading in the forward channel. Moreover, they derived lower bounds on the coverage and capacity of the network.

In the present chapter, we study a more generic and close to practical network setup. In our setup both the PBs and the BNs are distributed according to PPPs and we consider fading in both the forward and backward channel. We also consider that the BNs can harvest and backscatter energy from multiple nearby PBs. Then we utilize tools from

stochastic geometry to study the coverage and capacity of such a network.

3.1.2. Contributions and Outcomes

We develop a comprehensive model for the wireless powered backscatter IoT network in which the locations of PBs and BNs are distributed as independent PPPs. The BNs modulate the information on the unmodulated CW signal from the nearest PBs and reflect a portion of the signal to the receiver. The remaining energy is harvested for the operation of its integrated circuit. We study the coverage and capacity of this network for a typical BN where the capacity is defined as the number of successful transmissions between the BNs and their receivers in per unit area of the network. In a classical downlink cellular network, the coverage (and capacity) depends on a single channel (between a base station and a user equipment) and the density of the BSs, while in the uplink it depends on the channel and the density of the UEs. Furthermore, the BS has a constant transmit power in downlink while the UEs use power control in the uplink. Whereas, in our setup, the coverage probability (and capacity) depends on the double fading channel, the PPP of BNs and the joint probability distribution function (PDF) of the distances of the nearest PBs. In addition, the reflected power of a BN is a random quantity and depends on the forward channel and the PPP of the PBs. Thus all these unique features make the analysis very challenging.

To tackle these challenges, we use a dimensionality reduction technique in which we apply the expectation with respect to the forward channel to both the signal and interference power, before the analysis is carried out. This makes the analysis tractable and we find insightful and adequately accurate expressions for both the coverage and capacity of the network. Our analysis captures the effect of instantaneous energy harvesting from multiple PBs, backscatter modulations of the composite signal and the double fading channel in a single tractable expression. This significantly contrasts with [79] that uses a constant transmit power for the BNs and derives only the lower bound on the coverage probability and capacity of the network.

To get further insight, our coverage probability expression can be simplified into a single integral form when the BN harvests energy from a single nearest PB and the path-loss exponent of both the forward and backward channel is the same. It can be further simplified to a closed form solution when we consider that the BNs reflect the signal with the mean harvested power. We further consider a network scenario in which the BN harvests from all the PBs in the network and backscatters their signal. This case is even more challenging because the coverage probability depends on the PPPs of both PBs and BNs, and the double fading channel; therefore, we only find the approximation for this case. The accuracy of the analysis is verified with extensive Monte Carlo simulations.

Leveraging the above analysis, we are in a position to ask and answer some important and new questions/trade-offs that emerge in the wireless powered backscattered IoT network. Firstly, increasing the density of the PBs improves the harvested and reflected power, but

at the same time it increases the amount of interference. So, how does the coverage of the network vary with the density of the PBs? Secondly, what is the impact of the density of the BNs on the coverage and the capacity of the network? Finally, can the wireless powered backscattered network give the same coverage as of the classical cellular network where BNs are powered with a reliable power source rather than through backscattering? The answers to these questions are outlined below:

- We observe that increasing the density of the PBs increases the coverage probability of the BNs, where the coverage probability is defined as the probability that the instantaneous SINR at the randomly chosen receiver is greater than some predefined SINR threshold. However, when the SINR threshold is high, further increasing the density can decrease the coverage probability. This decrease in the coverage probability at a high SINR threshold is due to the increase in the interference power. The high SINR is achieved only by a very small fraction of the BNs, which are closer to the PBs and an increase in the density of the PBs increases both the signal and interfering power of the BNs. However, the increase in the interference power is more prominent than the increase in the signal power.

- The coverage probability can be considered as the individual link reliability while the capacity is the number of successful transmissions. Increasing the density of the BNs decreases the coverage probability, while it increases the capacity of the network. Therefore, the network provider should take into account the tradeoff between the individual link-reliability and the number of successful transmissions.

- We compare the wireless powered backscatter IoT network with the regular powered network in which the BNs are supplied with a reliable power source having the same transmit power as of the PBs. We observe that the coverage of the wireless powered backscatter network approaches to the coverage of the regular powered network for a very high density of the PBs. We further observe that up to a certain extent, increasing the density of PBs gives rapid increase in the coverage probability. However, beyond a certain density, any further increase in the density of the PBs shows a very small improvement in the coverage probability. This suggests that it may not be cost-effective to keep increasing the density of PBs beyond a certain level.

The rest of the chapter is organized as follows. In Section 3.1, we present our system model and discuss our performance metrics. In Section 3.3, we conduct the analysis and find the coverage and capacity of the network, while in Section 3.4 we present the numerical and simulation results. Finally, the summary of this chapter is provided in Section 3.5.

The key notations used in this chapter are given in Table 3.1.

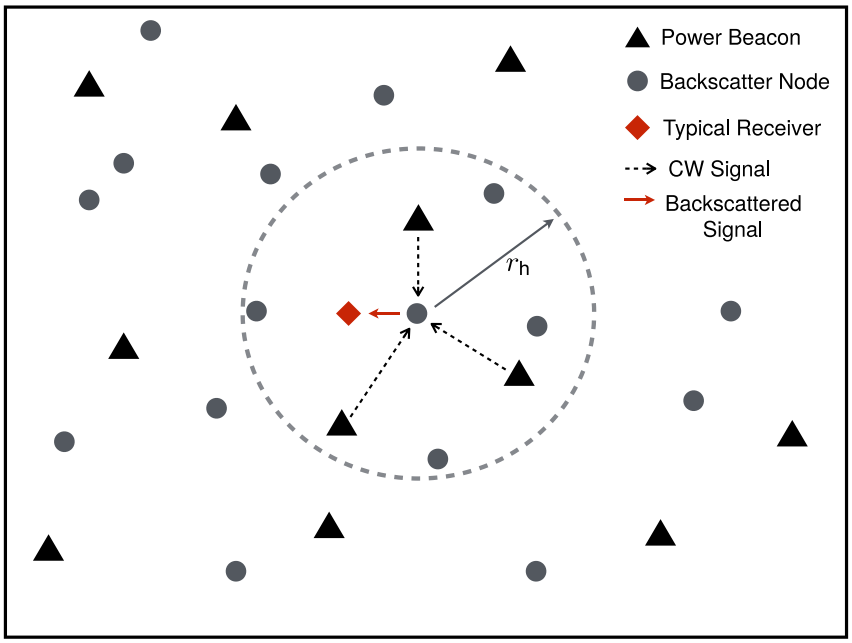

Figure 3.2.: Network model.

3.2. System Model

3.2.1. Network Model

We consider an ad-hoc network consisting of PBs and BNs. The positions of both the PBs and BNs are modeled as independent homogeneous Poisson point processes (PPPs). Let Φ_{PB} and Φ_{BN} be the 2-D PPPs with densities λ_{PB} and λ_{BN} of the PBs and BNs, respectively. The PBs transmit a CW isotropically and all the PBs use the same frequency. A BN harvests some energy from this carrier[2] and modulates its data on the carrier through backscatter modulation [73]. A BN receives a CW signal from multiple PBs and backscatters the signal. This reflected signal from the BN is received by a receiver, which can be located at a fixed distance from this BN in an isotropic direction. The network topology is shown in Fig. 3.2. Without loss of generality, the analysis is performed for a *typical* BN_0, which is transmitting the signal to its dedicated receiver R_0 [7]. In order to make the analysis tractable, we do not consider the circuit-power constraint and assume that the BNs modulate and backscatter the signal all the time. Moreover, we consider that the PBs and the BNs have a single antenna.

We assume that, around each BN, there is a region $z(Y, r_h) \subset \mathbb{R}^2$, which represents a disk of radius r_h centered at $Y \in \Phi_{BN}$. All the PBs inside this region contribute to the received power P_{BN} at the BN. We further assume that the power received from the PBs which are outside the harvesting region is negligible[3]. The number of PBs $\bar{N}_{PB}$ inside $z(Y, r_h)$ is a Poisson random variable with mean $N_{PB} = \pi r_h^2 \lambda_{PB}$. In order to avoid the expectation

[2] through AC-to-DC conversion
[3] later on we relax this condition

with respect to the probability density function (PDF) of the number of PBs $\bar{N}_{PB}$ inside the harvesting region in the analysis, we use the average number of PBs N_{PB} in the rest of this chapter. We adjust r_h such that N_{PB} is an integer number. The received power at BN_0 can be written as

$$P_{BN_0} = \left| \sum_{i=1}^{N_{PB}} \sqrt{P_{PB}} h_{0,i}^{f} x_{0,i}^{-\alpha^f/2} \right|^2, \tag{3.1}$$

where P_{PB} is the transmit power of a PB, $h_{0,i}^{f}$ represents the forward channel gain between BN_0 and its ith nearest PB and $h_{0,i}^{f} \sim \mathrm{CN}(0,1)$, $\alpha^f > 2$ represents the path-loss exponent of the forward channel i.e., between the PBs and BN_0, and $x_{0,i}$ is the distance between BN_0 and its ith nearest PB. The received signal by BN_0 is modulated and reflected to the receiver. The portion of the received power reflected back by BN_0 is modeled with a reflection coefficient $\beta \in [0,1]$, which we call backscattering efficiency. BN_0 reflects βP_{BN_0} amount of power while the remaining power $(1-\beta) P_{BN_0}$ is harvested (as shown in Fig. 3.1) [73, 83]. The harvested power is used by BN_0 to run its integrated circuit (IC).

The joint PDF of the distances from BN_0 to its nearest N_{PB} PBs will be used throughout the chapter, therefore, we present it here

$$f_x(x_{0,1}, \cdots, x_{0,N_{PB}}) = (2\pi\lambda_{PB})^{N_{PB}} \, x_{0,1}, \ldots, x_{0,N_{PB}} \mathrm{e}^{-\pi\lambda_{PB} x_{0,N_{PB}}^2}, \tag{3.2}$$

where $x_{0,1} < x_{0,2} \cdots < x_{0,N_{PB}}$ [84]. The joint PDF of the distances between the non-typical BNs to their nearest N_{PB} PBs is the same as (3.2); however, to make the distinction clear, we represent it by $f_x(x_1, \cdots, x_{N_{PB}})$ throughout the chapter. The SINR γ_{R_0} at a receiver R_0, when the BN_0 transmits under the above system model and in the presence of interference from other active BNs can be written as

$$\gamma'_{R_0} = \frac{\beta \mathbf{h}_{0,0}^{b} d_{0,0}^{-\alpha^b} \left| \sum_{i=1}^{N_{PB}} \sqrt{P_{PB}} h_{0,i}^{f} x_{0,i}^{-\alpha^f/2} \right|^2}{\beta \sum_{j \in \Phi_{BN} \setminus BN_0} \mathbf{h}_{0,j}^{b} d_{0,j}^{-\alpha^b} \left| \sum_{k=1}^{N_{PB}} \sqrt{P_{PB}} h_{j,k}^{f} x_{j,k}^{-\alpha^f/2} \right|^2 + N}, \tag{3.3}$$

where $\mathbf{h}_{i,j}^{b} = \left| h_{i,j}^{b} \right|^2$ is the backward channel gain between the ith receiver and the jth BN and $h_{i,j}^{b} \sim \mathrm{CN}(0,1)$, $h_{m,n}^{f}$ is the forward channel between the mth BN and the nth PB and $h_{m,n}^{f} \sim \mathrm{CN}(0,1)$, $d_{i,j}$ is the distance between the ith receiver and the jth BN, $x_{m,n}$ is the distance between the mth BN and the nth PB, α^b is the path-loss exponent of the backward channel i.e., between the BN and the receiver, and N is the variance of the additive white Gaussian noise (AWGN). In order to avoid the singularity in the forward link (infinite received power at a BN), we use the bounded path-loss model i.e., the path-loss is $\min\left\{1, x_{i,j}^{-\alpha^f}\right\}$ [7]. We assume that the distance between the receiver and the typical BS $d_{0,0}$ is fixed. We consider Rayleigh fading and assume that all channel gains are independent and identically distributed (i.i.d).

3.2.2. Performance Metrics

We consider two metrics to study the performance of this wireless powered backscatter communication network. The first metric is the coverage probability, $\mathcal{C}$, which is the success probability that the receiver R_0 can successfully decode the signal of BN_0. Given a threshold Θ, we defined the coverage probability as

$$\mathcal{C} = \mathbb{P}\left[\gamma'_{R_0} \geq \Theta\right], \tag{3.4}$$

which gives us the percentage of BNs having successful transmission in the network. Our second metric is the transmission capacity, $\mathcal{T}$, defined as

$$\mathcal{T} = \lambda_{BN}\mathcal{C}, \tag{3.5}$$

which is the number of successful transmissions between the BNs and their corresponding receivers per unit area of the network.

3.3. Coverage Probability Analysis

In this section, we find the coverage probability, $\mathcal{C}$, and the capacity, $\mathcal{T}$, of the network. For the coverage probability, we consider two cases. In the first case, we consider that a BN harvests energy from the nearest N_{PB} PBs as mentioned in the previous section, while for the second case, we assume that the BNs harvest energy from all the PBs in the network. The analysis depends on both the PPPs of PBs Φ_{PB} and of the BNs Φ_{BN}, and both the forward channel $\mathbf{h}^f_{i,j}$ and the backward channel $\mathbf{h}^b_{k,i}$. In conventional wireless networks, we do not have this extra tier of PBs, and both the BS and the UE have a reliable power source. The downlink analysis usually depends on the PPP of the BSs and the channel between the UE and the BS, while the uplink analysis depends on the PPP of UEs and the channel. Thus having the additional tier of PBs and the backscatter communications by the BNs make the analysis very challenging. Therefore, in order to make the analysis tractable, we make some assumption as discussed in the sequel. The second case is more complicated than the first one, therefore, we find an approximation for the coverage probability. The details of the derivation are given in the following subsections.

3.3.1. Coverage Probability when a BN harvests energy from N_{PB} nearby PBs

The transmission of a typical BN is successful when the SINR γ'_{R_0} exceeds the threshold Θ. It is very difficult to find the coverage probability of the network due to double fading (forward and backward channel) and its dependence on Φ_{BN} and N_{PB} nearest PBs. Therefore, in order to make the analysis tractable, we use a slightly modified definition of the SINR. The received power at the typical BN $\left|\sum_{i=1}^{N_{PB}} \sqrt{P_{PB}} h^f_{0,i} x_{0,i}^{-\alpha^f/2}\right|^2$ is exponen-

tially distributed with mean $P_{PB}\sum_{i=1}^{N_{PB}} x_{0,i}^{-\alpha^f}$. We replace the harvested power with its mean value in (3.3). The accuracy of this assumption is verified through simulations in the next section. It is important to mention that by doing so, we take the expectation only with respect to the forward channel and not with the location of the N_{PB} PBs. Similar approaches have been used in the literature to reduce the dimensionality of the problem when the analysis is very complicated and leads to intractable results [85–89]. More specifically in [85], and [86], the authors considered an averaging circle around the receiver of interest and modeled the interferers inside this region, while for the interference emanating from outside the region, they used the expected value of it. Similarly, in [87], the authors only considered the effect of two nearest interferers and for the rest of the interference, its average value is considered. We write the modified SINR γ_{R_0} as

$$\gamma_{R_0} = \frac{\mathbf{h}_{0,0}^b d_{0,0}^{-\alpha^b} \sum_{i=1}^{N_{PB}} x_{0,i}^{-\alpha^f}}{\sum_{j\in\Phi_{BN}\setminus BN_0} \mathbf{h}_{0,j}^b d_{0,j}^{-\alpha^b} \sum_{k=1}^{N_{PB}} x_{j,k}^{-\alpha^f} + \frac{N}{\beta P_{PB}}}. \tag{3.6}$$

Before deriving our main result for the coverage probability, we first find the average received power by a random BN in the following lemma.

Lemma 3.1. *The average received power at BN_0 when there are N_{PB} PBs in the harvesting zone is given by*

$$\bar{P}_{BN_0} = P_{PB}\left(2\pi\lambda_{PB}\right)^{N_{PB}} \int\limits_{0<x_{0,1}<x_{0,2}<\cdots<x_{0,N_{PB}}<\infty} \cdots \int x_{0,1},\ldots,x_{0,N_{PB}} \left(\sum_{i=1}^{N_{PB}} x_{0,i}^{-\alpha^f}\right) \mathrm{e}^{-\pi\lambda_{PB}x_{0,N_{PB}}^2} \mathrm{d}x_{0,1},\cdots,\mathrm{d}x_{0,N_{PB}}. \tag{3.7}$$

Proof. The average received power at a BN can be written as

$$\bar{P}_{BN_0} = \mathbb{E}\left[P_{BN_0}\right] = \mathbb{E}_{h_{i,0}^f, x_{0,1},\cdots,x_{0,N_{PB}}}\left[\left|\sum_{i=1}^{N_{PB}} \sqrt{P_{PB}} h_{0,i}^f x_{0,i}^{-\alpha^f/2}\right|^2\right] \overset{a}{=} \mathbb{E}_{x_{0,1},\cdots,x_{0,N_{PB}}}\left[P_{PB}\sum_{i=1}^{N_{PB}} x_{0,i}^{-\alpha^f}\right], \tag{3.8}$$

where (a) follows because $h_{0,i}^f$ is i.i.d distributed $\mathrm{CN}\left(0,1\right)$ and after taking the expectation with respect to $x_{0,1},\cdots,x_{0,N_{PB}}$, we obtained the final result. □

It can be noticed from (3.7) that $\bar{P}_{BN_0}$ increases with an increase in P_{PB}, N_{PB} and λ_{PB}. It is important to remember that on average, a BN harvests $\left(1-\beta\right)\bar{P}_{BN_0}$ while $\beta\bar{P}_{BN_0}$ is reflected back through the backscatter modulation. Moreover, it should be noted that we do not use the dimensionality reduction in the proof of Lemma 3.1 and the expression in (3.7) is exact.

It should be noted that our work significantly differs from [90, 91]. Both [90, 91] consider a cellular network while we consider an ad-hoc setup. In our work, each BN harvests energy from the PBs in its harvesting zone and then backscatters the signal to the receiver, while in [90, 91] multiple BSs cooperatively transmit to a receiver. Moreover, the authors [90, 91] first map the PPPs to a single one-dimensional PPP and then carry out the analysis, while we directly apply the probability generating functional (PGFL) of the 2-D PPP in the proof of Theorem 3.1 and Corollary 3.1. We present the SINR coverage probability in the following theorem.

Theorem 3.1. *The SINR coverage probability $\mathcal{C}$ when the BNs harvests from the nearest N_{PB} PBs is given by*

$$\mathcal{C} = \int_{0<x_{0,1}<x_{0,2}<\cdots<x_{0,N_{PB}}<\infty} \cdots \int \exp(-\frac{sN}{\beta P_{PB}})\mathcal{L}_I(s) f_x(x_{0,1}, \cdots, x_{0,N_{PB}}) \mathrm{d}x_{0,1}, \cdots, \mathrm{d}x_{0,N_{PB}} \tag{3.9}$$

where $s = \frac{\Theta d_{0,0}^{\alpha^f}}{\sum_{i=1}^{N_{PB}} x_{0,i}^{-\alpha^f}}$, $\mathcal{L}_I(s)$ is the Laplace transform of the interference and is given by

$$\mathcal{L}_I(s) = \exp\left(-\frac{2\pi^2 \lambda_{BN} s^{2/\alpha^b}}{\alpha^b \sin\left(\frac{2\pi}{\alpha^b}\right)} \mathbb{E}_{x_1,\cdots,x_{N_{PB}}} \left(\sum_{k=1}^{N_{PB}} x_k^{-\alpha^f}\right)^{2/\alpha^b}\right), \tag{3.10}$$

and $f_x(x_{0,1}, \cdots, x_{0,N_{PB}})$ is the joint PDF of the distances to the N_{PB} nearest PBs and given is in (3.2).

Proof. The proof is provided in Appendix B.1. □

Remark 3.1. *(Effect of β and P_{PB} on the coverage probability) It can be observed from* (3.9) *that the coverage probability $\mathcal{C}$ increases by increasing the backscattering efficiency β or by increasing the transmit power P_{PB} of the PBs.*

We observe that, as the number of PBs N_{PB} in the harvesting region increases, the numerical computation of the coverage probability $\mathcal{C}$ becomes very tedious. This is due to the integration over the joint PDF of the distances to the N_{PB} nearest PBs both in the expression for the $\mathcal{L}_I(s)$ and in the final expression of (3.9). Nonetheless, the coverage probability $\mathcal{C}$ can be simplified for the following plausible special cases.

Corollary 3.1. *When the BN harvests from the single nearest PB ($N_{PB} = 1$) and $\alpha^f = \alpha^b = \alpha$, then the coverage probability simplifies to*

$$\mathcal{C} = 2\pi\lambda_{PB} \int_0^\infty x_{0,1} \exp\left(-\left[\frac{sN}{\beta P_{PB}} + \pi\lambda_{PB} x_{0,1}^2 + \frac{2\pi^2 \lambda_{BN} s^{2/\alpha}}{\alpha \sin\left(\frac{2\pi}{\alpha}\right)} \left[1 - \mathrm{e}^{-\pi\lambda_{PB}} - \pi\lambda_{PB}\mathrm{Ei}\left(-\pi\lambda_{PB}\right)\right]\right]\right) \mathrm{d}x_{0,1}, \tag{3.11}$$

where $s = \Theta d_{0,0}^{\alpha} x_{0,1}^{\alpha}$ *and* $\mathrm{Ei}\,(z) = \int_z^{\infty} \mathrm{e}^{-t} t^{-1} \mathrm{d}t$ *is the exponential integral function [92]. The coverage probability can be computed by evaluating just a single integral.*

Proof. The proof follows similar steps as in the proof of Theorem 3.1. However, to be self-contained, we provide the main steps here. By using the marginal PDF of $x_{0,1}$, we write $\mathcal{C}$ as

$$\mathcal{C} = 2\pi\lambda_{PB} \int_0^{\infty} x_{0,1} \mathbb{P}\left[\gamma_{R_0} \geq \Theta | x_{0,1}\right] \exp\left(-\pi\lambda_{PB} x_{0,1}^2\right) \mathrm{d}x_{0,1}, \tag{3.12}$$

where, by utilizing the definition of γ_{R_0}, the probability $\mathbb{P}\left[\gamma_{R_0} \geq \Theta | x_{0,1}\right]$ can be written as

$$\mathbb{P}\left[\frac{\mathbf{h}_{0,0}^b d_{0,0}^{-\alpha} x_{0,1}^{-\alpha}}{\sum_{j \in \Phi_{BN} \setminus BN_0} \mathbf{h}_{0,j}^b d_{0,j}^{-\alpha} x_{j,1}^{-\alpha} + \frac{N}{\beta P_{PB}}} \geq \Theta\right] = \mathbb{P}\left[\mathbf{h}_{0,0}^b \geq s\left(I + \frac{N}{\beta P_{PB}}\right)\right]$$
$$= \exp(-\frac{sN}{\beta P_{PB}}) \mathcal{L}_I(s), \tag{3.13}$$

with $s = \Theta d_{0,0}^{\alpha} x_{0,1}^{\alpha}$ and $I = \sum_{j \in \Phi_{BN} \setminus BN_0} \mathbf{h}_{0,j}^b d_{0,j}^{-\alpha} x_{j,1}^{-\alpha}$. Now, to find $\mathcal{L}_I(s)$, we apply the same steps as we did to obtain (B.3) in the proof of Theorem 3.1 and we get

$$\mathcal{L}_I(s) = \exp\left(-\frac{2\pi^2 \lambda_{BN} s^{2/\alpha}}{\alpha \sin\left(\frac{2\pi}{\alpha}\right)} \mathbb{E}_{x_1}\left(x_1^{-2}\right)\right)$$
$$= \exp\left(-\frac{2\pi^2 \lambda_{BN} s^{2/\alpha}}{\alpha \sin\left(\frac{2\pi}{\alpha}\right)} \left(2\pi\lambda_{PB} \int_0^1 x_1 \mathrm{e}^{-\pi\lambda_{PB} x_1^2} \mathrm{d}x_1 + 2\pi\lambda_{PB} \int_1^{\infty} x_1^{-1} \mathrm{e}^{-\pi\lambda_{PB} x_1^2} \mathrm{d}x_1\right)\right), \tag{3.14}$$

where the last expression is obtained by utilizing the bounded path-loss model for $\mathbb{E}_{x_1}\left(x_1^{-2}\right)$. In (3.14), the first integral $2\pi\lambda_{PB} \int_0^1 x_1 \mathrm{e}^{-\pi\lambda_{PB} x_1^2} \mathrm{d}x_1 = 1 - \mathrm{e}^{-\pi\lambda_{PB}}$, and the second integral $2\pi\lambda_{PB} \int_1^{\infty} x_1^{-1} \mathrm{e}^{-\pi\lambda_{PB} x_1^2} \mathrm{d}x_1 = -\pi\lambda_{PB} \mathrm{Ei}\,(-\pi\lambda_{PB})$, where $\mathrm{Ei}\,(z)$ is the exponential integral function and $\mathrm{Ei}\,(z) = \int_z^{\infty} \mathrm{e}^{-t} t^{-1} \mathrm{d}t$ [92]. Thus evaluating both integrals in the above expression, inserting (3.14) in (3.13) and then inserting (3.13) back into (3.12), and doing some manipulations, we obtain (3.11). □

Remark 3.2. *(Effect of* λ_{PB} *on the coverage probability) The density of the PBs* λ_{PB} *appears both inside the exponential and outside the exponential in* (3.11)*. We expect that when* Θ *is small then the* λ_{PB} *outside the exponential dominates and as a result the coverage probability increases with an increase in* λ_{PB}*. However, when* Θ *is large enough then the exponential-term dominates due to which the coverage probability decreases with an increase in* λ_{PB}*.*

Remark 3.3. *(Effect of* λ_{BN} *on the coverage probability) The density of the BNs* λ_{BN} *is only inside the exponential in* (3.11)*, which suggests that an increase in* λ_{BN} *always decreases the coverage probability.*

Remark 3.4. *(Effect of* λ_{BN} *on the capacity of the network) The capacity* $\mathcal{T} = \lambda_{BN}\mathcal{C}$*, which shows that the density of BNs* λ_{BN} *is both inside the exponential term (in the ex-*

pression for $\mathcal{C}$) and outside the exponential term. This means that the λ_{BN} outside and inside the exponential affects the capacity $\mathcal{T}$ in a completely different way. We expect that for small Θ it will increase $\mathcal{T}$, whereas for large Θ it will decrease $\mathcal{T}$.

Corollary 3.2. *When $N_{PB} = 1, N = 0$ and $\alpha^f = \alpha^b = \alpha$ then (3.11) can be further simplified to*

$$\mathcal{C} = 2\pi\lambda_{PB}\int_0^\infty x_{0,1}\exp\left(-\left[\pi\lambda_{PB}x_{0,1}^2 + \frac{2\pi^2\lambda_{BN}s^{2/\alpha}}{\alpha\sin\left(\frac{2\pi}{\alpha}\right)}\times \left[1-\mathrm{e}^{-\pi\lambda_{PB}} - \pi\lambda_{PB}\mathrm{Ei}\left(-\pi\lambda_{PB}\right)\right]\right]\right)\mathrm{d}x_{0,1}, \quad (3.15)$$

where $s = \Theta d_{0,0}^{\alpha}x_{0,1}^{\alpha}$. The coverage probability becomes independent of the transmit power P_{PB} of the PB and the backscattering efficiency β.

Corollary 3.3. *When $N = 0$, but the BNs harvest energy from multiple nearby PBs then the coverage probability simplifies to*

$$\mathcal{C} = \int\limits_{0<x_{0,1}<x_{0,2}<\cdots<x_{0,N_{PB}}<\infty}\cdots\int \exp\left(-\frac{2\pi^2\lambda_{BN}s^{2/\alpha^b}}{\alpha^b\sin\left(\frac{2\pi}{\alpha^b}\right)}\mathbb{E}_{x_1,\cdots,x_{N_{PB}}}\left(\sum_{k=1}^{N_{PB}}x_k^{-\alpha^f}\right)^{2/\alpha^b}\right)\times f_x(x_{0,1},\cdots,x_{0,N_{PB}})\mathrm{d}x_{0,1}\cdots\mathrm{d}x_{0,N_{PB}}, \quad (3.16)$$

where $s = \frac{\Theta d_{0,0}^{\alpha^b}}{\sum_{i=1}^{N_{PB}}x_{0,i}^{-\alpha^f}}$ and $\mathcal{C}$ is independent of the transmit power P_{PB} of PBs and the backscattering efficiency β.

Corollary 3.4. *The coverage probability can be further simplified to*

$$\mathcal{C} = \exp\left(-s\left[\frac{N}{\beta\bar{P}_{BN_0}} + \frac{2\pi^2\lambda_{BN}s^{2/\alpha^b-1}}{\alpha^b\sin\left(\frac{2\pi}{\alpha^b}\right)}\right]\right), \quad (3.17)$$

if the BNs reflect the average power $\beta\bar{P}_{BN_0}$ instead of the instantaneous power βP_{BN_0}. The coverage probability is in closed form. The network behaves like a conventional ad-hoc network with BNs having the transmit power $\beta\bar{P}_{BN_0}$ and $s = \Theta d_{0,0}^{\alpha^b}$. Similarly, when $N = 0$ and the BNs reflect the average power $\beta\bar{P}_{BN_0}$, then (3.17) further simplifies to

$$\mathcal{C} = \exp\left(-\frac{2\pi^2\lambda_{BN}\Theta^{2/\alpha^b}d_{0,0}^2}{\alpha^b\sin\left(\frac{2\pi}{\alpha^b}\right)}\right), \quad (3.18)$$

which depends only on the path-loss exponent α^b, density of the BN λ_{BN}, and the distance $d_{0,0}$ between the BN and its receiver. The network acts like a conventional ad-hoc network and the coverage is independent of the transmit power of the BNs.

Proof. We first replace the instantaneous βP_{BN_0} in (3.6) with the average harvested power $\bar{P}_{BN_0}$, and the rest of the proof follows similar steps as in Theorem 3.1. □

3.3.2. Coverage Probability when a BN harvests energy from all PBs

In contrast to the previous subsection, here we assume that a BN harvests energy from all the PBs in the network. We write the received power at the typical BN as

$$P_{BN_0} = \left| \sum_{i \in \Phi_{PB}} \sqrt{P_{PB}} h^f_{0,i} x^{-\alpha^f/2}_{0,i} \right|^2, \tag{3.19}$$

where the summation is over the Φ_{PB}. Similarly, we write the SINR γ'_{R_0} as

$$\gamma'_{R_0} = \frac{\beta \mathbf{h}^b_{0,0} d^{-\alpha^b}_{0,0} \left| \sum_{i \in \Phi_{PB}} \sqrt{P_{PB}} h^f_{0,i} x^{-\alpha^f/2}_{0,i} \right|^2}{\beta \sum_{j \in \Phi_{BN} \setminus BN_0} \mathbf{h}^b_{0,j} d^{-\alpha^b}_{0,j} \left| \sum_{k \in \Phi_{PB}} \sqrt{P_{PB}} h^f_{j,k} x^{-\alpha^f/2}_{j,k} \right|^2 + N}. \tag{3.20}$$

It is more challenging than the previous section to find the coverage probability based on the above SINR expression because it depends on the PPPs of both PBs and BNs, and both the forward and backward channel. Therefore, in order to make the analysis tractable, we make some modifications to the above expression and consider SIR instead of SINR. We write the modified expression for SIR as

$$\gamma_{R_0} = \frac{\mathbf{h}^b_{0,0} d^{-\alpha^b}_{0,0} \sum_{i \in \Phi_{PB}} x^{-\alpha^f}_{0,i}}{\sum_{j \in \Phi_{BN} \setminus BN_0} \mathbf{h}^b_{0,j} d^{-\alpha^b}_{0,j} \sum_{k \in \Phi_{PB}} x^{-\alpha^f}_{j,k}}, \tag{3.21}$$

where we use the average of $\left| \sum_{i \in \Phi_{PB}} \sqrt{P_{PB}} h^f_{0,i} x^{-\alpha^f/2}_{0,i} \right|^2$, which is $P_{PB} \sum_{i \in \Phi_{PB}} x^{-\alpha^f}_{0,i}$ [7]. It is important to mention that in (3.21), we only take the average with respect to the forward channel and not the Φ_{PB}. The coverage probability still depends on the Φ_{PB}, Φ_{BN} and $\mathbf{h}^b_{j,k}$. Similar approaches have been used in [85–89] to reduce the complexity of the problem and to get tractable results.

Before presenting the main result of this section, we first find the average power at a BN in the following lemma.

Lemma 3.2. *The average power at a BN when it harvests from all PBs in the network is given by*

$$\bar{P}_{BN_0} = \frac{P_{PB} \pi \lambda_{PB} \alpha^f}{\alpha^f - 2}. \tag{3.22}$$

It is important to mention that a power $(1-\beta)\,\bar{P}_{BN_0}$ is harvested while the remaining power $\beta \bar{P}_{BN_0}$ is reflected through backscatter modulation. Similar to Lemma 3.1, we do not use the dimensionality reduction in the proof of Lemma 3.2 and the expression in (3.22) is exact.

Proof. The average harvested power $\bar{P}_{BN}$ in this setup can be written as

$$\bar{P}_{BN_0} = \mathbb{E}\left[P_{BN_0}\right] = \mathbb{E}_{h^f_{0,i},\Phi_{PB}}\left[\left|\sum_{i\in\Phi_{PB}} \sqrt{P_{PB}} h^f_{0,i} x_{0,i}^{-\alpha^f/2}\right|^2\right] \overset{a}{=} \mathbb{E}_{\Phi_{PB}}\left[P_{PB}\sum_{i\in\Phi_{PB}} x_{0,i}^{-\alpha^f}\right], \tag{3.23}$$

where a follows because $h^f_{0,i}$ is an i.i.d distributed $\mathrm{CN}(0,1)$ and the final result follows from Campbell's theorem [7]. □

We know that the SIR coverage probability depends on both the Φ_{PB}, Φ_{BN}, and its exact expression cannot be obtained. Therefore, we utilize Jensen's inequality and find the approximated expression for the coverage probability in the following proposition.

Proposition 3.1. *The SIR coverage probability when the BNs harvest energy from all the PBs is approximated by*

$$\mathcal{C} \approx \exp\left(-\frac{2\pi^2\lambda_{BN}\Theta^{2/\alpha^b} d_{0,0}^2}{\alpha^b \sin\left(\frac{2\pi}{\alpha^b}\right)}\right). \tag{3.24}$$

Proof. See Appendix B.2. □

The above expression is the same as of (3.18), which makes sense because (3.18) is the SIR coverage probability when the BNs use the average transmit power and we know that SIR coverage is independent of the transmit power of the BNs.

3.4. Simulation Results and Discussion

In this section, we present numerical results to validate the accuracy of the analysis and the tradeoffs that emerge in this wireless powered backscatter network. The system model of Section 3.2 is carefully reproduced in the Monte Carlo simulations. We fix $P_{PB} = 40$dBm, $\beta = 0.5$, $d_{0,0} = 1$, $N = -40$dB, and $\alpha^f = \alpha^b = \alpha$. Both λ_{PB} and λ_{BN} are in per square meters $\left(/m^2\right)$ and we consider a unit area of $100m^2$ when computing the capacity $\mathcal{T}$ of the network. If we do not mention α and N_{PB} then we keep $\alpha = 4$ and $N_{PB} = 1$, otherwise, we state it.

In Fig. 3.3, we plot the average received power at a BN $\bar{P}_{BN}$ against the density of the PBs λ_{PB}. It can be seen that the numerical results obtained through Lemma 3.1 and 3.2 exactly match with the simulations results. It can be observed that $\bar{P}_{BN}$ is greater for a small path-loss exponent i.e., $\alpha = 3$. Furthermore, it can be noticed that $\bar{P}_{BN}$ increases with an increase in λ_{PB} for both Fig. 3.3a and Fig. 3.3b. However, for Lemma 3.1 in Fig. 3.3a, it saturates to 10W (40dBm) for $\lambda_{PB} = 1$, which is the transmit power P_{PB} of a PB. This implies that when $\lambda_{PB} = 1$, $N_{PB} = 1$ and the path-loss model is $\min\{1, x^{-\alpha}\}$, the received power is on average equal to the transmit power of a PB. Whereas, in Lemma 3.2

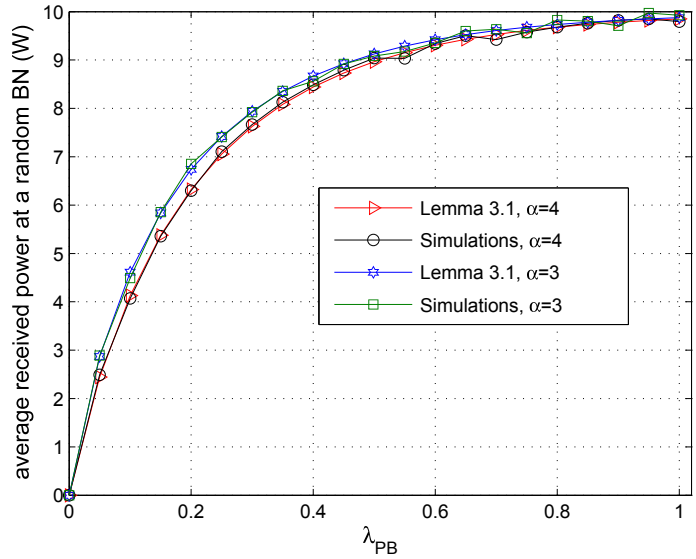

(a) Lemma 3.1 (harvesting energy from the nearest PB)

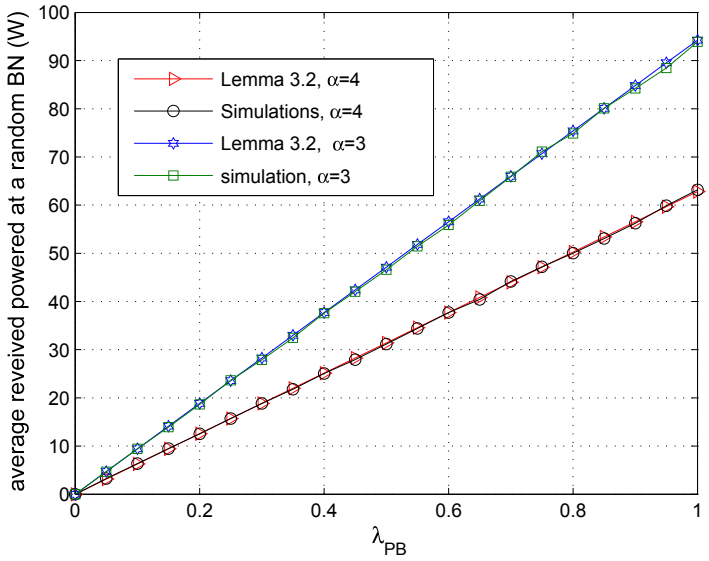

(b) Lemma 3.2 (harvesting energy from the whole network)

Figure 3.3.: Simulations vs analysis (Lemma 3.1 and 3.2).

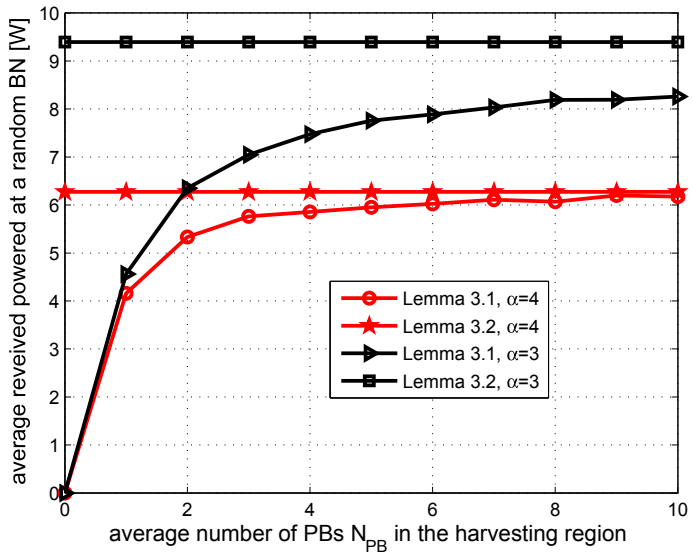

Figure 3.4.: Impact of the number of PBs N_{PB} in the harvesting zone on the $\bar{P}_{BN}$, ($\lambda_{PB} = 0.1$).

the BNs harvest power from all the PBs, therefore, in Fig. 3.3b the $\bar{P}_{BN}$ does not saturate and keep increasing with λ_{PB}.

Fig. 3.4 illustrates the impact of the number of PBs N_{PB} in the harvesting zone on the average received power $\bar{P}_{BN}$. It can be noticed that, for Lemma 3.1, the average received power $\bar{P}_{BN}$ increases with an increase in N_{PB}, whereas, for Lemma 3.2, the $\bar{P}_{BN}$ is constant because the harvesting zone is the whole network in Lemma 3.2. The important observation is that most of the power is harvested from the nearest PBs especially for $\alpha = 4$. In the case of $\alpha = 4$, the contribution from the far away PBs is very small, therefore, $\bar{P}_{BN}$ quickly converges to the maximum value. On the other hand, for $\alpha = 3$, the contribution from those far away nodes is still significant and therefore convergence is not achieved.

In Fig. 3.5, we compare the Monte Carlo simulations results with the numerical results for various network parameters. It can be noticed that the numerical and simulations curves are matching well for both Theorem 3.1 and Corollary 3.4, which shows the accuracy of the analysis. It is important to remember that, in the proof of Theorem 3.1, we used a simplified expression for the SINR in order to make the analysis tractable. Similarly, in Corollary 3.4, we defined the averaged received power $\bar{P}_{BN}$ as the harvested power at BN.

Similar to Fig. 3.5, we compare the numerical and simulation results in Fig. 3.6 for Proposition 3.1. It can be noticed that there are two different curves for the simulations. The first one is obtained when the BNs utilize the average harvested power (given in Lemma 3.2), while the second is obtained when the BNs utilize the instantaneous harvested power. It can be noticed that the numerical curve is very close to the simulations' curve, which is obtained when the BNs transmit with the average harvested power. Whereas, the second simulations curve provides the lower bound. This illustrates that the random transmit

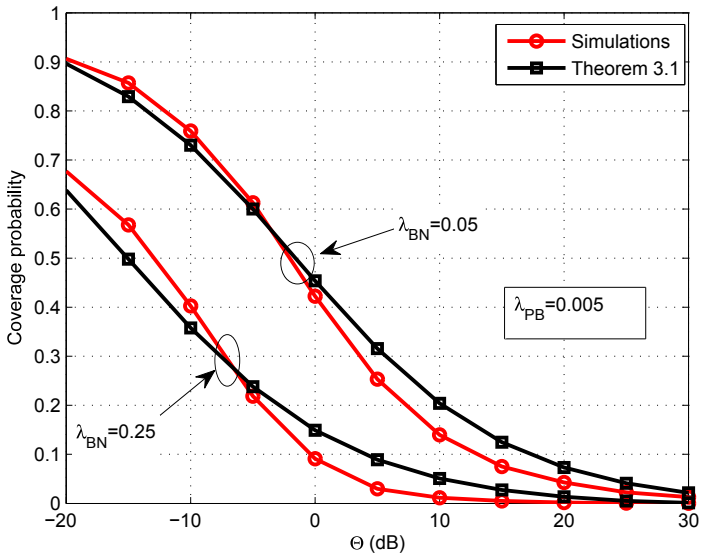

(a) Theorem 3.1

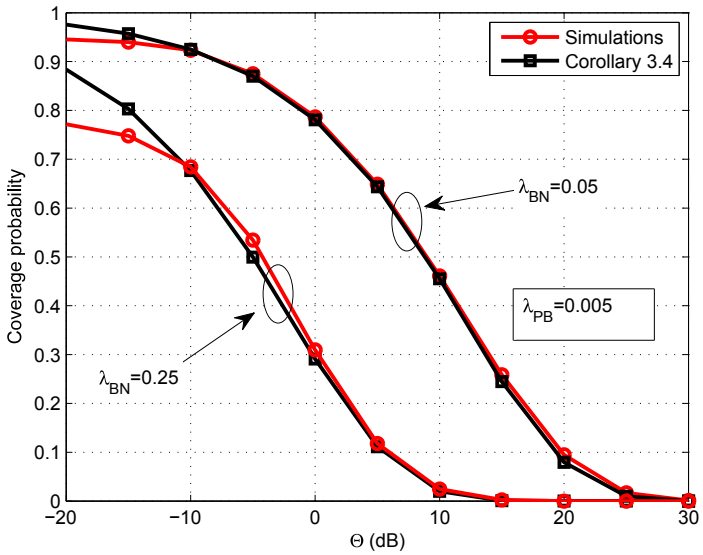

(b) Corollary 3.4

Figure 3.5.: Simulations versus analysis (Theorem 3.1 and Corollary 3.4).

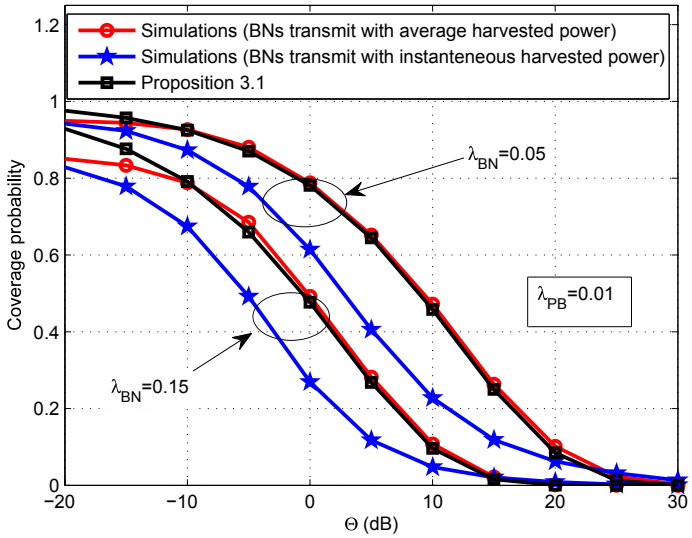

Figure 3.6.: Simulations vs analysis (Proposition 3.1).

power of the BNs degrades the coverage probability of the network. The rest of the results in the current chapter are obtained numerically.

Fig. 3.7 shows the impact of the density of the PBs on the coverage probability for different SINR thresholds. It can be noticed from Fig. 3.7a that the coverage probability increases with an increase in density of the PBs for different values of λ_{BN}. This improvement in the coverage probability is due to the increase in the received (and reflected) power at the BNs as a result of the dense deployment of the PBs. However, for a large Θ, the dense deployment of PBs can reduce the SINR coverage probability, as shown in Fig. 3.7b. From Fig. 3.7b, we observe that the coverage probability reaches a maximum point and then starts decreasing with the increase in λ_{PB}. This decrease in the coverage probability at higher SINR thresholds is due to the increase in the interference power. The high SINR is achieved only by a very small fraction of the BNs, which are very close to the PBs. The distance between the PBs and BNs decreases with an increase in λ_{PB}, which improves the harvested and reflected power of the BNs. As a result the interference power also increases and the coverage probability drops. This confirms our earlier observation in Remark 3.2 and suggests that in order to achieve the optimal coverage, the density of the PBs should be adjusted by taking Θ into account.

Fig. 3.8 depicts the impact of the density of the BNs on the coverage probability and capacity of the network. It can be observed from both Fig. 3.8a and Fig. 3.8c that an increase in the density of the BNs decreases the coverage probability, which is due to the increase in the number of interferers. However, a more appropriate metric in this scenario might be the capacity of network, which is the number of successful transmissions in some unit area. Therefore, we plot the capacity corresponding to Fig. 3.8a and Fig. 3.8c in Fig. 3.8b and Fig. 3.8d, respectively. In contrast to the coverage probability, both Fig. 3.8b and

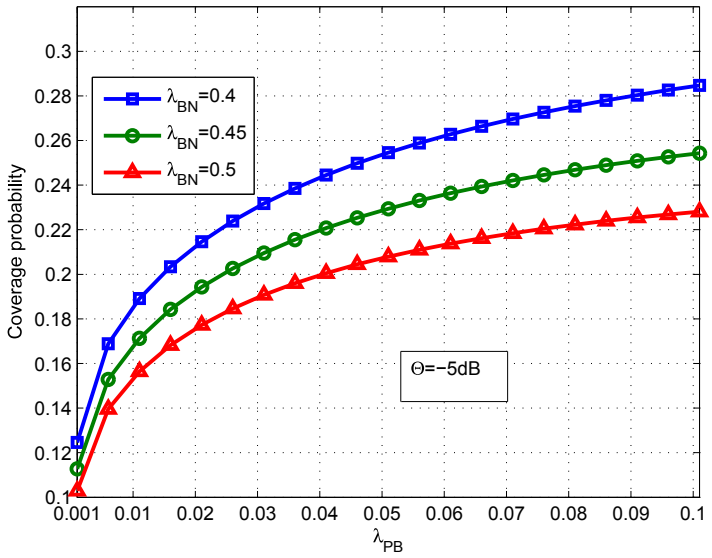

(a) $\Theta = -5$dB

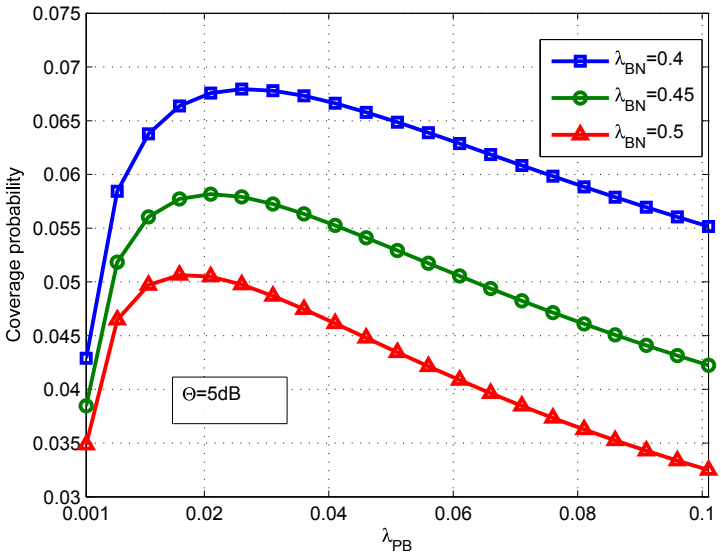

(b) $\Theta = 5$dB

Figure 3.7.: Impact of the density of the PBs λ_{PB} on the coverage probability $\mathcal{C}$.

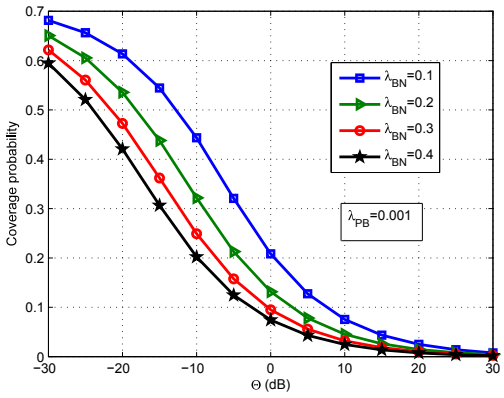

(a) Coverage probability $\mathcal{C}$

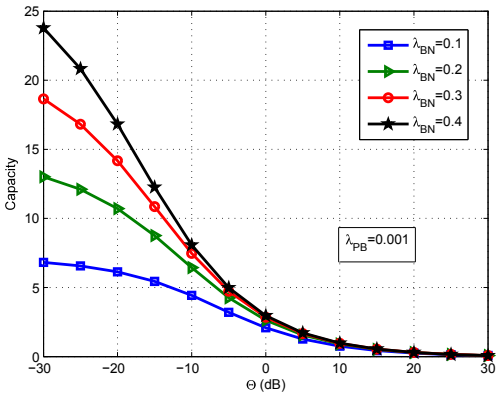

(b) Capacity $\mathcal{T}$

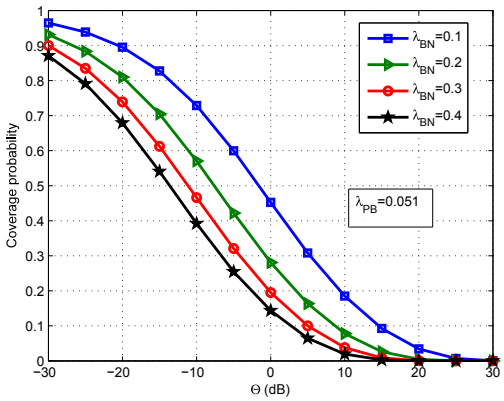

(c) Coverage probability $\mathcal{C}$

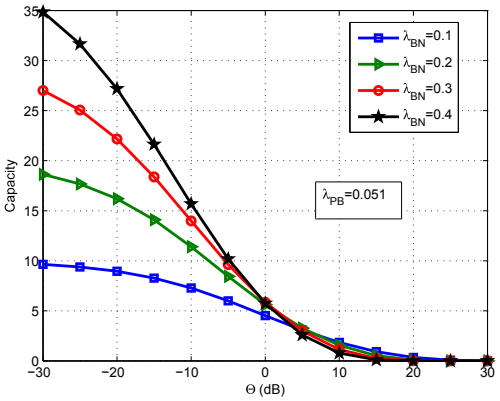

(d) Capacity $\mathcal{T}$

Figure 3.8.: Impact of density of the BNs λ_{BN} on the coverage probability $\mathcal{C}$ and capacity $\mathcal{T}$ of the network.

Fig. 3.8d show that the capacity of the network increases with increase in the density of the BNs. However, at the higher SINR threshold in Fig. 3.8d the capacity decreases with an increase in the density of the BNs. The high SINR threshold is achieved by the BNs which are in close vicinity of the PBs. The number of interfering BNs and the interference increase with an increase in λ_{BN}, due to which, the BNs can not achieve such a high Θ and therefore, the capacity drops. The insights from Fig. 3.8 again validate our earlier observations in Remark 3.3 and 3.4. The coverage probability can be seen as an objective function of an individual user, whereas the capacity is a network wide metric that the service provider would be more interested in. The network provider would like to maximize the capacity of the network given that certain minimum quality of service (coverage probability here) should be satisfied. Therefore, in order to get an optimal performance the tradeoff between the coverage and capacity should be considered along with Θ.

In Fig. 3.9, we compare the coverage of a regularly powered network (RPN) with the wireless powered backscatter communications network (WPBN). In RPN there is no PB tier and each BN has a constant transmit power equal to the transmit power of a PB i.e., P_{PB}. Since, the transmit power of each BN is P_{PB}, its coverage probability is the same for different values of λ_{PB}, as shown in the figure. In contrast, for the WPBN, the coverage probability increases with an increase in the density of the PBs. It can be noticed that when $\lambda_{PB} = 0.6$, the coverage probability of the WPBN approaches the coverage probability of the RPN. Another key point that can be observed from both Fig. 3.9a and 3.9b is that the coverage of WPBN increases very rapidly with increases in λ_{PB} initially, while after a certain increase in λ_{PB} the gain in coverage is very small. For instance, in both Fig. 3.9a and 3.9b the increase in the coverage probability is very significant when λ_{PB} goes from 0.01 to 0.3, whereas from 0.3 to 0.6 the improvement in the coverage is almost negligible. This suggests that after a certain point, further densification of the WPBN with more PBs would not improve the coverage significantly.

3.5. Chapter Summary

In this chapter, a general framework to study the performance of wireless powered backscattered IoT networks is presented. To make the analysis tractable, a dimensionality reduction technique has been applied. The coverage and the capacity of the network in the form of tractable and numerically computable expressions are derived with the help of stochastic geometry. These expressions can be further simplified for some relevant special cases. It has been noticed that the coverage of the network can either increase or decrease with the increase in the density of the PBs depending upon the SINR threshold. Furthermore, the capacity of the network increases with an increase in the density of the BNs, whereas the coverage probability decreases. Finally, the coverage of the wireless powered backscatter network has been compared with the coverage of the regularly powered network and it has been observed that for a very high density of the PBs, the coverage of the wireless powered

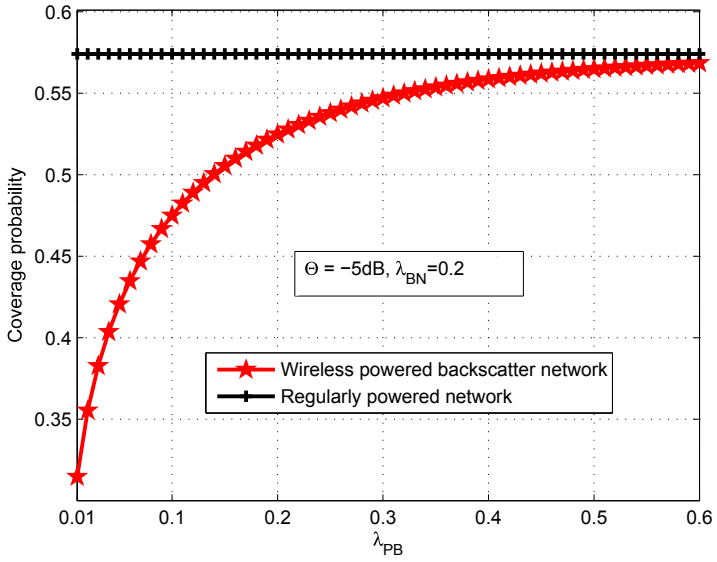

(a)

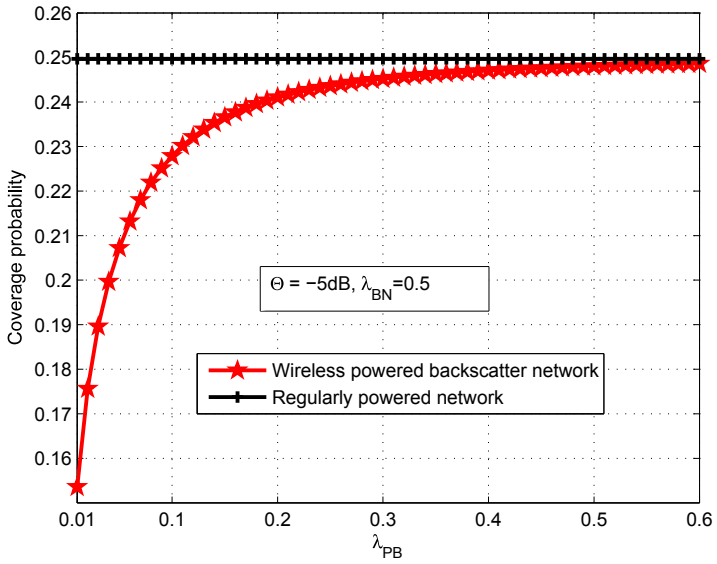

(b)

Figure 3.9.: Regularly powered vs a wireless powered backscatter network.

backscattered network approaches the coverage of the regular powered network.

In the next chapter, we develop a stochastic geometry-based tractable analytical framework to study the performance of our proposed scheduling algorithm for the cellular networks. This scheduling algorithm is motivated by the optimality condition of the famous interference management technique, known as treating interference as noise. We further carry out asymptotic analysis to show that, for the optimized parameters, our proposed scheduling algorithm provides significant gains over the scheduling algorithm for the conventional cellular networks.

4. Treating Interference as Noise in Cellular Networks

The interference management technique that treats interference as noise (TIN) is optimal when the interference is sufficiently low. Scheduling algorithms based on the TIN optimality condition have recently been proposed, e.g., for application to device-to-device communications. TIN, however, has never been applied to cellular networks. In this work, we propose a scheduling algorithm for application to cellular networks that is based on the TIN optimality condition. In the proposed scheduling algorithm, each base station (BS) first randomly selects a user equipment (UE) in its coverage region, and then checks the TIN optimality conditions. If the latter conditions are not fulfilled, the BS is turned off. In order to assess the performance of TIN applied to cellular networks, we introduce an analytical framework with the aid of stochastic geometry theory. We develop, in particular, tractable expressions of the signal-to-interference-and-noise ratio (SINR) coverage probability and average rate of cellular networks. In addition, we carry out asymptotic analysis to find the optimal system parameters that maximize the SINR coverage probability. By using the optimized system parameters, it is shown that TIN applied to cellular networks yields significant gains in terms of SINR coverage probability and average rate. Specifically, the numerical results show that average rate gains of the order of 21% over conventional scheduling algorithms are obtained.

4.1. Introduction

Interference has always been one of the main limiting factors in cellular networks due to its indeterministic nature. In order to cope with interference, different solutions have been proposed. For example, coordinated multipoint (CoMP) [93] and intercell interference coordination (ICIC) [94] have been considered for the long term evolution-advanced (LTE-A) communications standards. In CoMP operation, multiple base stations (BSs) cooperate over a backhaul link and jointly transmit data to the cell-edge user equipments (UEs) in order to mitigate the intercell interference and hence improve the network throughput [95]. The ICIC blanking of macrocells has been proposed for application to heterogeneous networks in order to reduce the amount of interference to the UEs of small cells [96]. Fractional power control (FPC) is considered to be an essential feature in the uplink (UL) of the LTE and LTE-A communication standards [97, 98]. FPC, however, still generates high levels of interference and limits the UL performance. Another approach is interference

aware fractional power control (IAFPC), which limits the maximum amount of interference that a UE can generate. If the interference generated is greater than a maximum threshold, the UE adjusts its transmit power so as to reduce the interference to a given maximum value [99]. These few examples confirm the relevance that mitigating interference in cellular networks plays, as well as the research efforts that have been put towards this end. All these approaches, however, are heuristic in nature and do not rely upon any information theoretic optimality conditions.

Treating interference as noise (TIN) is a known interference management technique that is optimal if the strength of the intended link is greater than or equal to the interference strength that the intended link receives multiplied by the interference strength that the intended link creates [100]. It is not just the optimality of TIN that makes it attractive to the research community, but also its low complexity and robustness to channel uncertainty [100–103]. Despite its optimality and simplicity, TIN has never been applied to cellular networks. In the present chapter, we investigate the application of TIN to cellular networks and introduce a tractable analytical framework in order to optimize its parameters and quantify its achievable performance. To this end, the mathematical tools of stochastic geometry and Poisson point processes are employed.

4.1.1. Related Work

A spectrum sharing mechanism for application in device-to-device (D2D) communications, which is referred to as ITLinQ, has been proposed in [85]. ITLinQ is based on the TIN optimality condition and it has been shown to provide performance gains compared with other heuristic spectrum sharing algorithms. The authors of [85] provide a distributed version of ITLinQ, which guarantees some fairness among the links. ITLinQ has further been improved in [104], where ITLinQ+ has been introduced. By using stochastic geometry, a semi-analytical framework for analyzing ITLinQ has been introduced in [105]. Therein, some adjustable parameters are considered, which can be optimized to get high gain over other D2D scheduling algorithms.

An analytical framework to study the performance of UL heterogeneous cellular networks that employ IAFPC has been proposed in [106]. According to the IAFPC scheme, the UEs that generate higher interference than a maximum threshold limit their transmit power so that the interference is below an admissible maximum value. A similar approach that turns off the UEs that generate more interference than a maximum threshold has been studied in [107]. In both [106] and [107], stochastic geometry tools have been used for performance analysis and optimization. Gains in terms of average rate and power consumption have been shown. Another stochastic geometry based framework that studies the problem of BS cooperation in the downlink for heterogeneous networks can be found in [90]. The analysis of BS cooperation with retransmissions can be found in [91]. Simulations based studies that consider interference aware power control can be found in [58, 108, 109].

The existing works that employ the TIN optimality condition for interference man-

agement are limited to D2D communications [85, 104, 105], whereas the works that employ interference awareness methods in cellular networks are based on heuristic criteria [58, 90, 91, 99, 106–109]. In the present chapter, we propose a scheduling algorithm based on the TIN optimality condition and develop a tractable analytical framework for its analysis and optimization by using tools from stochastic geometry.

4.1.2. Contributions and Outcomes

Designing a cellular network based on the TIN optimality conditions and developing an analytical framework for its analysis and optimization is a challenging task. To this end, in fact, a centralized controller that keeps track of all the channels of the cellular network and that identifies the strongest interference received and the strongest interference created on each link of the cellular network is needed. The complexity of such a centralized scheduler may be too high for application to large-scale networks. The resulting scheduling algorithm, in addition, would be intractable from the analytical standpoint and, therefore, difficult to optimize without using extensive system-level simulations.

To deal with the issues of implementation complexity and analytical intractability, we propose and study the performance of a simplified two-step version of the (optimal or centralized) TIN-based scheduling algorithm, which can be implemented in a distributed manner and requires only the channel state information (CSI) of neighboring BSs. In the first step, each BS randomly selects a UE in its coverage region, similar to conventional cellular networks that do not employ TIN. In the second step, only the BSs that fulfill the TIN optimality conditions schedule for transmission the UE in their coverage region. The rest of the BSs, on the other hand, are turned off. In order to make the TIN scheduling algorithm suitable for application to cellular networks, we introduce two design parameters (M and μ) that are optimized in order to control the number of BSs that are turned off. The optimization of these two parameters is important in order to identify a suitable trade-off between the potential reduction of interference and the potential loss of average rate that turning some BSs off entails. In spite of the latter potential loss of average rate, our analysis shows that the proposed TIN-based scheduling algorithm outperforms conventional cellular networks in terms of average rate, thanks to its effective interference reduction capability.

The proposed two-step TIN-based scheduling algorithm is simple to implement in cellular networks. Its analysis and optimization are, however, still challenging. The main reason is the lack of analytical results for the distribution of the downlink distances within the typical cell of a Voronoi tessellation [38,43]. To overcome this limitation, we introduce some approximations that lead to a tractable analytical framework, which is shown to be suitable for system optimization yet sufficiently accurate. We approximate, in particular, the typical cell of a Voronoi tessellation with the so-called Crofton cell [43], and the distribution of the distance between a BS and its most interfered UE with the distribution of the distance between the typical UE and the BS that creates the highest interference to it. These two approximations result in a lower bound for the coverage probability of the proposed

two-step TIN-based scheduling algorithm.

The unique contributions and outcomes of the present work can be summarized as follows:

- We derive tractable analytical expressions for the SINR coverage probability and average rate of the proposed two-step (distributed) TIN scheduling protocol. For specific system parameters, the analytical formulas are proved to reduce to the SINR coverage probability and average rate of conventional cellular networks.
- We show that unique values of M and μ that maximize the SINR coverage probability and average rate exist. In order to compute such optimal M and μ, we carry out asymptotic analysis of the SINR coverage probability and provide a simple optimization algorithm. By setting $M = 1$, more precisely, we identify the optimal value of μ for high and low values of the SINR decoding threshold.
- We observe that the optimal value of μ decreases as the SINR threshold increases. This implies that, in order to achieve a high SINR decoding threshold, more BSs need to be turned off. If, on the other hand, the SINR threshold is small, we show that no BSs need to be turned off, which implies that optimal performance can be obtained by using the conventional scheduling algorithm.
- We further show that TIN-based scheduling algorithms with optimized parameters significantly improve the SINR coverage probability and average rate. For example, the exact implementation (through simulation without any approximation) of the two-step TIN-based scheduling improves the SINR coverage probability by 67% and the mathematically tractable implementation (lower bound) of the two-step TIN-based scheduling improves the SINR coverage probability by 36%, if the SINR decoding threshold is set to 10 dB. In addition, the corresponding increase of the average rate is 21% and 11%, respectively, despite the fact that some BSs are turned off, compared to the classical scheduling algorithm.

The rest of the present chapter is organized as follows. In Section 4.2, we introduce the network model and the TIN-based scheduling algorithm. In Section 4.3, we provide a tractable analytical framework of the SINR coverage probability and average rate. In Section 4.4, we carry out asymptotic analysis in order to find the optimal system parameters that optimize the SINR coverage probability. In Section 4.5, simulation and numerical results are presented. Finally, Section 4.6 provides a summary of this chapter. The key notations used in this chapter are given in Table 4.1.

4.2. System Model

4.2.1. Network Model

We consider a single-tier downlink cellular network in which the locations of BSs and UEs are modeled as points of two bi-dimensional and mutually independent homogeneous

Table 4.1.: List of Notations for Chapter 4

Notation	Description
Φ_b, Φ_u, λ_b, λ_u	PPP of the BSs, PPP of the UEs, density of the BSs, density of the UEs
P, N, α	transmit power of each BS, power of the AWGN noise, path-loss exponent
λ_I, $\mathcal{R}_I$, $\mathbb{P}[\mathbb{A}_{\mathbb{UE}}]$	density of the interfering BSs, inhomogeneity ball, probability that the typical UE is active
X_{11}, X_{12}, X_{21}	distance between the typical UE and the typical BS, distance between the typical BS and the most interefered UE, distance between the typcial UE and the nearest interfering BS
$\max(.,.)$, $\min(.,.)$, Θ	the maximum operator, the minimum operator, SINR decoding threshold
$\mathcal{C}$, $\mathcal{C}_{net}$	SINR coverage probability of an active UE, effective SINR coverage probability
$\mathcal{RSE}$, $\mathcal{RSE}_{net}$	SINR average rate of an active UE, effective SINR average rate
$\Gamma(a)$	The gamma function $\Gamma(a) = \int_0^\infty x^{a-1}\mathrm{e}^{-x}\mathrm{d}x$

Poisson point processes (PPPs). We denote by Φ_b and Φ_u the PPPs, and by λ_b and λ_u the densities of BSs and UEs, respectively. The density of UEs is assumed to be much greater than the density of BSs. Thus, all the BSs are active and have UEs to serve in every resource block (carrier frequency, time slot, etc.), if no scheduling for interference management is applied. We assume full frequency reuse, i.e., all the BSs share the same transmission bandwidth. Each UE is associated with the nearest BS. Accordingly, the coverage regions of the BSs constitute a Poisson-Voronoi tessellation in the plane. The BSs and UEs have a single antenna. The standard unbounded path-loss model with path-loss exponent $\alpha > 2$ is considered. The fast-fading is assumed to follow a Rayleigh distribution. More general system models may be analyzed. In the present work, however, we consider the so-called standard modeling assumptions [43], in order to focus our attention on the impact and potential benefits of TIN.

4.2.2. Treating Interference as Noise

Treating interference as noise is a scheduling algorithm that has attracted major interest for practical and theoretical reasons. From the implementation point of view, TIN is attractive due to its simplicity and adaptability to channel uncertainties. From the theoretical standpoint, it is a promising solution due to its optimality under certain conditions [100].

The TIN optimality conditions, more precisely, can be stated as follows: In a wireless network with n transmitter and receiver pairs, if the strength of the intended link (from an intended BS to an intended UE) is greater than or equal to the product of the strengths of the strongest interference that the intended BS creates and of the strongest interference

that the intended UE receives, then TIN achieves the whole capacity region to within a constant gap of $\log 3n$ [100]. In mathematical terms, the TIN optimality conditions can be formulated as follows:

$$\mathrm{SNR}_i \geqslant \max_{j \neq i} \mathrm{INR}_{ij} \max_{k \neq i} \mathrm{INR}_{ki} \quad \forall i = 1, ..., n, \tag{4.1}$$

where SNR_i and INR_{ij} denote the signal-to-noise ratio (SNR) of link i and the interference-to-noise ratio (INR) of source j at destination i, respectively. It is worth mentioning, in particular, that the SNRs and INRs in (4.1) depend on both the path-loss and the fast fading.

4.2.3. TIN-Based Scheduling Algorithm

The scheduling algorithm based on the TIN optimality conditions in (4.1) may be difficult to realize in large-scale cellular networks, since a centralized controller that is aware of the (instantaneous) channel state information of all the links available in the networks is necessary. In the present chapter, this approach is referred to as *centralized TIN scheduling*.

To overcome this issue, we propose a two-step distributed scheduling algorithm inspired by (4.1), which, in addition, does not necessitate the instantaneous channel state information of the links. This approach is referred to as *two-step or distributed TIN scheduling*. In the first step, for each available resource block, each BS randomly selects a UE that lies in its coverage region. In the second step, the BSs that do not fulfill the following (simplified) TIN optimality conditions:

$$M\overline{\mathrm{SNR}}_i^{\mu} \geqslant \max_{j \neq i} \overline{\mathrm{INR}}_{ij} \max_{k \neq i} \overline{\mathrm{INR}}_{ki} \quad \forall i = 1, ..., n, \tag{4.2}$$

are turned off, where $\overline{\mathrm{SNR}}_i$ and $\overline{\mathrm{INR}}_{ij}$ have the same meaning as in (4.1) except that they are averaged with respect to the fast fading in order to dispense the scheduler from requiring the instantaneous channel state information of the links. Equation (4.2), as opposed to (4.1), is applied by each BS independently of the other BSs, which makes it suitable for a distributed implementation and requires only the average channel state information of neighboring BSs. In (4.2), in addition, we have introduced two design parameters, M and μ, for system optimization, which allow us to control the number of BSs that are turned off, and, thus, are instrumental for interference management. In particular, M is a positive real number greater than or equal to one ($M \geq 1$), and μ is a positive real number greater than or equal to one and less than or equal to two ($1 \leq \mu \leq 2$).

In order to get deeper understanding and insight from (4.2), we rewrite it with the aid of a more explicit notation by taking as an example the cellular network realization depicted in Fig. 4.1. For any realization of the cellular network under analysis, we select one cell (BS) at random that is referred to as *the typical cell or the typical BS*. Among the UEs that lay in its coverage region, we select one UE at random for every available resource block.

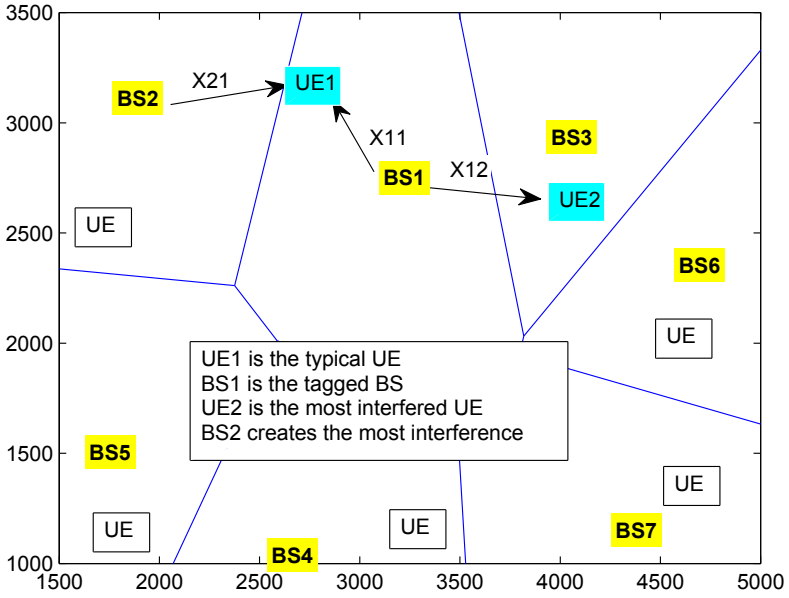

Figure 4.1.: Network model.

We focus our attention on a randomly chosen resource block and the UE that is scheduled for transmission on it is referred to as the *typical UE*. Let X_{11} denote the downlink distance between the typical UE (UE1 in Fig. 4.1) and the typical BS (BS1 in Fig. 4.1), X_{12} denote the downlink distance between the typical BS and the most interfered UE (UE2 in Fig. 4.1) by it, and X_{21} denote the downlink distance between the typical UE and the BS (BS2 in Fig. 4.1) that creates the highest interference to it. With the aid of this explicit notation, (4.2) can be re-formulated as follows:

$$M\left(\frac{PX_{11}^{-\alpha}}{N}\right)^{\mu} \geq \frac{PX_{12}^{-\alpha}}{N}\frac{PX_{21}^{-\alpha}}{N}, \tag{4.3}$$

where P is the transmit power of the BSs, N is the noise power at the UE, and α is the path-loss exponent. From (4.3), it follows that the typical BS necessitates only three average SNRs to check the TIN optimality conditions, and, thus, a network-level controller is not necessary.

Equivalently, (4.3) can be written as follows:

$$X_{11} \leq M^{\frac{1}{\alpha\mu}}\left(\frac{N}{P}\right)^{\frac{2-\mu}{\alpha\mu}}(X_{12}X_{21})^{\frac{1}{\mu}}. \tag{4.4}$$

During the second step of the proposed TIN-based scheduling algorithm, the typical UE is scheduled for transmission if X_{11} fulfills the constraint in (4.4). Otherwise, the typical BS is turned off and the UEs that lay in its coverage region are not scheduled for transmission. This implies that the interference can be potentially reduced at the cost of reducing the

average rate and the fairness among the UEs, since some of them are not scheduled for transmission at a given time instance. In the present chapter, we employ the pair of parameters M and μ to find the good balance in order to reduce the interference while increasing both the SINR coverage probability and the average rate. We do not explicitly study, on the other hand, the issue of fairness among the UEs. This is postponed to future research. It is important to mention, however, that the fairness among the UEs may not be a critical issue in a well designed system. If in a given time instance, e.g., a time-slot, the TIN optimality condition in (4.4) is not fulfilled, it may be likely fulfilled in another (the next) time instance. The local interference conditions that are considered in (4.4) may, in fact, change at every time instance for two main reasons. i) In each resource block, the BSs select the UEs at random. Accordingly, the interference perceived by the typical UE may change every time that a random UE is chosen by the BSs. ii) Mobility and shadowing, which are not explicitly considered in the present work, may change the interference perceived by the typical UE as well. The system parameters M and μ, in addition, may be tuned in order to account for specific fairness requirements. By setting, for example, M to a very large value, the scheduling criterion in (4.4) is deactivated and the typical fairness requirements among the UEs can be guaranteed. In the sequel, it is shown, more precisely, that our system model reduces to the original cellular network model without TIN-based scheduling by setting $M = 1$ and $\mu = 2$. Due to space limitations, the analysis and optimization of M and μ in order to find a good trade-off between average rate and user fairness is postponed to future research.

To better understand the impact of the proposed TIN-based scheduling algorithm on the downlink distances in (4.4), we analyze the joint probability density function of the distance pairs (X_{11}, X_{21}) and (X_{11}, X_{12}). We compare, in particular, a cellular network where TIN is not applied (i.e., each BS selects a UE at random in its coverage region, which is always scheduled for transmission) and the same cellular network where the scheduling criterion in (4.4) is applied. From Fig. 4.2a, if TIN is not applied, we evince that X_{21} is always greater than X_{11}, but the most interfering BS may be located just outside the coverage region of the typical BS. If TIN is applied, on the other hand, Fig. 4.2b shows that, as opposed to Fig. 4.2a, the most interfering BS is located further away from the coverage boundary of the typical BS. This confirms that TIN is capable of reducing the interference at the typical UE. From Fig. 4.2c, if TIN is not applied, we evince that X_{12} may be greater or less than X_{11}. This implies that the most interfered UE may be located farther or closer than the typical UE. If TIN is applied, on the other hand, Fig. 4.2d shows that the most interfered UE is located farther than the typical UE. This highlights that TIN is capable of reducing the interference towards the UEs.

In summary, the TIN-based scheduling algorithm is capable of reducing the interference in cellular networks by turning off those BSs that create a high level of interference, as well as those BSs whose tagged UEs receive a high level of interference. The proposed TIN-based scheduling algorithm, in particular, is different from those reported in [106] and [107],

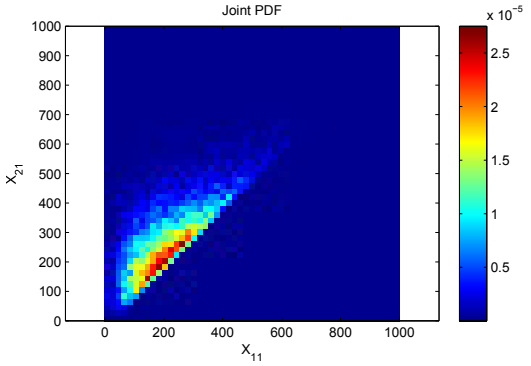

(a) Conventional cellular network.

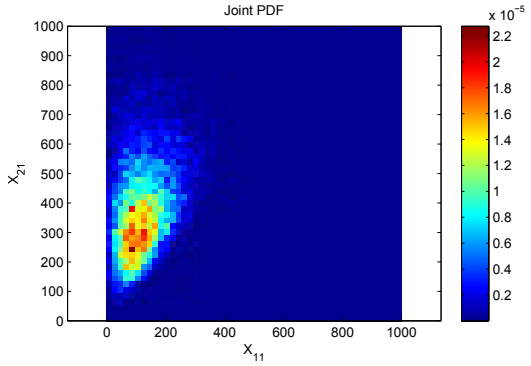

(b) TIN-based cellular network.

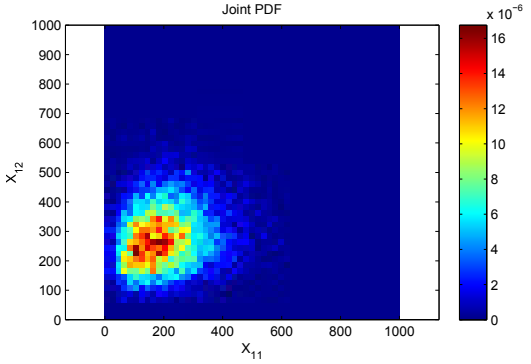

(c) Conventional cellular network.

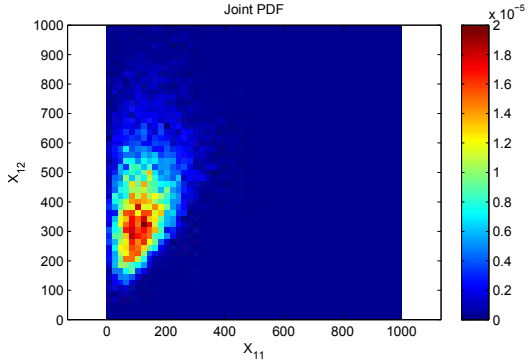

(d) TIN-based cellular network.

Figure 4.2.: Top view of the joint probability density functions of (X_{11}, X_{21}) and (X_{11}, X_{12}) in conventional and TIN-based cellular networks ($\lambda_b = 5$, $M = 1$, $\mu = 1.8$).

where the rationale is to compare the signal strengths against a maximum but fixed level of tolerable interference. In the proposed TIN-based scheduling algorithm, the level of tolerable interference depends on the signal strengths themselves, which makes TIN robust to channel uncertainty as well. Also, the proposed TIN-based scheduling not only accounts for the amount of interference that is received but also for the amount of interference that is generated.

4.3. Coverage and Spectral Efficiency Analysis

In this section, we introduce analytical frameworks for computing the SINR coverage probability and average rate of TIN-based cellular networks. The obtained analytical frameworks are instrumental to quantify the performance gains offered by TIN, to compare conventional against TIN-based cellular networks, as well as to optimize the system parameters in order to identify the correct tradeoff between interference reduction and the required average rate.

To this end, some enabling results are needed. In particular, the probability that a random UE satisfies the TIN optimality conditions in (4.4), and the joint and marginal distributions of the distances X_{11}, X_{12}, and X_{21} are needed. However, they are not available in the open technical literature. To overcome this analytical challenge, we resort to some approximations that are introduced, motivated, and discussed in the following section for ease of exposition, since they are applied throughout the rest of the present chapter.

4.3.1. Approximations for Tractable Analytical Modeling

Three main approximations are used, which are detailed as follows.

- In our network model, the distribution of the downlink distances within the typical Poisson-Voronoi cell are needed. It is known, however, that these distributions are unknown [38,43]. A tractable and accurate approximation that is typically employed to overcome this limitation consists of approximating the typical cell with the Crofton (or zero) cell. The Crofton cell of a Poisson-Voronoi tessellation is the cell that contains the origin. It is known that the Crofton cell is larger than the typical cell, but the two cells are equal in law [110]. Some discussions accompanied by empirical results are available in [111]. To obtain a tractable yet accurate analytical framework of the SINR coverage probability and average rate, we conduct the analysis for the Crofton cell instead of for the typical cell. This approach is motivated by the fact that the marginal and joint distributions of X_{11} and X_{21} are available in closed-form for the Crofton cell of a Poisson-Voronoi tessellation [84]. Since it is known that large cells are more likely to contain the origin, the Crofton cell is larger than the typical cell defined through the Palm measure [112]. This implies that, with the proposed approximation, the distances X_{11} and X_{21} are overestimated.

- In our network model, the distribution of the downlink distance, X_{12}, between the typical BS and its most interfered UE is needed. To the best of our knowledge, the distribution of this distance is not available in closed-form. In order to overcome this limitation, we still rely on the Crofton cell approximation, and, in addition, we propose to approximate the distribution of X_{12} with the distribution of X_{21}, i.e., with the distance between the typical UE and its most interfering BS. This approximation is empirically supported by comparing Fig. 4.2b and Fig. 4.2d, where it is shown that, if TIN is applied, the conditional probability density functions of X_{12} and X_{21} are similar. In Fig. 4.3, in addition, we depict the corresponding cumulative distribution functions of X_{12} and X_{21}. We observe that they are not so different from each other, especially for short distances. Furthermore, it is apparent that X_{21} overestimates X_{12}.

- By applying the TIN-based scheduling algorithm, some BSs are turned off if the TIN optimality conditions in (4.3) are not fulfilled. Even though the point process of BSs is a PPP, the point process of the active BSs after applying TIN is not a PPP anymore. The TIN-based scheduling algorithm, in fact, introduces some spatial correlations among the set of active BSs that depend on the amount of downlink interference generated and received throughout the entire cellular network. To the best of our knowledge, no exact analytical characterization of the point process of the active BSs exists in the open technical literature. For analytical tractability, and similar to [106, 107, 113], we approximate the point process of the active BSs with an inhomogeneous PPP. The spatial inhomogeneity is, in particular, determined by the spatial constraints imposed by the TIN optimality conditions in (4.3), which allows us to account, at least in part, for the spatial correlations among the active BSs. The details of the approximating inhomogeneous PPP are provided in the sequel.

Based on the Crofton cell approximation, the joint probability density function of X_{11} and X_{21} is approximated as follows [84]:

$$f_{X_{11},X_{21}}(x_{11},x_{21}) \approx (2\pi\lambda_b)^2 \, x_{11}x_{21}\mathrm{e}^{-\pi\lambda_b x_{21}^2}, \tag{4.5}$$

if $x_{11} < x_{21}$ and $f_{X_{11},X_{21}}(x_{11},x_{21}) = 0$ otherwise. Also, we have $f_{X_{11}}(x_{11}) \approx 2\pi\lambda_b x_{11}\mathrm{e}^{-\pi\lambda_b x_{11}^2}$ and $f_{X_{11},X_{21}}(x_{11},x_{21}) \approx f_{X_{11}}(x_{11})f_{X_{21}|X_{11}}(x_{21}|x_{11})$, where $f_{X_{21}|X_{11}}(x_{21}|x_{11})$ is the conditional probability density function of X_{21}. Based on the second approximation, furthermore, we assume $f_{X_{12}}(x_{12}) \approx f_{X_{21}}(x_{21})$. By capitalizing on the Crofton cell approximation, in addition, the typical UE can be assumed to be at the origin without loss of generality.

Based on the inhomogeneous PPP approximation, the point process of the interfering BSs after applying the TIN optimality conditions is approximated with an inhomogeneous

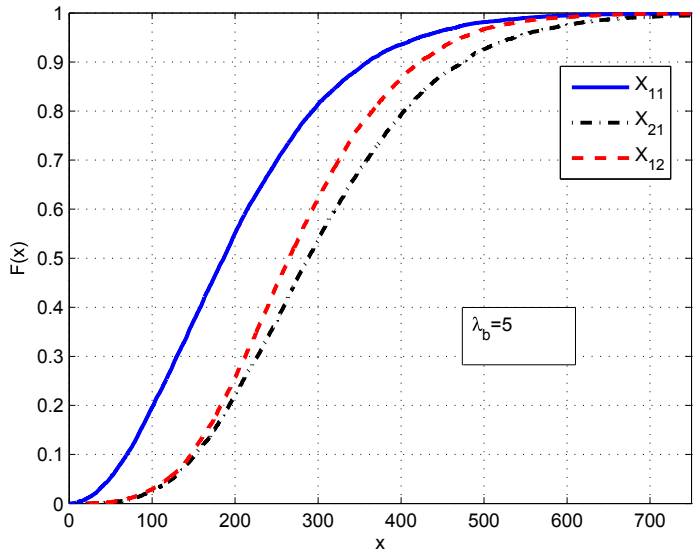

(a)

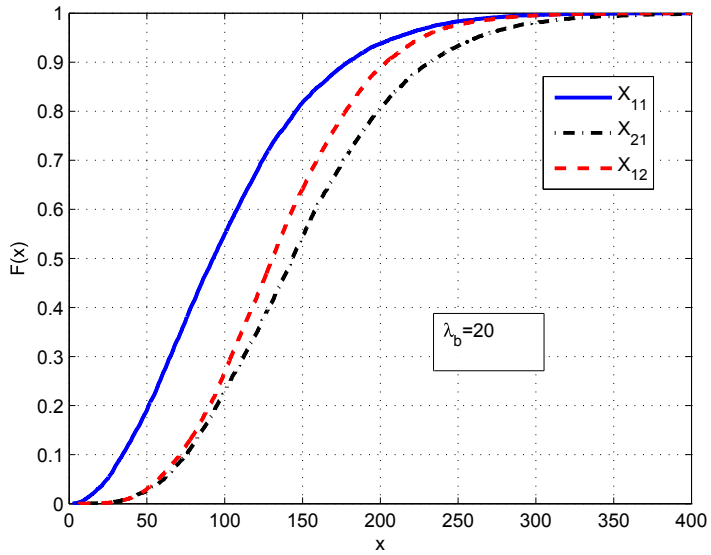

(b)

Figure 4.3.: Empirical cumulative distribution functions of X_{11}, X_{21} and X_{12}

PPP of distance-dependent density $\lambda_I(r)$ defined as follows:

$$\begin{cases} \lambda_I(r) = 0 & \text{if} \quad r < \mathcal{R}_{\mathcal{I}} \\ \lambda_I(r) = \lambda_b \mathbb{P}\left[\mathbb{A}_{\mathbb{UE}}\right] & \text{if} \quad r \geq \mathcal{R}_{\mathcal{I}}, \end{cases} \tag{4.6}$$

where $\mathbb{A}_{\mathbb{UE}}$ denotes the event that (4.3) is true, $\mathbb{P}\left[\mathbb{A}_{\mathbb{UE}}\right]$ is its probability of occurrence, and $\mathcal{R}_{\mathcal{I}}$ constitutes the smallest distance from the origin of any interfering BSs after applying TIN. $\mathcal{R}_{\mathcal{I}}$ is referred to as the *inhomogeneity ball* and can be formulated as follows:

$$\mathcal{R}_{\mathcal{I}} = \max(X_{11}, X_{11}^{\frac{\mu}{2}} \left(\frac{P}{N}\right)^{\frac{2-\mu}{2\alpha}} \left(\frac{1}{M}\right)^{\frac{1}{2\alpha}}), \tag{4.7}$$

where $\max(\cdot,\cdot)$ denotes the maximum operator, and its first and second arguments originate from the shortest distance cell association criterion and from the TIN-based optimality conditions in (4.3), respectively. From (4.7), the condition $X_{21} \geq \mathcal{R}_{\mathcal{I}}$ holds implicitly true.

The accuracy of the proposed approximations is analyzed in Section 4.5 with the aid of Monte Carlo simulations. It is shown that the proposed approximations lead to a tractable yet accurate analytical formulation of the SINR coverage probability and average rate. In the sequel, the proposed approximations are used for all the analytical derivations.

4.3.2. Probability of TIN

In this section, we compute the probability that a randomly selected UE satisfies the TIN optimality conditions in (4.4). Based on the approximations in Section 4.3.1, the event, $\mathbb{A}_{\mathbb{UE}}$, that the typical UE fulfills the TIN optimality conditions can be formulated as follows:

$$\mathbb{A}_{\mathbb{UE}} = \left[X_{11} \leq M^{\frac{1}{\alpha\mu}} \left(\frac{N}{P}\right)^{\frac{2-\mu}{\alpha\mu}} X_{21}^{\frac{2}{\mu}} \right]. \tag{4.8}$$

The probability that the typical UE fulfills the event $\mathbb{A}_{\mathbb{UE}}$ is given in the following lemma.

Lemma 4.1. *The probability that the typical UE is active can be formulated as follows:*

$$\begin{aligned} \mathbb{P}\left[\mathbb{A}_{\mathbb{UE}}\right] &= \mathbb{P}\left[X_{11} \leq M^{\frac{1}{\alpha\mu}} \left(\frac{N}{P}\right)^{\frac{2-\mu}{\alpha\mu}} X_{21}^{\frac{2}{\mu}} \right] \\ &= \int_0^\infty 2\left(\pi\lambda_b\right)^2 x_{21} \mathrm{e}^{-\pi\lambda_b x_{21}^2} \min{}^2\left(x_{21}, M^{\frac{1}{\alpha\mu}} \left(\frac{N}{P}\right)^{\frac{2-\mu}{\alpha\mu}} x_{21}^{\frac{2}{\mu}} \right) \mathrm{d}x_{21}, \end{aligned} \tag{4.9}$$

where $\min(\cdot,\cdot)$ *denotes the minimum function.*

Proof. The probability that a UE is active can be written as follows:

$$\mathbb{P}\left[\mathbb{A}_{\mathbb{UE}}\right] = \mathbb{E}_{X_{11},X_{21}} \left[\mathbf{1}\left(X_{11} \leq X_{21}\right) \times \mathbf{1}\left(X_{11} \leq \left(M^{\frac{1}{\alpha\mu}} \left(\frac{N}{P}\right)^{\frac{2-\mu}{\alpha\mu}} X_{21}^{\frac{2}{\mu}} \right) \right) \right], \tag{4.10}$$

where the fist indicator function, $\mathbf{1}(\cdot)$, is due to the cell association criterion based on the shortest distance and the second indicator function is due to the TIN optimality conditions. The expectation in (4.10) can be computed from the joint probability density function in (4.5), which results in the following integral:

$$\mathbb{P}\left[\mathbb{A}_{\mathbb{UE}}\right] = \int_0^{\infty} \int_0^{\min\left(X_{21}, M^{\frac{1}{\alpha\mu}} \left(\frac{N}{P}\right)^{\frac{2-\mu}{\alpha\mu}} X_{21}^{\frac{2}{\mu}}\right)} (2\pi\lambda_b)^2 x_{11} x_{21} \mathrm{e}^{-\pi\lambda_b x_{21}^2} \mathrm{d}x_{11} \mathrm{d}x_{21}.$$

By solving the inner integral with respect to x_{11}, the expression in (4.9) is obtained. This concludes the proof. □

It is worth noting that $\mathbb{P}\left[\mathbb{A}_{\mathbb{UE}}\right] = 1$ if $M = 1$ and $\mu = 2$. This corresponds to the scenario where the TIN optimality conditions are inactive and the system model reduces to a conventional cellular network without TIN.

4.3.3. Probability Density Function of X_{11} Conditioned Upon $\mathbb{A}_{\mathbb{UE}}$

In this section, we compute the probability density function of the distance, X_{11}, between the typical BS and the typical UE conditioned upon the event $\mathbb{A}_{\mathbb{UE}}$, i.e., the TIN optimality conditions are fulfilled. It is formally stated in the following lemma.

Lemma 4.2. *The probability density function of X_{11} conditioned upon $\mathbb{A}_{\mathbb{UE}}$ in (4.8) can be formulated as follows:*

$$f_{X11}\left(x_{11} | \mathbb{A}_{\mathbb{UE}}\right) = \frac{2\pi\lambda_b x_{11} \mathrm{e}^{-\pi\lambda_b \max^2\left(\mathrm{x}_{11}, \mathrm{x}_{11}^{\mu/2} \left(\frac{\mathrm{P}}{\mathrm{N}}\right)^{\frac{2-\mu}{2\alpha}} \left(\frac{1}{\mathrm{M}}\right)^{\frac{1}{2\alpha}}\right)}}{\mathbb{P}\left[\mathbb{A}_{\mathbb{UE}}\right]}, \tag{4.11}$$

where $\mathbb{P}\left[\mathbb{A}_{\mathbb{UE}}\right]$ is given in Lemma 4.1.

Proof. The probability density function of X_{11} conditioned upon $\mathbb{A}_{\mathbb{UE}}$ is defined as follows:

$$f_{X11}\left(x_{11} | \mathbb{A}_{\mathbb{UE}}\right) = \frac{\mathrm{d}}{\mathrm{d}x_{11}} \frac{\mathbb{P}\left[X_{11} \leq x_{11}, \mathbb{A}_{\mathbb{UE}}\right]}{\mathbb{P}\left[\mathbb{A}_{\mathbb{UE}}\right]}. \tag{4.12}$$

The numerator of (4.12) can be expressed as follows:

$$\begin{aligned}
\mathbb{P}\left[X_{11} \leq x_{11}, \mathbb{A}_{\mathbb{UE}}\right] &= \mathbb{E}_{X_{11}, X_{21}}\left[\mathbf{1}\left(X_{21} > X_{11}\right) \times \mathbf{1}\left(X_{21} > X_{11}^{\mu/2} \left(\frac{P}{N}\right)^{\frac{2-\mu}{2\alpha}} \left(\frac{1}{M}\right)^{1/2\alpha}\right)\right] \\
&= \int_0^{x_{11}} \int_{\max\left(x_{11}, x_{11}^{\mu/2} \left(\frac{P}{N}\right)^{\frac{2-\mu}{2\alpha}} \left(\frac{1}{M}\right)^{1/2\alpha}\right)}^{\infty} (2\pi\lambda_b)^2 x_{11} x_{21} \mathrm{e}^{-\pi\lambda_b x_{21}^2} \mathrm{d}x_{21} \mathrm{d}x_{11},
\end{aligned} \tag{4.13}$$

where the last equality is obtained by using (4.5). The proof follows by computing the inner integral with respect to x_{21} and then applying Leibniz's integration rule. This concludes the proof. □

It is worth noting that (4.11) reduces to the probability density function of the distance of the nearest BS to the origin of a conventional cellular network if $M = 1$ and $\mu = 2$. This corresponds to the scenario where TIN is not applied.

4.3.4. SINR Coverage Probability

In this section, we provide a tractable analytical framework for computing the SINR coverage probability of cellular networks in which the TIN-based scheduling algorithm is applied.

By capitalizing on the three approximations in Section 4.3.1, the SINR at the typical UE can be formulated as follows:

$$\mathrm{SINR} = \frac{h_{11} X_{11}^{-\alpha}}{\sum_{i \in \Phi_b'} h_i D_i^{-\alpha} \mathbf{1}\left(D_i \geq \max(X_{11}, X_{11}^{\frac{\mu}{2}} \left(\frac{P}{N}\right)^{\frac{2-\mu}{2\alpha}} \left(\frac{1}{M}\right)^{\frac{1}{2\alpha}})\right) + \frac{N}{P}}, \tag{4.14}$$

where h_i is the channel gain of the ith interfering BS, h_{11} is the channel gain of the intended link, D_i is the distance between the ith interfering BS and the typical UE, Φ_b' is the inhomogeneous PPP of interfering BSs whose density is defined in (4.6), and the indicator function makes explicit that the interfering BSs must lie outside the inhomogeneity radius defined in (4.7).

We are interested in computing the *effective* SINR coverage probability, $\mathcal{C}_{net}$, of the typical UE, which accounts for the fact that the typical UE may not be served by the typical BS if it is turned off because it does not fulfill the TIN optimality conditions. $\mathcal{C}_{net}$ can be formulated as follows:

$$\mathcal{C}_{net} = \mathbb{P}\left[\mathbb{A}_{\mathbb{UE}}\right] \mathcal{C}, \tag{4.15}$$

where $\mathbb{P}\left[\mathbb{A}_{\mathbb{UE}}\right]$ is the probability that the typical UE is active, which is given in (4.9), and $\mathcal{C}$ is the SINR coverage probability of the typical active UE. This latter probability is defined and computed in the following theorem.

Theorem 4.1. *Let Θ be the SINR decoding threshold. The SINR coverage probability of the typical active UE, $\mathcal{C} = \mathbb{P}\left[\mathrm{SINR} \geq \Theta\right]$, can be formulated as follows:*

$$\mathcal{C} = \frac{2\pi\lambda_b}{\mathbb{P}\left[\mathbb{A}_{\mathbb{UE}}\right]} \int_0^\infty x_{11} \mathrm{e}^{-\pi\lambda_b \max^2\left(x_{11}, x_{11}^{\mu/2} \left(\frac{P}{N}\right)^{\frac{2-\mu}{2\alpha}} \left(\frac{1}{M}\right)^{\frac{1}{2\alpha}}\right)} \mathrm{e}^{\left(-\frac{x_{11}^\alpha \Theta N}{P}\right)} \mathcal{L}_{\mathcal{I}}\left(x_{11}^\alpha \Theta\right) \mathrm{d}x_{11}, \tag{4.16}$$

where $\mathcal{L}_{\mathcal{I}}(s)$ is the Laplace transform of the interference:

$$\mathcal{L}_{\mathcal{I}}(s) = \exp\left(\frac{-2\pi\lambda_b \mathbb{P}\left[\mathbb{A}_{\mathbb{UE}}\right]}{\alpha - 2} s \left(\max^2\left(x_{11}, x_{11}^{\mu/2} \left(\frac{P}{N}\right)^{\frac{2-\mu}{2\alpha}} \left(\frac{1}{M}\right)^{\frac{1}{2\alpha}}\right)\right)^{1-\frac{\alpha}{2}} \right.$$
$$\left. {}_2\mathrm{F}_1\left[1, 1 - \frac{2}{\alpha}, 2 - \frac{2}{\alpha}; -s\left(\max^2\left(x_{11}, x_{11}^{\mu/2} \left(\frac{P}{N}\right)^{\frac{2-\mu}{2\alpha}} \left(\frac{1}{M}\right)^{\frac{1}{2\alpha}}\right)\right)^{-\frac{\alpha}{2}}\right]\right). \tag{4.17}$$

Proof. See Appendix C.1. □

Corollary 4.1. *If $M = 1$ and $\mu = 2$, the SINR coverage probability in Theorem 4.1 simplifies as follows:*

$$\mathcal{C} = 2\pi\lambda_b \int_0^\infty x_{11} \mathrm{e}^{-\left(\pi\lambda_b x_{11}^2 + \frac{x_{11}^\alpha \Theta N}{P} + \pi\lambda_b x_{11}^2 \Theta^{\frac{2}{\alpha}} \int_{\Theta^{\frac{-2}{\alpha}}}^\infty \frac{1}{1+z^{\alpha/2}} \mathrm{d}z\right)} \mathrm{d}x_{11}, \tag{4.18}$$

which is the SINR coverage probability of a conventional cellular network when TIN is not applied [28].

4.3.5. SINR Average Rate

In this section, we provide a tractable analytical framework for computing the average rate of cellular networks in which the TIN-based scheduling algorithm is applied.

Similar to the SINR coverage probability, we are interested in computing the *effective* SINR average rate, $\mathcal{R}_{\mathcal{SE}_{net}}$, of the typical UE, which accounts for the fact that the typical UE may not be served by the typical BS if it is turned off because it does not fulfill the TIN optimality conditions. $\mathcal{R}_{\mathcal{SE}_{net}}$ can be formulated as follows:

$$\mathcal{R}_{\mathcal{SE}_{net}} = \mathbb{P}\left[\mathbb{A}_{\mathbb{UE}}\right] \mathcal{R}_{\mathcal{SE}}, \tag{4.19}$$

where a similar notation as in (4.15) is used and $\mathcal{R}_{\mathcal{SE}}$ is the SINR average rate of the typical active UE. This latter average rate is defined and computed in the following theorem and is measured in nats/sec/Hz.

Theorem 4.2. *Let $\mathcal{R}_{\mathcal{SE}} = \mathbb{E}\left[\ln\left[1 + \mathrm{SINR}\right]\right]$, where the SINR is given in (4.14). The SINR average rate of the typical active UE, $\mathcal{R}_{\mathcal{SE}}$, can be formulated as follows:*

$$\mathcal{R}_{\mathcal{SE}} = \frac{2\pi\lambda_b}{\mathbb{P}\left[\mathbb{A}_{\mathbb{UE}}\right]} \int_0^\infty x_{11} \mathrm{e}^{\left(-\pi\lambda_b \max^2\left(x_{11}, x_{11}^{\mu/2}\left(\frac{P}{N}\right)^{\frac{2-\mu}{2\alpha}}\left(\frac{1}{M}\right)^{\frac{1}{2\alpha}}\right)\right)} \int_{\tau>0}^\infty \mathrm{e}^{\left(-\frac{N}{P}x_{11}^\alpha(\mathrm{e}^\tau - 1)\right)} \times \mathcal{L}_{\mathcal{I}}\left(x_{11}^\alpha\left(\mathrm{e}^\tau - 1\right)\right) \mathrm{d}\tau \mathrm{d}x_{11}, \tag{4.20}$$

where $\mathcal{L}_{\mathcal{I}}(\cdot)$ is the Laplace transform of the interference:

$$\mathcal{L}_{\mathcal{I}}\left(x_{11}^\alpha\left(\mathrm{e}^\tau - 1\right)\right) = \exp\left(\frac{-2\pi\lambda_b \mathbb{P}\left[\mathbb{A}_{\mathbb{UE}}\right]}{\alpha - 2} x_{11}^\alpha\left(\mathrm{e}^\tau - 1\right)\left(\max^2\left(x_{11}, x_{11}^{\mu/2}\left(\frac{P}{N}\right)^{\frac{2-\mu}{2\alpha}}\left(\frac{1}{M}\right)^{\frac{1}{2\alpha}}\right)\right)^{1-\frac{\alpha}{2}}\right.$$
$$\left. {}_2\mathrm{F}_1\left[1, 1 - \frac{2}{\alpha}, 2 - \frac{2}{\alpha}; -x_{11}^\alpha\left(\mathrm{e}^\tau - 1\right)\left(\max^2\left(x_{11}, x_{11}^{\mu/2}\left(\frac{P}{N}\right)^{\frac{2-\mu}{2\alpha}}\left(\frac{1}{M}\right)^{\frac{1}{2\alpha}}\right)\right)^{-\frac{\alpha}{2}}\right]\right) \tag{4.21}$$

Proof. By definition of SINR average rate, we have:

$$\begin{aligned}
&\mathcal{R}_{\mathcal{SE}} = \mathbb{E}\left[\ln\left[1+\mathrm{SINR}\right]\right] \\
&= \frac{2\pi\lambda_b}{\mathbb{P}\left[\mathbb{A}_{\mathbb{UE}}\right]}\int_0^\infty \mathbb{E}\left[\ln\left[1+\frac{h_{11}x_{11}^{-\alpha}}{I+\frac{N}{P}}\right]\right] x_{11}\mathrm{e}^{-\pi\lambda_b \max^2\left(x_{11},x_{11}^{\mu/2}\left(\frac{P}{N}\right)^{\frac{2-\mu}{2\alpha}}\left(\frac{1}{M}\right)^{\frac{1}{2\alpha}}\right)}\mathrm{d}x_{11} \\
&= \frac{2\pi\lambda_b}{\mathbb{P}\left[\mathbb{A}_{\mathbb{UE}}\right]}\int_0^\infty x_{11}\mathrm{e}^{-\pi\lambda_b \max^2\left(x_{11},x_{11}^{\mu/2}\left(\frac{P}{N}\right)^{\frac{2-\mu}{2\alpha}}\left(\frac{1}{M}\right)^{\frac{1}{2\alpha}}\right)}\int_{\tau>0}^\infty \mathbb{P}\left[\ln\left[1+\frac{h_{11}x_{11}^{-\alpha}}{I+\frac{N}{P}}\right]\geq\tau\right]\mathrm{d}\tau\mathrm{d}x_{11} \\
&= \frac{2\pi\lambda_b}{\mathbb{P}\left[\mathbb{A}_{\mathbb{UE}}\right]}\int_0^\infty x_{11}\mathrm{e}^{-\pi\lambda_b \max^2\left(x_{11},x_{11}^{\mu/2}\left(\frac{P}{N}\right)^{\frac{2-\mu}{2\alpha}}\left(\frac{1}{M}\right)^{\frac{1}{2\alpha}}\right)}\int_{\tau>0}^\infty \mathrm{e}^{-x_{11}^{\alpha}(\mathrm{e}^{\tau}-1)\frac{N}{P}}\mathcal{L}_I\left(x_{11}^{\alpha}\left(\mathrm{e}^{\tau}-1\right)\right)\mathrm{d}\tau\mathrm{d}x_{11},
\end{aligned} \tag{4.22}$$

where I denotes the other-cell interference and its Laplace transform $\mathcal{L}_I\left(x_{11}^{\alpha}\left(\mathrm{e}^{\tau}-1\right)\right)$ can be computed by using the same analytical steps as for the SINR coverage probability in Theorem 4.1. This concludes the proof. □

Corollary 4.2. *If $M=1$ and $\mu=2$, the SINR average rate in Theorem 4.2 simplifies as follows:*

$$\mathcal{R}_{\mathcal{SE}} = 2\pi\lambda_b\int_0^\infty x_{11}\mathrm{e}^{\left(-\pi\lambda_b x_{11}^2\right)}\int_{\tau>0}^\infty \mathrm{e}^{-\left(\frac{N}{P}x_{11}^{\alpha}(\mathrm{e}^{\tau}-1)+\pi\lambda_b x_{11}^2(\mathrm{e}^{\tau}-1)^{\frac{2}{\alpha}}\int_{(\mathrm{e}^{\tau}-1)^{-\frac{2}{\alpha}}}^\infty \frac{1}{1+z^{\alpha/2}}\mathrm{d}z\right)}\mathrm{d}\tau\mathrm{d}x_{11}, \tag{4.23}$$

which is the SINR average rate of a conventional cellular network if TIN is not applied [28].

4.4. Asymptotic Analysis and Optimization Problem

The aim of this section is to study the existence and optimal setup for the pair of system parameters M and μ, in order to maximize the effective SINR coverage probability. We focus our attention, in particular, on the effective SINR coverage probability, since the corresponding analytical framework is more tractable than (4.20).

The effective SINR coverage probability can be formulated as follows:

$$\mathcal{C}_{net} = 2\pi\lambda_b\int_0^\infty x_{11}\mathrm{e}^{-\pi\lambda_b \max^2\left(x_{11},x_{11}^{\mu/2}\left(\frac{P}{N}\right)^{\frac{2-\mu}{2\alpha}}\left(\frac{1}{M}\right)^{\frac{1}{2\alpha}}\right)}\mathrm{e}^{\left(-\frac{sN}{P}\right)}\mathcal{L}_{\mathcal{I}}\left(s\right)\mathrm{d}x_{11}, \tag{4.24}$$

where $s = x_{11}^{\alpha}\Theta$, and $\mathcal{L}_{\mathcal{I}}\left(\cdot\right)$ is given in (4.17).

For simplicity, and without loss of generality, we assume $M=1$ and focus our attention on optimizing $\mu\in[1,2]$. In order to find the optimal value of μ, it is convenient to have a closed form solution of the integral in (4.24). To this end, we employ the following approach.

First, we rewrite the $\max(\cdot,\cdot)$ function, which allows us to split the integration range as

follows:

$$\mathcal{C}_{net} = 2\pi\lambda_b \int_0^{\Upsilon^{\frac{1}{\alpha}}} x_{11} \mathrm{e}^{\left(-\pi\lambda_b x_{11}^{\mu} \Upsilon^{\frac{2-\mu}{\alpha}}\right)} \mathrm{e}^{\left(-\frac{x_{11}^{\alpha}\Theta}{\Upsilon}\right)} \mathrm{e}^{\left(-\pi\lambda_b \mathbb{P}[\mathbb{A}_{\mathbb{UE}}] x_{11}^2 \Theta^{\frac{2}{\alpha}} \int_{x_{11}^{\mu-2}\Theta^{\frac{-2}{\alpha}}\Upsilon^{\frac{2-\mu}{\alpha}}}^{\infty} \frac{1}{1+z^{\alpha/2}} \mathrm{d}z\right)} \mathrm{d}x_{11}$$
$$+ 2\pi\lambda_b \int_{\Upsilon^{\frac{1}{\alpha}}}^{\infty} x_{11} \mathrm{e}^{\left(-\pi\lambda_b x_{11}^2\right)} \mathrm{e}^{\left(-\frac{x_{11}^{\alpha}\Theta}{\Upsilon}\right)} \mathrm{e}^{\left(-\pi\lambda_b \mathbb{P}[\mathbb{A}_{\mathbb{UE}}] x_{11}^2 \Theta^{\frac{2}{\alpha}} \int_{\Theta^{\frac{-2}{\alpha}}}^{\infty} \frac{1}{1+z^{\alpha/2}} \mathrm{d}z\right)} \mathrm{d}x_{11}, \quad (4.25)$$

where we introduce the notation $\Upsilon = \frac{P}{N}$.

In (4.25), the second integral is negligible compared with the first integral for sufficiently high values of the SNR Υ (high SNR regime). Under this assumption, (4.25) can be approximated as follows:

$$\mathcal{C}_{net} \approx 2\pi\lambda_b \int_0^{\Upsilon^{\frac{1}{\alpha}}} x_{11} \mathrm{e}^{\left(-\pi\lambda_b x_{11}^{\mu} \Upsilon^{\frac{2-\mu}{\alpha}}\right)} \mathrm{e}^{\left(-\frac{x_{11}^{\alpha}\Theta}{\Upsilon}\right)} \mathrm{e}^{\left(-\pi\lambda_b \mathbb{P}[\mathbb{A}_{\mathbb{UE}}] x_{11}^2 \Theta^{\frac{2}{\alpha}} \int_{x_{11}^{\mu-2}\Theta^{\frac{-2}{\alpha}}\Upsilon^{\frac{2-\mu}{\alpha}}}^{\infty} \frac{1}{1+z^{\alpha/2}} \mathrm{d}z\right)} \mathrm{d}x_{11}. \quad (4.26)$$

It is known that the integral inside the exponential function can be expressed in terms of the Gauss hypergeometric function for general values of the path-loss exponent $\alpha > 2$ [28]. In order to better highlight the proposed approach, we assume $\alpha = 4$ in the sequel. A similar approach can be applied for other values of α. This generalization is left to the reader. By letting $\alpha = 4$ and by using some algebraic manipulations, (4.26) can be written as follows:

$$\mathcal{C}_{net} \approx 2\pi\lambda_b \int_0^{\Upsilon^{\frac{1}{4}}} x_{11} \mathrm{e}^{\left(-\pi\lambda_b x_{11}^{\mu} \Upsilon^{\frac{2-\mu}{4}}\right)} \mathrm{e}^{\left(-\frac{x_{11}^{4}\Theta}{\Upsilon}\right)} \mathrm{e}^{\left(-\pi\lambda_b \mathbb{P}[\mathbb{A}_{\mathbb{UE}}] x_{11}^2 \sqrt{\Theta}\left(\frac{\pi}{2} - \arctan\left(\frac{x_{11}^{\mu-2}\Upsilon^{\frac{2-\mu}{4}}}{\sqrt{\Theta}}\right)\right)\right)} \mathrm{d}x_{11}. \quad (4.27)$$

The term $\mathrm{e}^{\left(-\frac{x_{11}^{4}\Theta}{\Upsilon}\right)}$ can be ignored, because when Υ is dominant then $\mathrm{e}^{\left(-\frac{x_{11}^{4}\Theta}{\Upsilon}\right)} \approx 1$ and when the $x_{11}^4\Theta$ dominates then the rest of the integral tends to 0. Therefore, (4.27) simplifies as follows:

$$\mathcal{C}_{net} \approx 2\pi\lambda_b \int_0^{\Upsilon^{\frac{1}{4}}} x_{11} \mathrm{e}^{\left(-\pi\lambda_b x_{11}^{\mu} \Upsilon^{\frac{2-\mu}{4}} - \pi\lambda_b \mathbb{P}[\mathbb{A}_{\mathbb{UE}}] x_{11}^2 \sqrt{\Theta}\left(\frac{\pi}{2} - \arctan\left(\frac{x_{11}^{\mu-2}\Upsilon^{\frac{2-\mu}{4}}}{\sqrt{\Theta}}\right)\right)\right)} \mathrm{d}x_{11}. \quad (4.28)$$

In the next two sections, we further simplify (4.28) by considering large and small values of Θ, respectively.

4.4.1. Large Θ

By definition, $\mu \in [1,2]$. In addition, the function $\arctan(\cdot)$ becomes small for large values of Θ, i.e., $\arctan(1/\Theta) \approx 0$. Thus, it can be ignored for large values of Θ:

$$\mathcal{C}_{net} \approx 2\pi\lambda_b \int_0^{\Upsilon^{\frac{1}{4}}} x_{11} \mathrm{e}^{\left(-\pi\lambda_b x_{11}^{\mu} \Upsilon^{\frac{2-\mu}{4}} - \frac{\pi^2 \lambda_b \mathbb{P}[\mathbb{A}_{\mathbb{UE}}] x_{11}^2 \sqrt{\Theta}}{2}\right)} \mathrm{d}x_{11} = 2\pi\lambda_b \int_0^{\Upsilon^{\frac{1}{4}}} x_{11} \mathrm{e}^{\left(-A_1 x_{11}^{\mu} - A_2 x_{11}^2\right)} \mathrm{d}x_{11}, \tag{4.29}$$

where $A_1 = \pi\lambda_b \Upsilon^{\frac{2-\mu}{4}}$ and $A_2 = \frac{\pi^2 \lambda_b \mathbb{P}[\mathbb{A}_{\mathbb{UE}}] \sqrt{\Theta}}{2}$.

The integral in (4.29) cannot be formulated in a simple closed-form expression that is suitable to get insight for system optimization. To circumvent this issue, we express the exponential $\mathrm{e}^{\left(-A_1 x_{11}^u\right)}$ by using its power series representation:

$$\mathcal{C}_{net} \approx 2\pi\lambda_b \int_0^{\Upsilon^{\frac{1}{4}}} x_{11} \left[1 - \frac{A_1 x_{11}^{\mu}}{1!} + \frac{A_1^2 x_{11}^{2\mu}}{2!} - \frac{A_1^3 x_{11}^{3\mu}}{3!} + \frac{A_1^4 x_{11}^{4\mu}}{4!} + \cdots\right] \mathrm{e}^{\left(-A_2 x_{11}^2\right)} \mathrm{d}x_{11}. \tag{4.30}$$

To further simplify the analysis, since the high SNR assumption is considered, the upper integration limit can be simplified as $\Upsilon^{1/\alpha} \to \infty$. With the aid of this approximation, we obtain:

$$\begin{aligned}
\mathcal{C}_{net} &\approx 2\pi\lambda_b \left[\int_0^{\infty} x_{11} \mathrm{e}^{\left(-A_2 x_{11}^2\right)} \mathrm{d}x_{11} - \frac{A_1}{1!} \int_0^{\infty} x_{11}^{\mu+1} \mathrm{e}^{\left(-A_2 x_{11}^2\right)} \mathrm{d}x_{11} \right. \\
&\quad \left. + \frac{A_1^2}{2!} \int_0^{\infty} x_{11}^{2\mu+1} \mathrm{e}^{\left(-A_2 x_{11}^2\right)} \mathrm{d}x_{11} - \frac{A_1^3}{3!} \int_0^{\infty} x_{11}^{3\mu+1} \mathrm{e}^{\left(-A_2 x_{11}^2\right)} + \mathrm{d}x_{11} \cdots\right] \\
&\approx \pi\lambda_b \left[\frac{\Gamma(1)}{A_2} - \frac{A_1 \Gamma\left(\frac{\mu+2}{2}\right)}{A_2^{\frac{\mu+2}{2}}} + \frac{A_1^2 \Gamma\left(\frac{2\mu+2}{2}\right)}{2! A_2^{\frac{2\mu+2}{2}}} - \frac{A_1^3 \Gamma\left(\frac{3\mu+2}{2}\right)}{3! A_2^{\frac{3\mu+2}{2}}} + \frac{A_1^4 \Gamma\left(\frac{4\mu+2}{2}\right)}{4! A_2^{\frac{4\mu+2}{2}}} + \cdots\right],
\end{aligned} \tag{4.31}$$

where the last expression is obtained by solving each integral and writing it in terms of the Gamma function, i.e., $\int_0^{\infty} x^m \mathrm{e}^{-\zeta x^n} \mathrm{d}x = \frac{\Gamma(\gamma)}{n\zeta^{\gamma}}$ where $\gamma = \frac{m+1}{n}$ [92].

Equation (4.31) can be formulated, in a more compact form, as follows:

$$\mathcal{C}_{net} \approx \frac{\pi\lambda_b}{A_2} \sum_{n=0}^{\infty} \frac{(-1)^n R^{\frac{n}{2}} \Gamma\left(\frac{n\mu+2}{2}\right)}{n!}, \tag{4.32}$$

where $R = A_1^2 / A_2^{\mu}$.

It is not possible, to the best of our knowledge, to compute the explicit result of the series for arbitrary values of μ. This is possible, however, for the special case $\mu = 2$:

$$\mathcal{C}_{net} \approx= \frac{\pi\lambda_b}{A_1 + A_2}.$$

In Fig. 4.4, we plot R as a function of μ. We observe that, for constant values of λ_b

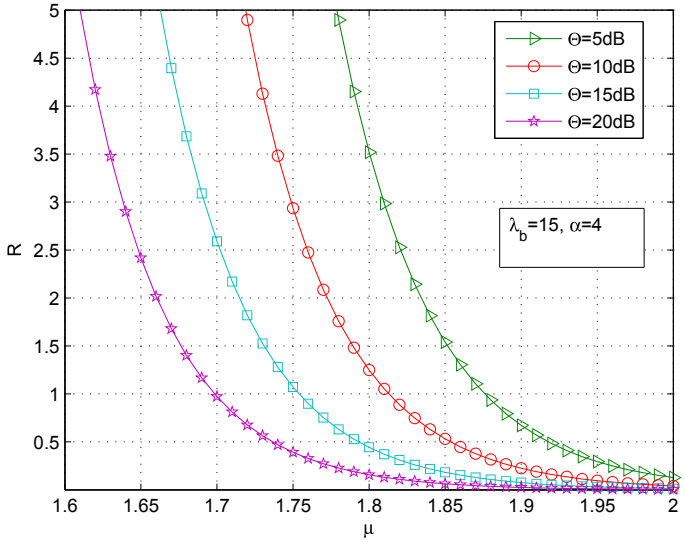

Figure 4.4.: R as a function of μ

and Υ, R decreases if μ increases. It is difficult, however, to find the analytical expression of the optimal value of μ that maximizes $\mathcal{C}_{net}$ in (4.32). To circumvent this issue, we have performed extensive Monte Carlo simulations and found that C_{net} is maximized by the value of μ that corresponds to $R = 1$.

As a result, the optimal value of μ that maximizes C_{net} is the unique solution of the following equation $R = 1$:

$$A_1^2 - A_2^{\mu} = \left(\pi^2 \lambda_b^2 \Upsilon^{\frac{2-\mu}{2}}\right) - \left(\frac{\pi^2 \lambda_b \mathbb{P}\left[\mathbb{A}_{\mathbb{UE}}\right] \sqrt{\Theta}}{2}\right)^{\mu} = 0. \tag{4.33}$$

To compute the optimal value of μ, a tractable expression of $\mathbb{P}\left[\mathbb{A}_{\mathbb{UE}}\right]$ is needed, which is itself a function of μ. From (4.9), $\mathbb{P}\left[\mathbb{A}_{\mathbb{UE}}\right]$ can be computed as follows:

$$\mathbb{P}\left[\mathbb{A}_{\mathbb{UE}}\right] = 2\left(\pi\lambda_b\right)^2 \int_0^{\infty} x_{21} \mathrm{e}^{-\pi\lambda_b x_{21}^2} \min^2\left(x_{21}, \Upsilon^{\frac{\mu-2}{4\mu}} x_{21}^{\frac{2}{\mu}}\right) \mathrm{d}x_{21} \approx \frac{2\,\Gamma\left(\frac{2}{u}\right)}{\mu\left(\pi\lambda_b\right)^{\frac{2}{\mu}-1} \Upsilon^{\frac{1}{\mu}-\frac{1}{2}}}, \tag{4.34}$$

where the approximation is obtained by using similar approximations as those used for computing C_{net} in the high SNR regime.

By inserting (4.34) in (4.33) and with the aid of some algebraic manipulations, we obtain:

$$\mu^{\mu}\left(\pi\lambda_b\right)^4 \Upsilon^{2-\mu} - \left(\pi^3 \lambda_b^2 \sqrt{\Theta}\,\Gamma\left(\frac{2}{\mu}\right)\right)^{\mu} = 0. \tag{4.35}$$

The optimization problem in (4.35) is much simpler to solve than (4.24). For example, it can be easily solved by using the `fzero` function in Matlab. By direct inspection of (4.35), in addition, the following conclusions can be drawn. The minuend term, $\mu^{\mu}\left(\pi\lambda_b\right)^4 \Upsilon^{2-\mu}$, is independent of Θ, and the subtrahend term, $\left(\pi^3 \lambda_b^2 \sqrt{\Theta}\,\Gamma\left(\frac{2}{\mu}\right)\right)^{\mu}$, is dependent on Θ. In

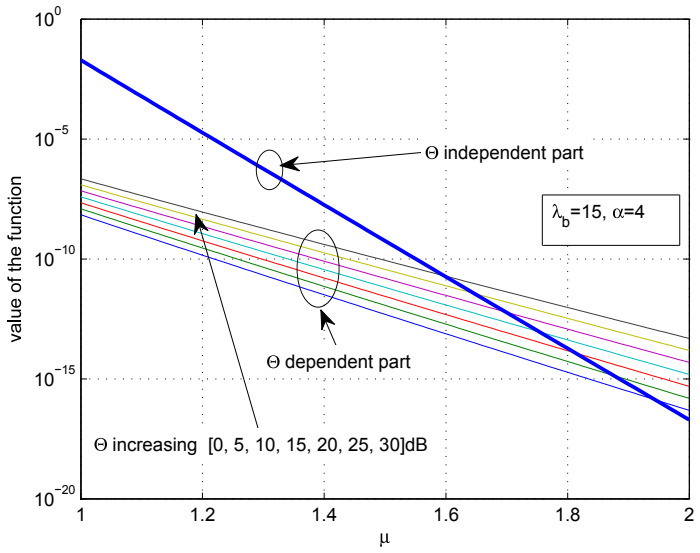

Figure 4.5.: Inspection of the optimization problem (4.35)

the minuend, the term μ^{μ} increases as μ increases from 1 to 2, but the term $\Upsilon^{2-\mu}$ decreases very rapidly with the same increase of μ. This suggests that the minuend is a decreasing function of μ. For fixed and realistic values of λ_b and Θ, the subtrahend decreases if μ increases. We plot both the minuend and subtrahend terms in Fig. 4.5. It can be observed that, for the given parameters, both the minuend and subtrahend decrease if μ increases. The minuend and subtrahend terms, however, cross each other in exactly one point, which guarantees that there is a unique optimal value of μ that maximizes the effective coverage probability.

In Fig. 4.6, we show that, for each value of Θ, an optimal value of μ exists. In addition, the accuracy of the solution of (4.35) compared with the exact values of μ that maximizes (4.24) is studied. A good accuracy is obtained. Fig. 4.6a, in particular, shows that the effective coverage probability is maximized for values of μ smaller than 2, which correspond to a conventional cellular network where TIN is not applied.

4.4.2. Small Θ

In this section, we study the existence of optimal values of μ for small values of the SINR threshold. If Θ is small, i.e. $\Theta \approx 0$, we have $\arctan\left(\frac{x_{11}^{\mu-2}\Upsilon^{\frac{2-\mu}{4}}}{\sqrt{\Theta}}\right) = \arctan(\infty) = \frac{\pi}{2}$, and (4.28) reduces to:

$$\mathcal{C}_{net} \approx 2\pi\lambda_b \int_0^{\infty} x_{11} \mathrm{e}^{\left(-\pi\lambda_b x_{11}^{\mu}\Upsilon^{\frac{2-\mu}{4}}\right)} \mathrm{d}x_{11} \approx \frac{2\,\Gamma\left(\frac{2}{u}\right)}{\mu\,(\pi\lambda_b)^{\frac{2}{\mu}-1}\,\Upsilon^{\frac{1}{\mu}-\frac{1}{2}}}. \tag{4.36}$$

By direct inspection of (4.36), we evince that $\mathcal{C}_{net}$ increases if μ increases. In particular, $\mathcal{C}_{net} = 1$ when $\mu = 2$. This finding suggests that there is no need to turn any BSs off if the

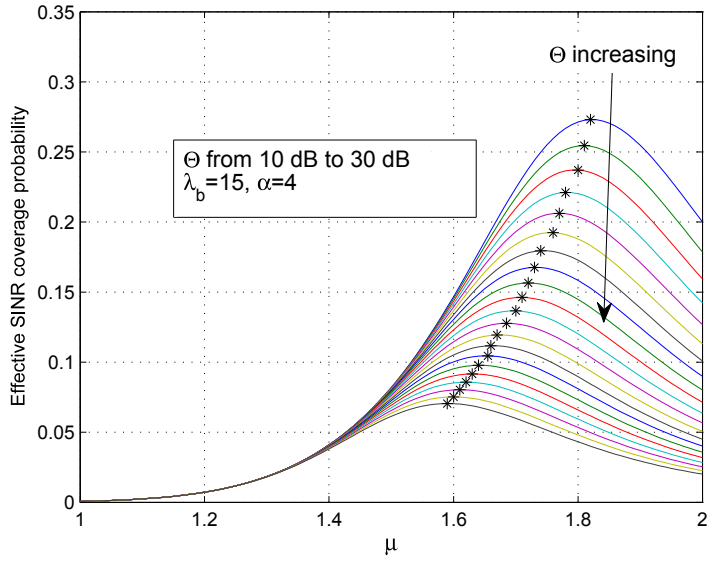

(a) Effective SINR Coverage probability

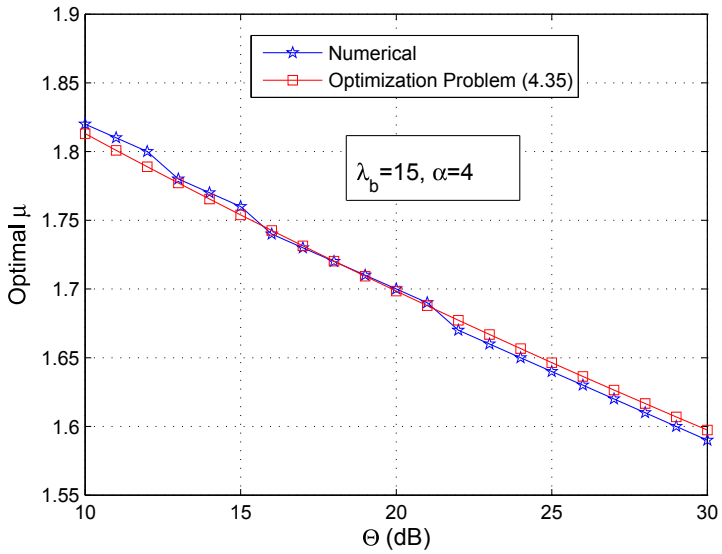

(b) Optimal μ

Figure 4.6.: Optimal μ for high SINR threshold Θ

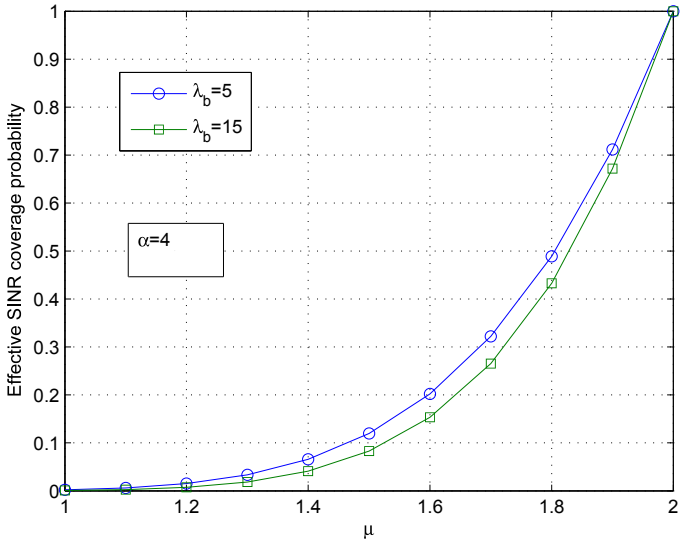

Figure 4.7.: Optimal μ when Θ is very small

SINR threshold is small. For small values of Θ, in other words, there is no need to apply TIN. Figure 4.7 confirms this conclusion.

4.5. Results and Discussion

In this section, we illustrate some numerical and simulation results. We emphasize that the Monte Carlo simulation results are generated without any approximations or assumptions that are exploited to obtain the analytical frameworks. As for the simulation setup, we set $P = 46$ dBm and $N = -110$ dBm/Hz.

In Fig. 4.8, we plot the probability of TIN against μ. The figure shows that the probability of TIN increases with μ. It can be observed that the probability of TIN is zero if $\mu = 1$ and tends to one if $M = 10$ and $\mu = 1.9$. Similarly, the probability tends to one if $M = 1$ and $\mu = 2$. We remind the reader that no BSs are turned off if the probability of TIN is equal to one. In other words, every BS schedules a UE in any given time slot, as in conventional cellular networks. This illustrates that both M and μ are tunable parameters that control the number of UEs to be scheduled. For simplicity, and without loss of generality, we keep $M = 1$ and vary μ in the rest of the results.

In Fig. 4.9, we plot the probability of TIN versus the density of the BS. It can be observed that, for a given value of μ, the probability of TIN decreases if λ_b increases. This result shows that, if we increase λ_b, the probability that the UEs satisfy the TIN criterion in (4.8) reduces. This is due to the increase of the amount of interference in the network.

Fig. 4.10 shows the effect of the path-loss exponent on the probability of TIN. It can be observed that the probability of TIN increases if α increases. If the path-loss exponent is large, the interference received at a UE is low, and, therefore, the probability that a UE

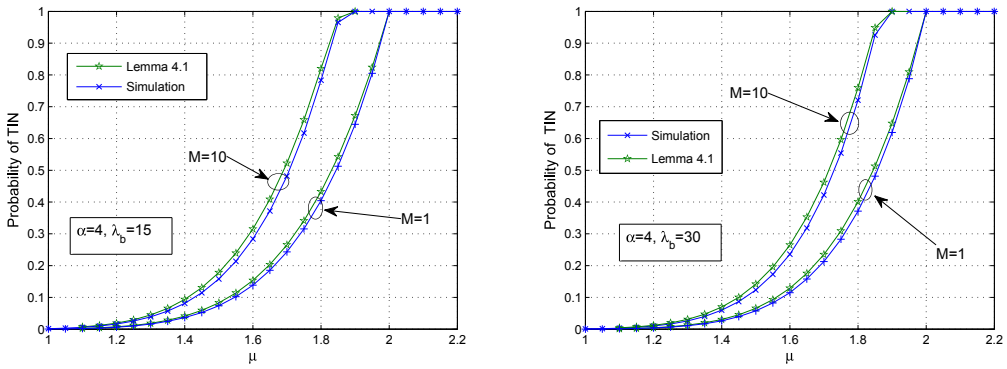

(a) (b)

Figure 4.8.: Probability of TIN versus μ

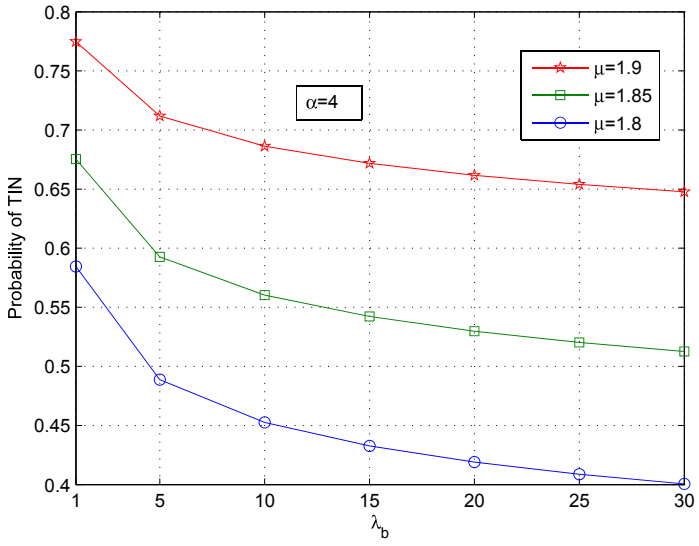

Figure 4.9.: Probability of TIN versus λ_b

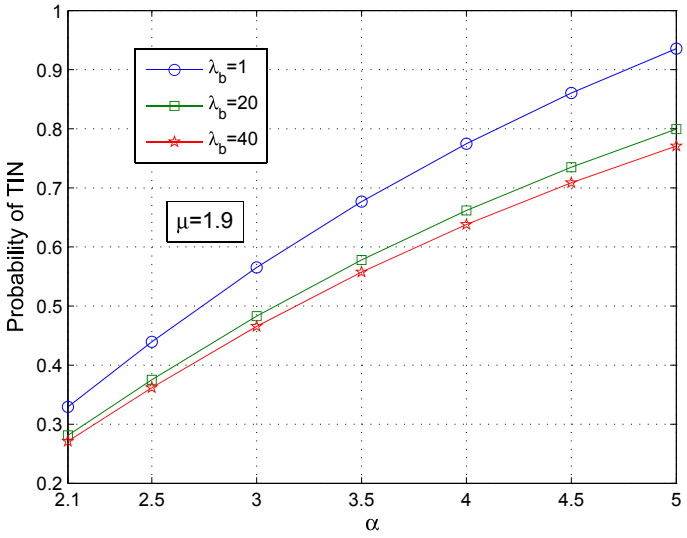

Figure 4.10.: Probability of TIN versus α

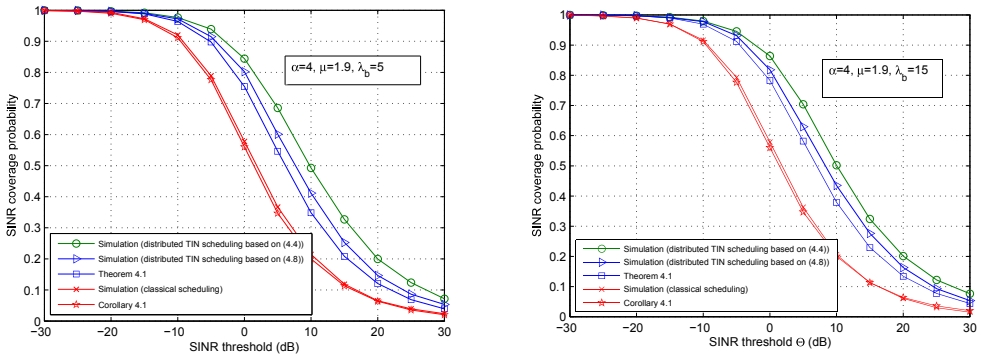

(a) (b)

Figure 4.11.: SINR coverage probability

satisfies the TIN criterion increases (4.8).

Fig. 4.11 compares the simulation and analytical curves of the SINR coverage probability. We remind the reader that the first simulation curve is obtained if the TIN-based scheduling is based on (4.4) and the second simulation curve is obtained if the TIN-based scheduling is based on (4.8). The curve corresponding to the classical scheduling is obtained by not turning any BSs off. The figure highlights that the analytical and simulation curves are quite close to each other, which substantiates the accuracy of our analysis. The small gap between the two curves originates from the approximations discussed in Section 4.3.1.

Fig. 4.12 illustrates the effect of λ_b and Θ on the optimal value of μ that maximizes the SINR coverage probability. The optimal value of μ is obtained as the solution of (4.35). The figure highlights that the optimal value of μ decreases if the SINR threshold increases. This shows that, for large values of the SINR threshold, more BSs need to be turned off

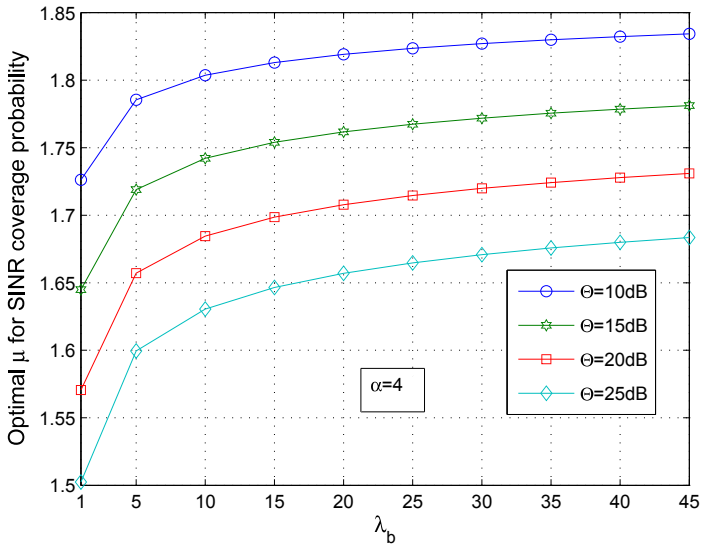

Figure 4.12.: Optimal μ for SINR coverage probability

to maximize the effective coverage probability. Furthermore, it can be observed that the optimal value of μ increases if the density of the BSs increases. To understand this effect, we need to consider the effect of λ_b on the probability of TIN. We have seen in Fig. 4.9 that the probability of TIN decreases if the density of the BS increases. Our optimization problem not only maximizes the SINR coverage probability, but, at the same time, tries to turn the smallest number of BSs off. Therefore, the optimal value of μ increases by increasing the density of the BS.

Fig. 4.13 shows the SINR coverage probability gain provided by our proposed distributed TIN-based scheduling scheme compared with the conventional scheduling scheme where no BSs are turned off. The optimal value of μ is obtained from (4.35) if the distributed TIN scheduling algorithm is based on (4.8). It is obtained through simulations, on the other hand, if the distributed TIN scheduling algorithm is based on (4.4). It can be observed that the improvement provided by the distributed TIN scheduling scheme over the conventional scheduling scheme changes with the SINR threshold. Specifically, it can be noticed that, if $\Theta = 10$dB, the improvement is 67% when the distributed TIN scheduling is based on (4.4), and 36% when the distributed TIN scheduling is based on (4.8).

In Fig. 4.14, we depict the effective average rate against the density of the BSs. The curves of the distributed TIN scheduling are obtained by setting $\mu = 1.9$. It can be observed that the distributed TIN scheduling based on (4.4) improves the average rate by 21%, whereas the distributed TIN scheduling based on (4.8) improves the average rate by 11%. Furthermore, it can be observed that the gain remains constant for various values of λ_b. From Fig. 4.13 and 4.14, it can be concluded that a simple distributed TIN-based scheduling algorithm significantly enhances the SINR effective coverage probability and the effective average rate.

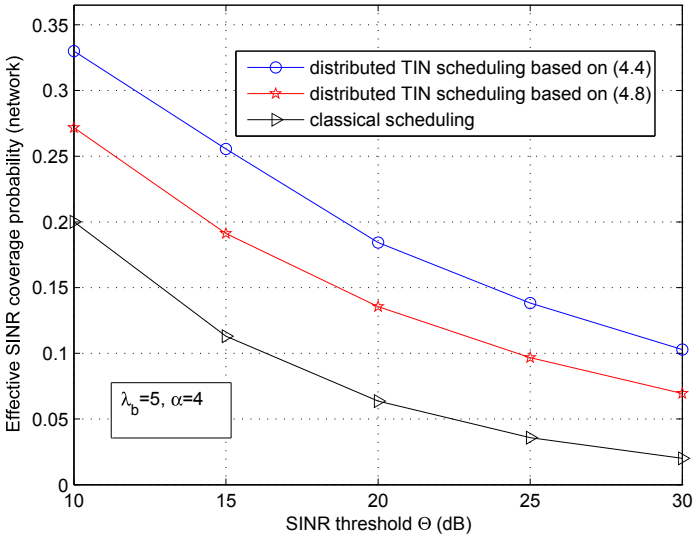

Figure 4.13.: SINR coverage probability gain

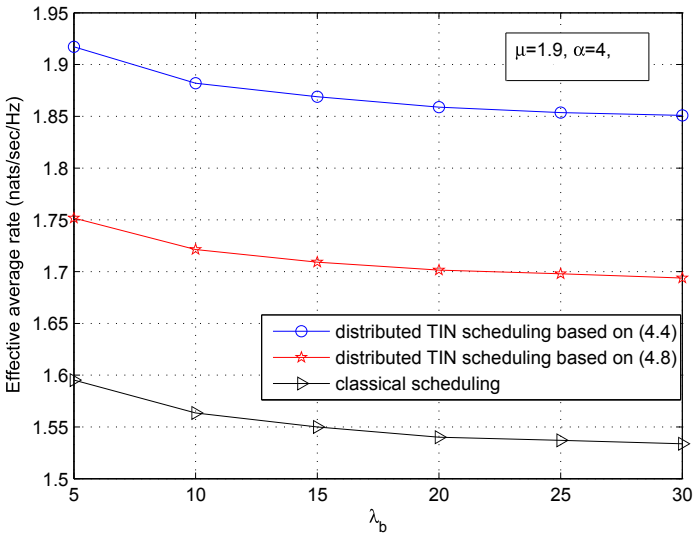

Figure 4.14.: Average rate gain

4.6. Chapter Summary

In this chapter, we have proposed a simple scheduling algorithm for application to cellular networks that is based on the TIN optimality condition. The original form of the scheduling algorithm is shown not to be mathematically tractable. To overcome this issue, we have proposed a simplified analytical framework to estimate the SINR effective coverage probability and the effective average rate by using stochastic geometry tools. To enable a simple optimization of the system parameters, we have developed simplified analytical frameworks in the high SNR regime, and for small and large values of the SINR decoding threshold. By optimizing the system with the aid of the proposed analytical frameworks, it is shown that the proposed TIN-based scheduling algorithm outperforms conventional cellular networks in terms of effective coverage probability and effective average rate.

In the next chapter, the work presented in this thesis is concluded and some future research directions are highlighted.

5. Conclusion

In this thesis, stochastic geometry tools have been used to model, analyze and design various large-scale wireless networks with random topologies. For the sake of the simplicity and tractability of the analysis, the Poisson point process based abstraction model for the spatial modeling of the network elements has been adopted.

We have seen in this thesis that stochastic geometry enables us to analytically model large-scale wireless networks, thanks to its amazing tractability. In Chapters 2, 3 and 4, we have seen that nice insights can be obtained, especially for the plausible special cases.

Correlation among the interfering nodes is difficult to model. However, correlation between the typical node and the interfering nodes can be modeled easily and we have realized in Chapters 2 and 4 that the resulting analysis is sufficiently accurate. Optimization in stochastic geometry is challenging; however, with some asymptotic simplification it can be performed. In the following, we provide chapter-wise details.

In Chapter 2, a tractable uplink model for the analysis and design of a two-tier heterogeneous network having multiple antennas at the BSs has been proposed. The performance of the network in term of SIR coverage probability and rate coverage probability has been quantified. Furthermore, the idea of downlink and uplink decoupling has been studied, and how to get the optimal performance in such a decoupled accessed networks has been shown.

In Chapter 3, a general framework has been presented to study the performance of an ad-hoc network that uses a combination of wireless power transfer and backscatter communications. The coverage and capacity of a such network in terms of easily computable expressions have been provided. The performance of this network is further compared with the regular powered network and it has been shown that for some parameters the performance of both the networks is comparable.

In Chapter 4, a scheduling algorithm for the cellular networks has been proposed that is based on a well-known interference management technique in information theory, known as treating interference as noise. The gains of this scheduling algorithm over the classical scheduling algorithm in term of SINR coverage probability and average rate of the network, for the downlink transmission, have been quantified. In order to obtain the optimal system parameters that provide the maximum gains, an asymptotic analysis has been performed. This asymptotic analysis resulted in a simple optimization algorithm for the optimal system parameters.

5.1. Future Work

There are many open and interesting research directions, related to the problems discussed in this thesis that can be studied. Some of them are the following:

- In Chapter 2, we considered multiple antennas at the BSs and single antennas at the UEs, future-work might study the performance of both the downlink and uplink for the MIMO networks, and find the optimal offloading strategy, which jointly optimizes both the downlink and the uplink performance. Another important research direction is to investigate the potential gain offered by using both the multiple antennas BSs and the interference cancellation scheme.

- In Chapter 3, the minimum circuit-power threshold is not considered, therefore, a future study might consider a minimum circuit-power threshold on the harvested power of the BN and if the harvested power threshold is not satisfied then the BN will not backscatter the signal. It would also be interesting to incorporate different collisions resolution schemes, such as using directional antennas and/or successive interference cancellation and study its effect on the performance of this wireless powered backscatter network.

- In Chapter 4, a TIN based scheduling algorithm has been proposed and its performance for the downlink transmissions in the cellular networks has been studied. A future work can study the performance of a such scheduling algorithm in the uplink. The exact analysis in the uplink is even more challenging than the downlink; however, we expect that a nice approximation can be obtained. In this work, we have proposed an optimization algorithm for the SINR coverage probability. A similar asymptotic analysis can be performed for the average rate. Another interesting extension would be to study the energy efficiency of this scheduling algorithm in cellular networks. Furthermore, the fairness of the scheduling algorithm is not investigated in this work. Hence, it is important and interesting to study the fairness of the proposed scheduling algorithm.

A. Proofs for Chapter 2

A.1. Proof of Lemma 2.1

The association criterion when a typical UE connects to a MBS both in the UL and DL is given by

$$\mathbb{P}\left[\left\{P_M\mathbb{E}\left\{\|\mathbf{h}_M\|^2\right\}X_M^{-\alpha_M} > P_F\mathbb{E}\left\{\|\mathbf{h}_F\|^2\right\}X_F^{-\alpha_F}\right\}\bigcap \left\{B_M\mathbb{E}\left\{\|\mathbf{h}_M\|^2\right\}X_M^{-\alpha_M} > B_F\mathbb{E}\left\{\|\mathbf{h}_F\|^2\right\}X_F^{-\alpha_F}\right\}\right]$$

where the expectation is over the channel fading. The $\mathbb{E}\left\{\|\mathbf{h}_M\|^2\right\} = N_M$, $\mathbb{E}\left\{|h_F|^2\right\} = N_F$, where N_M, and N_F are the array gains and represent the number of antennas at an MBS and FBS respectively [114]. B_F and B_M are bias factors towards the femto-tier and the macro-tier respectively. The above equation can be equivalently written as

$$\mathbb{P}\left[\left\{P_M N_M X_M^{-\alpha_M} > P_F N_F X_F^{-\alpha_F}\right\}\bigcap\left\{B_M N_M X_M^{-\alpha_M} > B_F N_F X_F^{-\alpha_F}\right\}\right].$$

We know that $P_F < P_M$ and when $\frac{B_F}{B_M} \geq \frac{P_F}{P_M}$, it can be easily observed that the common region in the above equation is $N_M X_M^{-\alpha_M} > \frac{B_F}{B_M} N_F X_F^{-\alpha_F}$, or equivalently $X_F > \left(\frac{B_F N_F}{B_M N_M}\right)^{(1/\alpha_F)} X_M^{\alpha_M/\alpha_F}$. Similarly, when $\frac{B_F}{B_M} < \frac{P_F}{P_M}$ then the common region is $X_F > \left(\frac{P_F N_F}{P_M N_M}\right)^{(1/\alpha_F)} X_M^{\alpha_M/\alpha_F}$ and the probability is calculated as

$$\mathbb{P}\left(case1\right) = \mathbb{P}\left(X_F > a\right) = \int_0^\infty \left(1 - F_{X_F}\left(a\right)\right) f_{X_M}\left(X_M\right) \mathrm{d}_{\mathrm{X_M}},$$

where $a = \Upsilon_1^{1/\alpha_F} X_M^{\alpha_M/\alpha_F}$, while for $\frac{B_F}{B_M} \geq \frac{P_F}{P_M}$, $\Upsilon_1 = \frac{B_F N_F}{B_M N_M}$ and for $\frac{B_F}{B_M} < \frac{P_F}{P_M}$, $\Upsilon_1 = \frac{P_F N_F}{P_M N_M}$. Using the null probability of 2-D PPP, $F_{X_F}\left(X_M\right) = 1 - e^{-\pi\lambda_F X_M^2}$, $f_{X_M}\left(X_M\right) = 2\pi\lambda_M X_M e^{-\pi\lambda_M X_M^2}$ and evaluating the integral we obtain (2.4).

A.2. Proof of Lemma 2.4

The distance X_K between a typical UE and the tagged BS is a random variable. The event $X_K > x$ is equivalent to the event that $X_K > x$ given that a typical user is attached to the

Kth tier (proof follows a similar method as in [29])

$$\mathbb{P}\left[X_K > x\right] = \mathbb{P}\left[X_K > x | n = K\right] = \frac{\mathbb{P}\left[X_K > x, n = K\right]}{\mathcal{A}_K}, \tag{A.1}$$

where $\mathbb{P}\left[n = K\right] = \mathcal{A}_K$ is the tier association probability given by (2.7). Let Pr_K and Pr_J respectively be the biased received power from a typical UE at the nearest Kth tier and Jth tier BS then the joint probability $\mathbb{P}\left[X_K > x, n = K\right]$ can be expressed as

$$\begin{aligned}\mathbb{P}\left[X_K > x, n = K\right] &= \mathbb{P}\left[X_K > x, Pr_K(X_K) > Pr_j\right] \\ &= \int_x^\infty \mathbb{P}\left[B_K N_K X_K^{-\alpha_K} > B_J N_J X_J^{-\alpha_J}\right] f_{X_K}\left(X_K\right) \mathrm{d}_{\mathrm{X_K}} \\ &= \int_x^\infty \mathbb{P}\left[X_J > \left(\frac{B_J N_J}{B_K N_K}\right)^{1/\alpha_J} X_K^{\alpha_K/\alpha_J}\right] f_{X_K}\left(X_K\right) \mathrm{d}_{\mathrm{X_K}}.\end{aligned}$$

From the 2-D null probability of PPP, we obtain $\mathbb{P}\left[X_J > \left(\frac{B_J N_J}{B_K N_K}\right)^{1/\alpha_J} X_K^{\alpha_K/\alpha_J}\right] = \exp\left\{-\pi\lambda_J \left(\frac{B_J N_J}{B_K N_K}\right)^{2/\alpha_J} \left(X_K^{\alpha_K/\alpha_J}\right)^2\right\}$, and $f_{X_K}\left(X_K\right) = 2\pi\lambda_K X_K \exp\left\{-\pi\lambda_K X_K^2\right\}$, and inserting in the above equation, we get

$$\begin{aligned}\mathbb{P}\left[X_K > x, n = K\right] = 2\pi\lambda_K \int_x^\infty X_K \times \\ \exp\left\{-\pi\left(\lambda_K X_K^2 + \lambda_J \left(\frac{B_J N_J}{B_K N_K}\right)^{2/\alpha_J}\right)\left(X_K^{\alpha_K/\alpha_J}\right)^2\right\} \mathrm{d}_{\mathrm{X_K}}.\end{aligned} \tag{A.2}$$

By inserting (A.2) in (A.1), we get the following

$$\mathbb{P}\left[X_K > x\right] = \frac{2\pi\lambda_K}{\mathcal{A}_K} \int_x^\infty X_K \exp\left\{-\pi\left(\lambda_K X_K^2 + \lambda_J \left(\frac{B_J N_J}{B_K N_K}\right)^{2/\alpha_J}\right)\left(X_K^{\alpha_K/\alpha_J}\right)^2\right\} \mathrm{d}_{\mathrm{X_K}}, \tag{A.3}$$

which is the complementary cumulative distribution function (CCDF) of X_K, while it CDF is $F_{X_K}(x) = 1 - \mathbb{P}\left[X_K > x\right]$, and probability density function is $f_{X_K}\left(x\right) = \frac{d}{dx} F_{X_K}\left(x\right)$. Thus, we obtain (2.9).

A.3. Proof of Theorem 2.1

We consider multiple antenna BSs and use MRC combining, therefore, the signal channel follows Gamma $\left(N_K, 1\right)$, whereas the interfering channel still follows an exponential distribution [61]. Let X_K be the distance between a typical UE and its serving Kth tier BS

then the coverage probability $\mathcal{C}_K$ for a given threshold can be written as

$$\mathcal{C}_K(\tau_K) \triangleq \mathbb{E}_{X_K}\left[\mathbb{P}\left[\mathrm{SIR}_{X_K} \geq \tau | X_K\right]\right] = \int_0^\infty \mathbb{P}\left[\mathrm{SIR}_{X_K} \geq \tau_K | X_K\right] f_{X_K}(X_K)\, \mathrm{d_X_K}$$
$$= \frac{2\pi\lambda_K}{\mathcal{A}_K} \int_0^\infty \mathbb{P}\left[\mathrm{SIR}_{X_K} \geq \tau_K | X_K\right] X_K$$
$$\exp\left\{-\pi\left(\lambda_K X_K^2 + \lambda_J \left(\frac{B_J N_J}{B_K N_K}\right)^{2/\alpha_J} X_K^{2(\alpha_K/\alpha_J)}\right)\right\} \mathrm{d_X_K}, \quad \text{(A.4)}$$

where the last expression follows by inserting $f_{X_K}(.)$ from (2.9). For an interference limited network, the $\mathbb{P}\left[\mathrm{SIR}_{X_K} > \tau_K | X_K\right]$ can be written as

$$\mathbb{P}\left[\mathrm{SIR}_{X_K} \geq \tau_K | X_K\right] \overset{1}{=} \mathbb{P}\left[\frac{\|\mathbf{h}_{K_0}\|^2 X_K^{\alpha_K(\eta-1)}}{\sum\limits_{i\in\Phi'_K\setminus u_0} \left|\frac{\mathbf{h}_{K_0}^H \mathbf{h}_{K_i}}{\|\mathbf{h}_{K_0}\|}\right|^2 X_{K_i}^{\alpha_K\eta} D_{K_i}^{-\alpha_K} + \sum\limits_{q\in\Phi'_J} \left|\frac{\mathbf{h}_{K_0}^H \mathbf{h}_{J_q}}{\|\mathbf{h}_{K_0}\|}\right|^2 X_{J_q}^{\alpha_J\eta} D_{J_q}^{-\alpha_K}} \geq \tau_K\right]$$
$$= \mathbb{P}\left[\|\mathbf{h}_{K_0}\|^2 > sI | X_K\right] \overset{2}{=} \mathbb{E}_I\left[\sum_{n=0}^{N_K-1} s^n I^n e^{-sI}\right] \overset{3}{=} \sum_{n=0}^{N_K-1} \frac{s^n (-1)^n}{n!} \frac{\mathrm{d}^n}{\mathrm{d}s^n} \mathcal{L}_I(s) \quad \text{(A.5)}$$

where $s = \tau_K X_K^{\alpha_K(1-\eta)}$, $I = \sum\limits_{i\in\Phi'_K\setminus u_0} g_i X_{K_i}^{\alpha_K\eta} D_{K_i}^{-\alpha_K} + \sum\limits_{q\in\Phi'_J} g_q X_{J_q}^{\alpha_J\eta} D_{J_q}^{-\alpha_K}$, $g_i = \left|\frac{\mathbf{h}_{K_0}^H \mathbf{h}_{K_i}}{\|\mathbf{h}_{K_0}\|}\right|^2$, and $g_q = \left|\frac{\mathbf{h}_{K_0}^H \mathbf{h}_{J_q}}{\|\mathbf{h}_{K_0}\|}\right|^2$. The expression after (1) follows due to the definition of SIR, (2) follows due to $\mathbf{h}_{K_0} \sim \mathrm{Gamma}(N_K, 1)$, and (3) follows due to the Laplace transform identity $\mathcal{L}\left\{I^n e^{-sI}\right\} = (-1)^n \frac{\mathrm{d}^n}{\mathrm{d}s^n}\mathcal{L}_I(s)$.

Next, we find the Laplace transform $\mathcal{L}_I(s)$ of the interference as follows:

$$\begin{aligned}
&\mathcal{L}_I(s) = \mathbb{E}_I\left[e^{-sI_K}\right] \\
&\overset{a}{=}\mathbb{E}_{g_i,X_{K_i},D_{K_i}}\left[\exp\left(-s\sum_{i\in\Phi'_K\setminus u_0} g_i X_{K_i}^{\alpha_K\eta} D_{K_i}^{-\alpha_K}\right)\right]\mathbb{E}_{g_q,X_{J_q},D_{J_q}}\left[\exp\left(-s\sum_{q\in\Phi'_J} g_q X_{J_q}^{\alpha_J\eta} D_{J_q}^{-\alpha_K}\right)\right] \\
&\overset{b}{=}\mathbb{E}_{X_{K_i},D_{K_i}}\left[\prod_{i\in\Phi'_K\setminus u_0}\mathbb{E}_{g_i}\left[\exp\left(-sg_i X_{K_i}^{\alpha_K\eta} D_{K_i}^{-\alpha_K}\right)\right]\right]\mathbb{E}_{X_{J_q},D_{J_q}}\left[\prod_{q\in\Phi'_J}\mathbb{E}_{g_q}\left[\exp\left(-sg_q X_{J_q}^{\alpha_J\eta} D_{J_q}^{-\alpha_K}\right)\right]\right] \\
&\overset{c}{=}\mathbb{E}_{D_{K_i}}\left[\prod_{i\in\Phi'_K\setminus u_0}\mathbb{E}_{X_{K_i}}\left[\frac{1}{1+sX_{K_i}^{\alpha_K\eta}D_{K_i}^{-\alpha_K}}\right]\right]\mathbb{E}_{D_{J_q}}\left[\prod_{q\in\Phi'_J}\mathbb{E}_{X_{J_q}}\left[\frac{1}{1+sX_{J_q}^{\alpha_J\eta}D_{J_q}^{-\alpha_K}}\right]\right] \\
&\overset{d}{=}\exp\left(-2\pi\lambda_K\int_{X_K}^{\infty}\left(1-\mathbb{E}_{X_{K_i}}\left[\frac{1}{1+sX_{K_i}^{\alpha_K\eta}u^{-\alpha_K}}\right]\right)u\mathrm{du}\right)\times \\
&\exp\left(-2\pi\lambda_J\int_{\left(\frac{N_JB_JX_K^{\alpha_K}}{N_KB_K}\right)^{1/\alpha_J}}^{\infty}\left(1-\mathbb{E}_{X_{J_q}}\left[\frac{1}{1+sX_{J_q}^{\alpha_J\eta}v^{-\alpha_K}}\right]\right)v\mathrm{dv}\right) \\
&\overset{e}{=}\exp\left(-2\pi\lambda_K\int_{X_K}^{\infty}\left(\int_0^u\frac{1}{1+s^{-1}X_{K_i}^{-\alpha_K\eta}u^{\alpha_K}}f_{X_{K_i}}(X_{K_i})\,\mathrm{d_{X_{K_i}}}\right)u\mathrm{du}\right)\times \\
&\exp\left(-2\pi\lambda_J\int_{\left(\frac{N_JB_JX_K^{\alpha_K}}{N_KB_K}\right)^{1/\alpha_J}}^{\infty}\left(\int_0^{\left(\frac{N_JB_Jv^{\alpha_K}}{N_KB_K}\right)^{1/\alpha_J}}\frac{1}{1+s^{-1}X_{J_q}^{-\alpha_J\eta}v^{\alpha_K}}f_{X_{J_q}}(X_{J_q})\,\mathrm{d_{X_{J_q}}}\right)v\mathrm{dv}\right) \\
&\overset{f}{=}\exp\left(-\pi\lambda_K\int_0^{\infty}s^{2/\alpha_K}X_{K_i}^{2\eta}\left(\int_{s^{-2/\alpha_K}X_{K_i}^{2(1-\eta)}}^{\infty}\frac{1}{1+Z_K^{\alpha_K/2}}\mathrm{d_{Z_K}}\right)f_{X_{K_i}}(X_{K_i})\,\mathrm{d_{X_{K_i}}}\right)\times \\
&\exp\left(-\pi\lambda_J\int_0^{\infty}s^{2/\alpha_K}X_{J_q}^{2\alpha_J\eta/\alpha_K}\left(\int_{\zeta^{-2/\alpha_K}s^{-2/\alpha_K}X_{J_q}^{2\alpha_J(1-\eta)/\alpha_K}}^{\infty}\frac{1}{1+Z_J^{\alpha_K/2}}\mathrm{d_{Z_J}}\right)f_{X_{J_q}}(X_{J_q})\mathrm{d_{X_{J_q}}}\right) \\
&\overset{g}{=}\exp\left(\frac{-2\pi\lambda_K s}{\alpha_K-2}\int_0^{\infty}X_{K_i}^{2-\alpha_K(1-\eta)}{}_2\mathrm{F}_1\left[1,1-\frac{2}{\alpha_K},2-\frac{2}{\alpha_K};-sX_{K_i}^{-\alpha_K(1-\eta)}\right]f_{X_{K_i}}(X_{K_i})\,\mathrm{d_{X_{K_i}}}\right)\times \\
&\exp\left(\frac{-2\pi\lambda_J\zeta^{1-2/\alpha_K}s}{\alpha_K-2}\int_0^{\infty}X_{J_q}^{2\alpha_J/\alpha_K-\alpha_J(1-\eta)}\times\right. \\
&\left.{}_2\mathrm{F}_1\left[1,1-\frac{2}{\alpha_K},2-\frac{2}{\alpha_K};-s\zeta X_{J_i}^{-\alpha_J(1-\eta)}\right]f_{X_{J_q}}(X_{J_q})\,\mathrm{d_{X_{J_q}}}\right) \qquad \text{(A.6)}
\end{aligned}$$

where (a) follows because the interference is from both the femto-tier and macro-tier's scheduled users, and they are also independent of each other, (b) is due to the independent and identically distributed assumption of g_i and g_q, and both g_i and g_q are further independent of point process Φ, (c) is due to $g_i \sim \exp(1)$ and $g_q \sim \exp(1)$, and (d) follows due to the probability generating functional (PGFL) of PPP, which converts an expectation over a point process to an integral $\mathbb{E}\left[\prod_{x\in\Phi} f(x)\right] = \exp\left(-\lambda\int_{\mathbb{R}^2}(1-f(x))\,\mathrm{dx}\right)$ [7]. It is important to mention that in step (d) the integration limits in both of the integrals are not the same, i.e., the closest interferer of the serving tier can be at a distance X_K from the

typical BS, whereas the closest interferer of the non serving tier should be at a distance $\left(\frac{N_J B_J X_K^{\alpha_K}}{N_K B_K}\right)^{1/\alpha_J}$, as mentioned in Remark 2.2. In step (e), we apply the inner expectations, which are required for power control. Again, it is important to note that the distance distribution of an interfering UE to its serving BS is different from that of the typical UE to the tagged BS and for different tiers the distance distribution of an interfering UE to its serving BS are also different, as mentioned in Remark 2.1. This difference can be seen by the limits of the inner integral in both exponentials. Step (f) follows by changing the integration order, inserting $\zeta = \frac{N_J B_J}{N_K B_K}$ and some algebraic manipulations while (g) follows by writing the inner integrals as Gauss hypergeometric functions [92]. We combine the two exponentials and inserting it in (A.5) and then (A.5) into (A.4). Thus the proof is completed.

B. Proofs for Chapter 3

B.1. Proof of Theorem 3.1

By using the definition of γ_{R_0} in (3.6), we write $\mathcal{C}$ as

$$\mathcal{C} = \mathbb{P}\left[\gamma_{R_0} \geq \Theta\right] = \int_{0<x_{0,1}<x_{0,2}<\cdots<x_{0,N_{PB}}<\infty} \cdots \int \mathbb{P}\left[\gamma_{R_0} \geq \Theta | x_{0,1}, \cdots, x_{0,N_{PB}}\right] f_x(x_{0,1}, \cdots, x_{0,N_{PB}}) \mathrm{d}x_{0,1}, \cdots, \mathrm{d}x_{0,N_{PB}}, \quad \text{(B.1)}$$

where the integration is over the joint PDF of the distances $x_{0,1}, \cdots, x_{0,N_{PB}}$ to nearest N_{PB} PBs. Now, the conditional probability $\mathbb{P}\left[\gamma_{R_0} \geq \Theta | x_{0,1}, \cdots, x_{0,N_{PB}}\right]$ can be written as

$$\mathbb{P}\left[\gamma_{R_0} \geq \Theta | x_{0,1}, \cdots, x_{0,N_{PB}}\right] = \mathbb{P}\left[\frac{\mathbf{h}_{0,0}^b d_{0,0}^{-\alpha^b} \sum_{i=1}^{N_{PB}} x_{0,i}^{-\alpha^f}}{\sum_{j \in \Phi_{BN} \setminus BN_0} \mathbf{h}_{0,j}^b d_{0,j}^{-\alpha^b} \sum_{k=1}^{N_{PB}} x_{j,k}^{-\alpha^f} + \frac{N}{\beta P_{PB}}} \geq \Theta\right]$$
$$= \mathbb{P}\left[\mathbf{h}_{0,0}^b \geq s\left(I + \frac{N}{\beta P_{PB}}\right)\right] \overset{a}{=} \mathbb{E}_I\left[\exp(-s\left(I + \frac{N}{\beta P_{PB}}\right))\right] = \exp(-\frac{sN}{\beta P_{PB}})\mathcal{L}_I(s), \quad \text{(B.2)}$$

where $s = \frac{\Theta d_{0,0}^{\alpha^b}}{\sum_{i=1}^{N_{PB}} x_{0,i}^{-\alpha^f}}$, $I = \sum_{j \in \Phi_{BN} \setminus BN_0} \mathbf{h}_{0,j}^b d_{0,j}^{-\alpha^b} \sum_{k=1}^{N_{PB}} x_{j,k}^{-\alpha^f}$, (a) follows because $\mathbf{h}_{0,0}^b \sim \exp(1)$, and $\mathcal{L}_I(s) = \mathbb{E}_I\left[\exp\left(-sI\right)\right]$ is the Laplace transform of the interference I evaluated

at s. Next, we find the Laplace transform as

$$\mathcal{L}_I(s) = \mathbb{E}_I\left[\exp(-sI)\right] = \mathbb{E}_{\mathbf{h}^b_{0,j},d_{0,j},x_{j,1},\cdots,x_{j,N_{PB}}}\left[\exp\left(-s\sum_{j\in\Phi_{BN}\setminus BN_0}\mathbf{h}^b_{0,j}d^{-\alpha^b}_{0,j}\sum_{k=1}^{N_{PB}}x^{-\alpha^f}_{j,k}\right)\right]$$

$$\stackrel{a}{=}\mathbb{E}_{d_{0,j},x_{j,1},\cdots,x_{j,N_{PB}}}\left[\prod_{j\in\Phi_{BN}\setminus BN_0}\mathbb{E}_{\mathbf{h}^b_{0,j}}\left[\exp\left(-s\mathbf{h}^b_{0,j}d^{-\alpha^b}_{0,j}\sum_{k=1}^{N_{PB}}x^{-\alpha^f}_{j,k}\right)\right]\right]$$

$$\stackrel{b}{=}\mathbb{E}_{d_{0,j}}\left[\prod_{j\in\Phi_{BN}\setminus BN_0}\mathbb{E}_{x_{j,1},\cdots,x_{j,N_{PB}}}\left[\frac{1}{1+sd^{-\alpha^b}_{0,j}\sum_{k=1}^{N_{PB}}x^{-\alpha^f}_{j,k}}\right]\right]$$

$$\stackrel{c}{=}\exp\left(-2\pi\lambda_{BN}\int_0^\infty\mathbb{E}_{x_1,\cdots,x_{N_{PB}}}\left[\frac{1}{1+\frac{u^{\alpha^b}}{s\sum_{k=1}^{N_{PB}}x_k^{-\alpha^f}}}\right]u\mathrm{d}u\right),$$

$$\stackrel{d}{=}\exp\left(-\frac{2\pi^2\lambda_{BN}s^{2/\alpha^b}}{\alpha^b\sin\left(\frac{2\pi}{\alpha^b}\right)}\mathbb{E}_{x_1,\cdots,x_{N_{PB}}}\left(\sum_{k=1}^{N_{PB}}x_k^{-\alpha^f}\right)^{2/\alpha^b}\right) \quad \text{(B.3)}$$

where (a) follows due to the independence of $\mathbf{h}^b_{0,j}$, (b) follows from the fact that $\mathbf{h}^b_{0,j}\sim\exp(1)$ and the independence of $\mathbb{E}_{x_{j,1},\cdots,x_{j,N_{PB}}}$, (c) follows from the probability generating functional (PGFL) of 2-D PPP [7], changing the coordinates to the polar coordinates and evaluating one of the integrals, and (d) follows by changing the order of integration and expectation, and then computing the integral. The last expectation $\mathbb{E}_{x_1,\cdots,x_{N_{PB}}}$ can be computed by using the joint PDF given in (3.2). By inserting (B.3) in (B.2), and then (B.2) in (B.1), we get the final expression for $\mathcal{C}$.

B.2. Proof of Proposition 3.1

The SIR coverage probability can be written as

$$\mathcal{C}\approx\mathbb{P}\left[\gamma_{R_0}\geq\Theta\right]=\mathbb{P}\left[\frac{\mathbf{h}^b_{0,0}d^{-\alpha^b}_{0,0}\sum_{i\in\Phi_{PB}}x^{-\alpha^f}_{0,i}}{\sum_{j\in\Phi_{BN}\setminus BN_0}\mathbf{h}^b_{0,j}d^{-\alpha^b}_{0,j}\sum_{k\in\Phi_{PB}}x^{-\alpha^f}_{j,k}}\geq\Theta\right], \quad \text{(B.4)}$$

where we insert (3.21) for γ_{R_0}. We know that $\mathbf{h}^b_{0,0}$ is exponentially distributed with a unit mean, due to which the above expression becomes

$$\mathcal{C}\approx\mathbb{E}_{\Phi_{BN},\Phi_{PB},\mathbf{h}^b_{0,j}}\left[\exp\left(-\frac{\Theta\sum_{j\in\Phi_{BN}\setminus BN_0}\mathbf{h}^b_{0,j}d^{-\alpha^b}_{0,j}\sum_{k\in\Phi_{PB}}x^{-\alpha^f}_{j,k}}{d^{-\alpha^b}_{0,0}\sum_{i\in\Phi_{PB}}x^{-\alpha^f}_{0,i}}\right)\right], \quad \text{(B.5)}$$

where the expectation should be with respect to Φ_{BN}, Φ_{PB}, and $\mathbf{h}_{0,j}^{b}$. Due to the independence of $\mathbf{h}_{0,j}^{b}$ the previous expression can be written as

$$\begin{aligned}
\mathcal{C} &\approx \mathbb{E}_{\Phi_{BN},\Phi_{PB}}\left[\prod_{j\in\Phi_{BN}\setminus BN_0}\mathbb{E}_{\mathbf{h}_{0,j}^{b}}\left[\exp\left(-\frac{\Theta\mathbf{h}_{0,j}^{b}d_{0,j}^{-\alpha^b}\sum_{k\in\Phi_{PB}}x_{j,k}^{-\alpha^f}}{d_{0,0}^{-\alpha^b}\sum_{i\in\Phi_{PB}}x_{0,i}^{-\alpha^f}}\right)\right]\right] \\
&\overset{a}{=} \mathbb{E}_{\Phi_{BN}}\left[\prod_{j\in\Phi_{BN}\setminus BN_0}\mathbb{E}_{\Phi_{PB}}\left[\frac{1}{1+\frac{\Theta d_{0,j}^{-\alpha^b}\sum_{k\in\Phi_{PB}}x_{j,k}^{-\alpha^f}}{d_{0,0}^{-\alpha^b}\sum_{i\in\Phi_{PB}}x_{0,i}^{-\alpha^f}}}\right]\right] \\
&\overset{b}{=} \exp\left(-2\pi\lambda_{BN}\int_0^{\infty}\left(1-\mathbb{E}_{\Phi_{PB}}\left[\frac{1}{1+\frac{\Theta u^{-\alpha^b}\sum_{k\in\Phi_{PB}}x_{j,k}^{-\alpha^f}}{d_{0,0}^{-\alpha^b}\sum_{i\in\Phi_{PB}}x_{0,i}^{-\alpha^f}}}\right]\right)u\mathrm{d}u\right) \\
&\overset{c}{\geq} \exp\left(-2\pi\lambda_{BN}\int_0^{\infty}\left(1-\frac{1}{1+\frac{\Theta u^{-\alpha^b}}{d_{0,0}^{-\alpha^b}}\mathbb{E}_{\Phi_{PB}}\left[\frac{\sum_{k\in\Phi_{PB}}x_{j,k}^{-\alpha^f}}{\sum_{i\in\Phi_{PB}}x_{0,i}^{-\alpha^f}}\right]}\right)u\mathrm{d}u\right), \quad \text{(B.6)}
\end{aligned}$$

where (a) follows because $\mathbf{h}_{0,j}^{b}\sim\exp(1)$ and both Φ_{BN} and Φ_{PB} are independent, (b) follows due the probability generating functional of 2-D PPP [7], while in (c) we utilize the Jensen's inequality. Now, to find the last expectation $\mathbb{E}_{\Phi_{PB}}$, we use Jensen's inequality and write $\mathbb{E}_{\Phi_{PB}}\left[\frac{\sum_{k\in\Phi_{PB}}x_{j,k}^{-\alpha^f}}{\sum_{i\in\Phi_{PB}}x_{0,i}^{-\alpha^f}}\right] \geq \frac{\mathbb{E}_{\Phi_{PB}}\left[\sum_{k\in\Phi_{PB}}x_{j,k}^{-\alpha^f}\right]}{\mathbb{E}_{\Phi_{PB}}\left[\sum_{i\in\Phi_{PB}}x_{0,i}^{-\alpha^f}\right]} = 1$, where to find $\mathbb{E}_{\Phi_{PB}}$, we utilize Lemma 3.2. The final expression in (3.24) is obtained by doing some algebraic manipulations.

C. Proofs for Chapter 4

C.1. Proof of Theorem 4.1

The SINR coverage probability of the typical UE given that it satisfies the TIN optimality conditions can be expressed as follows:

$$\begin{aligned}\mathcal{C} &= \int_0^\infty \mathbb{P}\left[\text{SINR} \geq \Theta\right] f_{X_{11}}\left(x_{11}|\mathbb{A}_{\mathbb{UE}}\right) \mathrm{d}x_{11} \\ &\overset{(a)}{=} \frac{2\pi\lambda_b}{\mathbb{P}\left[\mathbb{A}_{\mathbb{UE}}\right]} \int_0^\infty \mathbb{P}\left[\frac{h_{11}x_{11}^{-\alpha}}{I+\frac{N}{P}} \geq \Theta\right] x_{11} \mathrm{e}^{-\pi\lambda_b \max^2\left(x_{11}, x_{11}^{\mu/2}\left(\frac{P}{N}\right)^{\frac{2-\mu}{2\alpha}}\left(\frac{1}{M}\right)^{\frac{1}{2\alpha}}\right)} \mathrm{d}x_{11} \\ &\overset{(b)}{=} \frac{2\pi\lambda_b}{\mathbb{P}\left[\mathbb{A}_{\mathbb{UE}}\right]} \int_0^\infty \mathrm{e}^{-x_{11}^\alpha \Theta \frac{N}{P}} \mathbb{E}_I\left[\mathrm{e}^{-x_{11}^\alpha \Theta I}\right] x_{11} \mathrm{e}^{-\pi\lambda_b \max^2\left(x_{11}, x_{11}^{\frac{\mu}{2}}\left(\frac{P}{N}\right)^{\frac{2-\mu}{2\alpha}}\left(\frac{1}{M}\right)^{\frac{1}{2\alpha}}\right)} \mathrm{d}x_{11},\end{aligned} \tag{C.1}$$

where I denotes the other-cell interference, (a) follows by using $f_{X_{11}}\left(x_{11}|\mathbb{A}_{\mathbb{UE}}\right)$ in (4.11), (b) follows because $h_{11} \sim \exp\left(1\right)$ is an exponential random variable, and $\mathbb{E}_I\left[\mathrm{e}^{-x_{11}^\alpha \Theta I}\right] = \mathcal{L}_I\left(x_{11}^\alpha \Theta\right)$ is the Laplace transform of the other-cell interference I.

Let us define $s = x_{11}^\alpha \Theta$. The Laplace transform $\mathcal{L}_I\left(s\right)$ can be written as follows:

$$\begin{aligned}\mathcal{L}_I\left(s\right) &= \mathbb{E}_I\left[\mathrm{e}^{-sI}\right] = \mathbb{E}_{h_i, D_i}\left[\mathrm{e}^{-s\sum_{i\in\Phi_b'} h_i D_i^{-\alpha}}\right] \\ &= \mathbb{E}_{D_i} \prod_{i\in\Phi_b'} \mathbb{E}_{h_i}\left[\mathrm{e}^{-s h_i D_i^{-\alpha}}\right] \overset{(c)}{=} \mathbb{E}_{D_i} \prod_{i\in\Phi_b'} \frac{1}{1+sD_i^{-\alpha}} \\ &\overset{(d)}{=} \exp\left(-2\pi\lambda_b \mathbb{P}\left[\mathbb{A}_{\mathbb{UE}}\right] \int_{\max\left(x_{11}, x_{11}^{\mu/2}\left(\frac{P}{N}\right)^{\frac{2-\mu}{2\alpha}}\left(\frac{1}{M}\right)^{\frac{1}{2\alpha}}\right)}^\infty \left(1-\frac{1}{1+su^{-\alpha}}\right) u \mathrm{d}u\right) \\ &= \exp\left(-\pi\lambda_b \mathbb{P}\left[\mathbb{A}_{\mathbb{UE}}\right] s^{\frac{2}{\alpha}} \int_{s^{\frac{-2}{\alpha}} \max^2\left(x_{11}, x_{11}^{\mu/2}\left(\frac{P}{N}\right)^{\frac{2-\mu}{2\alpha}}\left(\frac{1}{M}\right)^{\frac{1}{2\alpha}}\right)}^\infty \frac{1}{1+z^{\alpha/2}} \mathrm{d}z\right),\end{aligned} \tag{C.2}$$

where (c) follows by computing the expectation with respect to h_i, and (d) follows from the probability generating functional theorem of PPPs [28] by assuming that the point process of interfering BSs is an inhomogeneous PPP whose density is given in (4.6). The proof follows with the aid of simple algebraic manipulations.

Bibliography

[1] A. D. Wyner, "Shannon-theoretic approach to a gaussian cellular multiple-access channel," *IEEE Transactions on Information Theory*, vol. 40, no. 6, pp. 1713–1727, Nov 1994.

[2] J. Xu, J. Zhang, and J. G. Andrews, "On the accuracy of the wyner model in cellular networks," *IEEE Transactions on Wireless Communications*, vol. 10, no. 9, pp. 3098–3109, September 2011.

[3] V. Tarokh, C.-B. Chae, I. Hwang, and R. W. Heath Jr, "Interference aware-coordinated beamforming system in a two-cell environment," *Technical Report*, 2009. [Online]. Available: http://dash.harvard.edu/handle/1/3293263.

[4] V. H. M. Donald, "Advanced mobile phone service: The cellular concept," *The Bell System Technical Journal*, vol. 58, no. 1, pp. 15–41, Jan 1979.

[5] H. ElSawy, E. Hossain, and M. Haenggi, "Stochastic geometry for modeling, analysis, and design of multi-tier and cognitive cellular wireless networks: A survey," *IEEE Communications Surveys Tutorials*, vol. 15, no. 3, pp. 996–1019, Third 2013.

[6] H. ElSawy, A. Sultan-Salem, M.-S. Alouini, and M. Z. Win, "Modeling and analysis of cellular networks using stochastic geometry: A tutorial," *IEEE Communications Surveys & Tutorials*, vol. 19, no. 1, pp. 167–203, 2017.

[7] M. Haenggi and R. K. Ganti, *Interference in large wireless networks*. Now Publishers Inc, 2009.

[8] F. Baccelli and B. Baszczyszyn, "Stochastic geometry and wireless networks: Volume I theory," *Foundations and Trends in Networking*, vol. 3, no. 34, pp. 249–449, 2010. [Online]. Available: http://dx.doi.org/10.1561/1300000006

[9] ——, "Stochastic geometry and wireless networks: Volume II applications," *Foundations and Trends in Networking*, vol. 4, no. 12, pp. 1–312, 2010. [Online]. Available: http://dx.doi.org/10.1561/1300000026

[10] M. Haenggi, J. G. Andrews, F. Baccelli, O. Dousse, and M. Franceschetti, "Stochastic geometry and random graphs for the analysis and design of wireless networks," *IEEE Journal on Selected Areas in Communications*, vol. 27, no. 7, pp. 1029–1046, September 2009.

[11] C. h. Lee and M. Haenggi, "Interference and outage in Poisson cognitive networks," *IEEE Transactions on Wireless Communications*, vol. 11, no. 4, pp. 1392–1401, April 2012.

[12] E. M. Stein and R. Shakarchi, *Real analysis: measure theory, integration, and Hilbert spaces*. Princeton University Press, 2009.

[13] J. G. Andrews, A. K. Gupta, and H. S. Dhillon, "A primer on cellular network analysis using stochastic geometry," *arXiv preprint arXiv:1604.03183*, 2016.

[14] M. C. Valenti, D. Torrieri, and S. Talarico, "A direct approach to computing spatially averaged outage probability," *IEEE Communications Letters*, vol. 18, no. 7, pp. 1103–1106, 2014.

[15] M. Di Renzo and W. Lu, "The equivalent-in-distribution (EiD)-based approach: On the analysis of cellular networks using stochastic geometry," *IEEE Communications Letters*, vol. 18, no. 5, pp. 761–764, 2014.

[16] M. Di Renzo, A. Guidotti, and G. E. Corazza, "Average rate of downlink heterogeneous cellular networks over generalized fading channels: A stochastic geometry approach," *IEEE Transactions on Communications*, vol. 61, no. 7, pp. 3050–3071, 2013.

[17] M. D. Renzo and P. Guan, "Stochastic geometry modeling of coverage and rate of cellular networks using the gil-pelaez inversion theorem," *IEEE Communications Letters*, vol. 18, no. 9, pp. 1575–1578, Sept 2014.

[18] "1000x data challenge and mobile traffic — Qualcomm," 2014. [Online]. Available: https://www.qualcomm.com/invention/1000x

[19] J. G. Andrews, H. Claussen, M. Dohler, S. Rangan, and M. C. Reed, "Femtocells: Past, present, and future," *IEEE Journal on Selected Areas in Communications*, vol. 30, no. 3, pp. 497–508, April 2012.

[20] J. G. Andrews, "Seven ways that hetnets are a cellular paradigm shift," *IEEE Communications Magazine*, vol. 51, no. 3, pp. 136–144, March 2013.

[21] F. Boccardi, J. Andrews, H. Elshaer, M. Dohler, S. Parkvall, P. Popovski, and S. Singh, "Why to decouple the uplink and downlink in cellular networks and how to do it," *arXiv preprint arXiv:1503.06746*, 2015.

[22] F. Boccardi, R. W. Heath, A. Lozano, T. L. Marzetta, and P. Popovski, "Five disruptive technology directions for 5G," *IEEE Communications Magazine*, vol. 52, no. 2, pp. 74–80, 2014.

[23] H. Elshaer, F. Boccardi, M. Dohler, and R. Irmer, "Downlink and uplink decoupling: A disruptive architectural design for 5G networks," in *IEEE Global Communications Conference (GLOBECOM)*, 2014, pp. 1798–1803.

[24] K. Smiljkovikj, P. Popovski, and L. Gavrilovska, "Analysis of the decoupled access for downlink and uplink in wireless heterogeneous networks," *IEEE Wireless Communications Letters*, vol. 4, no. 2, pp. 173–176, 2015.

[25] K. Smiljkovikj, H. Elshaer, P. Popovski, F. Boccardi, M. Dohler, L. Gavrilovska, and R. Irmer, "Capacity analysis of decoupled downlink and uplink access in 5g heterogeneous systems," *arXiv preprint arXiv:1410.7270*, 2014.

[26] L. Zhang, F. Gang, and Q. Shuang, "A comparison study of coupled and decoupled uplink heterogeneous cellular networks," *arXiv preprint arXiv:1502.01887*, 2015.

[27] S. Singh, X. Zhang, and J. G. Andrews, "Joint rate and SINR coverage analysis for decoupled uplink-downlink biased cell associations in hetnets," *IEEE Transactions on Wireless Communications*, vol. 14, no. 10, pp. 5360–5373, 2015.

[28] J. G. Andrews, F. Baccelli, and R. K. Ganti, "A tractable approach to coverage and rate in cellular networks," *IEEE Transactions on Communications*, vol. 59, no. 11, pp. 3122–3134, 2011.

[29] H.-S. Jo, Y. J. Sang, P. Xia, and J. G. Andrews, "Heterogeneous cellular networks with flexible cell association: A comprehensive downlink SINR analysis," *IEEE Transactions on Wireless Communications*, vol. 11, no. 10, pp. 3484–3495, 2012.

[30] S. Singh and J. G. Andrews, "Joint resource partitioning and offloading in heterogeneous cellular networks," *IEEE Transactions on Wireless Communications*, vol. 13, no. 2, pp. 888–901, 2014.

[31] M. D. Renzo, A. Guidotti, and G. E. Corazza, "Average rate of downlink heterogeneous cellular networks over generalized fading channels: A stochastic geometry approach," *IEEE Transactions on Communications*, vol. 61, no. 7, pp. 3050–3071, July 2013.

[32] B. Blaszczyszyn, M. K. Karray, and H. P. Keeler, "Using Poisson processes to model lattice cellular networks," *in Proceedings of IEEE INFOCOM*, pp. 773–781, 2013.

[33] H. S. Dhillon and J. G. Andrews, "Downlink rate distribution in heterogeneous cellular networks under generalized cell selection," *IEEE Wireless Communications Letters*, vol. 3, no. 1, pp. 42–45, 2014.

[34] R. W. Heath, M. Kountouris, and T. Bai, "Modeling heterogeneous network interference using Poisson point processes," *IEEE Transactions on Signal Processing*, vol. 61, no. 16, pp. 4114–4126, 2013.

[35] S. Mukherjee, "Distribution of downlink SINR in heterogeneous cellular networks," *IEEE Journal on Selected Areas in Communications*, vol. 30, no. 3, pp. 575–585, 2012.

[36] S. Singh, H. S. Dhillon, and J. G. Andrews, "Offloading in heterogeneous networks: Modeling, analysis, and design insights," *IEEE Transactions on Wireless Communications*, vol. 12, no. 5, pp. 2484–2497, 2013.

[37] H. S. Dhillon, R. K. Ganti, F. Baccelli, and J. G. Andrews, "Modeling and analysis of k-tier downlink heterogeneous cellular networks," *IEEE Journal on Selected Areas in Communications*, vol. 30, no. 3, pp. 550–560, April 2012.

[38] A. Rajanna and M. Haenggi, "Enhanced cellular coverage and throughput using rateless codes," *IEEE Transactions on Communications*, vol. 65, no. 5, pp. 1899–1912, May 2017.

[39] M. Di Renzo, "Stochastic geometry modeling and analysis of multi-tier millimeter wave cellular networks," *IEEE Transactions on Wireless Communications*, vol. 14, no. 9, pp. 5038–5057, 2015.

[40] T. Bai and R. W. Heath, "Coverage and rate analysis for millimeter-wave cellular networks," *IEEE Transactions on Wireless Communications*, vol. 14, no. 2, pp. 1100–1114, 2015.

[41] S. Singh, M. N. Kulkarni, A. Ghosh, and J. G. Andrews, "Tractable model for rate in self-backhauled millimeter wave cellular networks," *IEEE Journal on Selected Areas in Communications*, vol. 33, no. 10, pp. 2196–2211, 2015.

[42] M. Di Renzo and W. Lu, "System-level analysis and optimization of cellular networks with simultaneous wireless information and power transfer: Stochastic geometry modeling," *IEEE Transactions on Vehicular Technology*, vol. 66, no. 3, pp. 2251–2275, 2017.

[43] M. D. Renzo, A. Zappone, T. T. Lam, and M. Debbah, "System-level modeling and optimization of the energy efficiency in cellular networks-a stochastic geometry framework," *IEEE Transactions on Wireless Communications*, vol. 17, no. 4, pp. 2539–2556, April 2018.

[44] H. S. Dhillon, Y. Li, P. Nuggehalli, Z. Pi, and J. G. Andrews, "Fundamentals of heterogeneous cellular networks with energy harvesting," *IEEE Transactions on Wireless Communications*, vol. 13, no. 5, pp. 2782–2797, 2014.

[45] A. H. Sakr and E. Hossain, "Analysis of k-tier uplink cellular networks with ambient rf energy harvesting," *IEEE Journal on Selected Areas in Communications*, vol. 33, no. 10, pp. 2226–2238, 2015.

[46] M. Bacha and B. Clerckx, "Backscatter communications for the internet of things: A stochastic geometry approach," *arXiv preprint arXiv:1711.07277*, 2018.

[47] Y. Wu, Y. Cui, and B. Clerckx, "Analysis and optimization of inter-tier interference coordination in downlink multi-antenna hetnets with offloading," *IEEE Transactions on Wireless Communications*, vol. 14, no. 12, pp. 6550–6564, 2015.

[48] Y. Cui, Y. Wu, D. Jiang, and B. Clerckx, "User-centric interference nulling in downlink multi-antenna heterogeneous networks," *IEEE Transactions on Wireless Communications*, vol. 15, no. 11, pp. 7484–7500, Nov 2016.

[49] H. S. Dhillon, M. Kountouris, and J. G. Andrews, "Downlink mimo hetnets: Modeling, ordering results and performance analysis," *Wireless Communications, IEEE Transactions on*, vol. 12, no. 10, pp. 5208–5222, 2013.

[50] A. K. Gupta, H. S. Dhillon, S. Vishwanath, and J. G. Andrews, "Downlink multi-antenna heterogeneous cellular network with load balancing," *Communications, IEEE Transactions on*, vol. 62, no. 11, pp. 4052–4067, 2014.

[51] ——, "Downlink coverage probability in MIMO hetnets with flexible cell selection," in *Global Communications Conference (GLOBECOM), 2014 IEEE*. IEEE, 2014, pp. 1534–1539.

[52] R. Tanbourgi, H. S. Dhillon, and F. K. Jondral, "Analysis of joint transmit–receive diversity in downlink MIMO heterogeneous cellular networks," *IEEE Transactions on Wireless Communications*, vol. 14, no. 12, pp. 6695–6709, 2015.

[53] H. Tabassum, A. H. Sakr, and E. Hossain, "Analysis of massive MIMO-enabled downlink wireless backhauling for full-duplex small cells," *IEEE Transactions on Communications*, vol. 64, no. 6, pp. 2354–2369, 2016.

[54] C. Li, J. Zhang, and K. B. Letaief, "Throughput and energy efficiency analysis of small cell networks with multi-antenna base stations," *IEEE Transactions on Wireless Communications*, vol. 13, no. 5, pp. 2505–2517, 2014.

[55] M. Di Renzo and P. Guan, "A mathematical framework to the computation of the error probability of downlink MIMO cellular networks by using stochastic geometry," *IEEE Transactions on Communications*, vol. 62, no. 8, pp. 2860–2879, 2014.

[56] T. D. Novlan, H. S. Dhillon, and J. G. Andrews, "Analytical modeling of uplink cellular networks," *Wireless Communications, IEEE Transactions on*, vol. 12, no. 6, pp. 2669–2679, 2013.

[57] H. ElSawy and E. Hossain, "On stochastic geometry modeling of cellular uplink transmission with truncated channel inversion power control," *IEEE Transactions on Wireless Communications*, vol. 13, no. 8, pp. 4454–4469, 2014.

[58] M. D. Renzo and P. Guan, "Stochastic geometry modeling and system-level analysis of uplink heterogeneous cellular networks with multi-antenna base stations," *IEEE Transactions on Communications*, vol. 64, no. 6, pp. 2453–2476, June 2016.

[59] W. P. Johnson, "The curious history of Faà di Bruno's formula," *The American mathematical monthly*, vol. 109, no. 3, pp. 217–234, 2002.

[60] W. Xiao, R. Ratasuk, A. Ghosh, R. Love, Y. Sun, and R. Nory, "Uplink power control, interference coordination and resource allocation for 3GPP E-UTRA," in *IEEE Vehicular Technology Conference*, Sept 2006, pp. 1–5.

[61] A. M. Hunter, J. G. Andrews, and S. Weber, "Transmission capacity of ad hoc networks with spatial diversity," *Wireless Communications, IEEE Transactions on*, vol. 7, no. 12, pp. 5058–5071, 2008.

[62] A. Guo and M. Haenggi, "Spatial stochastic models and metrics for the structure of base stations in cellular networks," *Wireless Communications, IEEE Transactions on*, vol. 12, no. 11, pp. 5800–5812, 2013.

[63] A. M. Hunter, J. G. Andrews, and S. Weber, "Transmission capacity of ad hoc networks with spatial diversity," *Wireless Communications, IEEE Transactions on*, vol. 7, no. 12, pp. 5058–5071, 2008.

[64] M. Kountouris and J. G. Andrews, "Transmission capacity scaling of SDMA in wireless ad hoc networks," in *Information Theory Workshop, 2009. ITW 2009. IEEE.* IEEE, 2009, pp. 534–538.

[65] C. Li, J. Zhang, and K. Letaief, "Throughput and energy efficiency analysis of small cell networks with multi-antenna base stations," *Wireless Communications, IEEE Transactions on*, vol. 13, no. 5, pp. 2505–2517, 2014.

[66] S. Singh, H. S. Dhillon, and J. G. Andrews, "Offloading in heterogeneous networks: Modeling, analysis, and design insights," *Wireless Communications, IEEE Transactions on*, vol. 12, no. 5, pp. 2484–2497, 2013.

[67] "Internet of things (IoT)." [Online]. Available: http://www.cisco.com/c/en/us/solutions/internet-of-things/overview.html

[68] M. Elkhodr, S. Shahrestani, and H. Cheung, "The internet of things: New interoperability, management and security challenges," *International Journal of Network Security & Its Applications (IJNSA)*, vol. 8, no. 2, pp. 85–102, 2016.

[69] "Powering IoT devices: Technologies and opportunities." [Online]. Available: http://iot.ieee.org/newsletter/november-2015/powering-iot-devices-technologies-and-opportunities.html

[70] Y. Zeng, B. Clerckx, and R. Zhang, "Communications and signals design for wireless power transmission," *IEEE Transactions on Communications*, vol. 65, no. 5, pp. 2264–2290, May 2017.

[71] B. Clerckx and E. Bayguzina, "Waveform design for wireless power transfer," *IEEE Transactions on Signal Processing*, vol. 64, no. 23, pp. 6313–6328, Dec 2016.

[72] B. Clerckx, Z. B. Zawawi, and K. Huang, "Wirelessly powered backscatter communications: Waveform design and snr-energy tradeoff," *IEEE Communications Letters*, vol. PP, no. 99, pp. 1–1, 2017.

[73] C. Boyer and S. Roy, "Backscatter communication and RFID: Coding, energy, and MIMO analysis," *Communications, IEEE Transactions on*, vol. 62, no. 3, pp. 770–785, 2014.

[74] W. Liu, K. Huang, X. Zhou, and S. Durrani, "Backscatter communications for internet-of-things: Theory and applications," *arXiv preprint arXiv:1701.07588*, 2017.

[75] R. Want, "An introduction to RFID technology," *IEEE Pervasive Computing*, vol. 5, no. 1, pp. 25–33, Jan 2006.

[76] V. Liu, A. Parks, V. Talla, S. Gollakota, D. Wetherall, and J. R. Smith, "Ambient backscatter: wireless communication out of thin air," *ACM SIGCOMM Computer Communication Review*, vol. 43, no. 4, pp. 39–50, 2013.

[77] B. Kellogg, A. Parks, S. Gollakota, J. R. Smith, and D. Wetherall, "Wi-fi backscatter: Internet connectivity for rf-powered devices," in *ACM SIGCOMM Computer Communication Review*, vol. 44, no. 4. ACM, 2014, pp. 607–618.

[78] G. Yang, Y. C. Liang, R. Zhang, and Y. Pei, "Modulation in the air: Backscatter communication over ambient OFDM carrier," *IEEE Transactions on Communications*, vol. 66, no. 3, pp. 1219–1233, March 2018.

[79] K. Han and K. Huang, "Wirelessly powered backscatter communication networks: Modeling, coverage, and capacity," *IEEE Transactions on Wireless Communications*, vol. 16, no. 4, pp. 2548–2561, 2017.

[80] C. Psomas and I. Krikidis, "Backscatter communications for wireless powered sensor networks with collision resolution," *IEEE Wireless Communications Letters*, vol. 6, no. 5, pp. 650–653, Oct 2017.

[81] W. Liu, K. Huang, X. Zhou, and S. Durrani, "Full-duplex backscatter interference networks based on time-hopping spread spectrum," *IEEE Transactions on Wireless Communications*, 2017.

[82] P. N. Alevizos, K. Tountas, and A. Bletsas, "Multistatic scatter radio sensor networks for extended coverage," *IEEE Transactions on Wireless Communications*, pp. 1–1, 2018.

[83] A. Bletsas, S. Siachalou, and J. N. Sahalos, "Anti-collision backscatter sensor networks," *IEEE Transactions on Wireless Communications*, vol. 8, no. 10, pp. 5018–5029, October 2009.

[84] D. Moltchanov, "Distance distributions in random networks," *Ad Hoc Networks*, vol. 10, no. 6, pp. 1146–1166, 2012.

[85] N. Naderializadeh and A. S. Avestimehr, "ITLinQ: A new approach for spectrum sharing in device-to-device communication systems," *IEEE Journal on Selected Areas in Communications*, vol. 32, no. 6, pp. 1139–1151, June 2014.

[86] G. George, R. K. Mungara, and A. Lozano, "An analytical framework for device-to-device communication in cellular networks," *IEEE Transactions on Wireless Communications*, vol. 14, no. 11, pp. 6297–6310, 2015.

[87] M. A. Kishk and H. S. Dhillon, "Joint uplink and downlink coverage analysis of cellular-based RF-powered IoT network," *IEEE Transactions on Green Communications and Networking*, vol. 2, no. 2, pp. 446–459, June 2018.

[88] S. Weber, J. G. Andrews, and N. Jindal, "The effect of fading, channel inversion, and threshold scheduling on ad hoc networks," *IEEE Transactions on Information Theory*, vol. 53, no. 11, pp. 4127–4149, Nov 2007.

[89] P. Madhusudhanan, J. G. Restrepo, Y. Liu, T. X. Brown, and K. R. Baker, "Downlink performance analysis for a generalized shotgun cellular system," *IEEE Transactions on Wireless Communications*, vol. 13, no. 12, pp. 6684–6696, Dec 2014.

[90] G. Nigam, P. Minero, and M. Haenggi, "Coordinated multipoint joint transmission in heterogeneous networks," *IEEE Transactions on Communications*, vol. 62, no. 11, pp. 4134–4146, 2014.

[91] ——, "Spatiotemporal cooperation in heterogeneous cellular networks," *IEEE Journal on Selected Areas in Communications*, vol. 33, no. 6, pp. 1253–1265, June 2015.

[92] D. Zwillinger, *Table of integrals, series, and products*. Elsevier, 2014.

[93] D. Lee, H. Seo, B. Clerckx, E. Hardouin, D. Mazzarese, S. Nagata, and K. Sayana, "Coordinated multipoint transmission and reception in LTE-advanced: deployment scenarios and operational challenges," *IEEE Communications Magazine*, vol. 50, no. 2, pp. 148–155, February 2012.

[94] D. Lopez-Perez, I. Guvenc, G. de la Roche, M. Kountouris, T. Q. S. Quek, and J. Zhang, "Enhanced intercell interference coordination challenges in heterogeneous networks," *IEEE Wireless Communications*, vol. 18, no. 3, pp. 22–30, June 2011.

[95] G. J. Foschini, K. Karakayali, and R. A. Valenzuela, "Coordinating multiple antenna cellular networks to achieve enormous spectral efficiency," *IEE Proceedings - Communications*, vol. 153, no. 4, pp. 548–555, August 2006.

[96] Q. Ye, M. Al-Shalashy, C. Caramanis, and J. G. Andrews, "On/off macrocells and load balancing in heterogeneous cellular networks," in *Global Communications Conference (GLOBECOM), 2013 IEEE*. IEEE, 2013, pp. 3814–3819.

[97] E. U. T. R. Access, "Physical layer procedures, 3GPP std," *TS*, vol. 36, p. V9, 2013.

[98] C. U. Castellanos, D. L. Villa, C. Rosa, K. I. Pedersen, F. D. Calabrese, P. H. Michaelsen, and J. Michel, "Performance of uplink fractional power control in UTRAN LTE," in *VTC Spring 2008 - IEEE Vehicular Technology Conference*, May 2008, pp. 2517–2521.

[99] H. Zhang, N. Prasad, S. Rangarajan, S. Mekhail, S. Said, and R. Arnott, "Standards-compliant LTE and LTE-A uplink power control," in *Communications (ICC), 2012 IEEE International Conference on*. IEEE, 2012, pp. 5275–5279.

[100] C. Geng, N. Naderializadeh, A. S. Avestimehr, and S. A. Jafar, "On the optimality of treating interference as noise," *IEEE Transactions on Information Theory*, vol. 61, no. 4, pp. 1753–1767, April 2015.

[101] A. S. Motahari and A. K. Khandani, "Capacity bounds for the Gaussian interference channel," *IEEE Transactions on Information Theory*, vol. 55, no. 2, pp. 620–643, 2009.

[102] V. S. Annapureddy and V. V. Veeravalli, "Gaussian interference networks: Sum capacity in the low-interference regime and new outer bounds on the capacity region," *IEEE Transactions on Information Theory*, vol. 55, no. 7, pp. 3032–3050, 2009.

[103] M. A. Charafeddine, A. Sezgin, Z. Han, and A. Paulraj, "Achievable and crystallized rate regions of the interference channel with interference as noise," *IEEE Transactions on Wireless Communications*, vol. 11, no. 3, pp. 1100–1111, 2012.

[104] X. Yi and G. Caire, "Optimality of treating interference as noise: A combinatorial perspective," *IEEE Transactions on Information Theory*, vol. 62, no. 8, pp. 4654–4673, 2016.

[105] R. K. Mungara, X. Zhang, A. Lozano, and R. W. Heath, "Analytical characterization of ITLinQ: Channel allocation for device-to-device communication networks," *IEEE Transactions on Wireless Communications*, vol. 15, no. 5, pp. 3603–3615, May 2016.

[106] F. J. Martin-Vega, G. Gomez, M. C. Aguayo-Torres, and M. D. Renzo, "Analytical modeling of interference aware power control for the uplink of heterogeneous cellular networks," *IEEE Transactions on Wireless Communications*, vol. 15, no. 10, pp. 6742–6757, Oct 2016.

[107] F. J. Martin-Vega, M. C. Aguayo-Torres, G. Gómez, and M. D. Renzo, "On muting mobile terminals for uplink interference mitigation in hetnets - system-level analysis via stochastic geometry," *CoRR*, vol. abs/1702.03726, 2017. [Online]. Available: http://arxiv.org/abs/1702.03726

[108] A. M. Rao, "Reverse link power control for managing inter-cell interference in orthogonal multiple access systems," in *Vehicular Technology Conference, 2007. VTC-2007 Fall. 2007 IEEE 66th.* IEEE, 2007, pp. 1837–1841.

[109] M. Boussif, N. Quintero, F. D. Calabrese, C. Rosa, and J. Wigard, "Interference based power control performance in lte uplink," in *Wireless Communication Systems. 2008. ISWCS'08. IEEE International Symposium on.* IEEE, 2008, pp. 698–702.

[110] P. Calka, "Precise formulae for the distributions of the principal geometric characteristics of the typical cells of a two-dimensional Poisson-voronoi tessellation and a Poisson line process," *Advances in Applied Probability*, vol. 35, no. 3, p. 551562, 2003.

[111] B. Yu, S. Mukherjee, H. Ishii, and L. Yang, "Dynamic TDD support in the LTE-B enhanced local area architecture," in *2012 IEEE Globecom Workshops*, Dec 2012, pp. 585–591.

[112] M. van Lieshout, "An introduction to planar random tessellation models," *Spatial Statistics*, vol. 1, pp. 40 – 49, 2012. [Online]. Available: http://www.sciencedirect.com/science/article/pii/S2211675312000036

[113] M. Bacha, Y. Wu, and B. Clerckx, "Downlink and uplink decoupling in two-tier heterogeneous networks with multi- antenna base stations," *IEEE Transactions on Wireless Communications*, vol. 16, no. 5, pp. 2760–2775, 2017.

[114] B. Clerckx and C. Oestges, *MIMO wireless networks: Channels, techniques and standards for multi-antenna, multi-user and multi-cell systems.* Academic Press, 2013.